Spring 5-15-2022

Assembly and Repair of Photosystem II

Virginia M. Johnson
Washington University in St. Louis

WASHINGTON UNIVERSITY IN ST. LOUIS

Division of Biology and Biomedical Sciences
Plant and Microbial Biosciences

Dissertation Examination Committee:
Himadri Pakrasi, Chair
Robert Blankenship
Arpita Bose
Joe Jez
Janice Robertson
Hani Zaher

Assembly and Repair of Photosystem II

by

Virginia M. Johnson

A dissertation presented to
The Graduate School
of Washington University in
partial fulfillment of the
requirements for the degree
of Doctor of Philosophy

May 2022
St. Louis, Missouri

Table of Contents

List of Figures vi

List of Tables viii

Acknowledgments x

Abstract xii

Chapter 1: Introduction: Advances in the understanding of the Photosystem II lifecycle in Cyanobacteria xii

1.1 Summary 2

1.2 Introduction: Photosystem II and Cyanobacteria 3

1.3 PSII structure 5

1.4 PSII assembly 6

1.5 PSII repair 13

1.6 Structural Advances in PSII research 14

1.7 Advances in Photoactivation 20

1.8 Use of CRISPR and CRISPR-inhibition to study photosynthetic protein complexes 22

1.9 Conclusions 23

1.10 References 24

Chapter 2: A Novel Antenna Protein Complex in the Lifecycle of Photosystem II 36

2.1 Summary 37

2.2 Introduction 38

2.3 Materials and Methods 41

2.3.1 Cell Culture, PSII purification, and Protein Analysis 41

2.3.2 Clear Native polyacrylamide gel electrophoresis 41

2.3.3 In-gel digestion and LC-MS/MS analysis 42

2.3.4 In-solution digestion and LC-MS/MS analysis 43

2.3.5 Mass Spectrometry of Intact Proteins 44

2.3.6 Ultrafast Time-Resolved Fluorescence Spectroscopy 46

2.3.7 Glycerol Gradient Ultracentrifugation 47

2.3.8 Analytical Sedimentation 48

2.3.9 Photosystem II Damage Induction 49

2.4 Results 50
2.4.1 Isolation of a Novel PSII Subcomplex 50
2.4.2 Determination of the Size of the NRC Complex 56
2.4.3 The NRC Complex Lacks a Functional Reaction Center 57
2.4.4 NRC Accumulates Under High Light Stress and in the Absence of Protein Synthesis 59
2.5 Discussion 61
2.6 Supplementary Datasets Legend 65
2.7 References 66
Chapter 3: A Reversibly Induced CRISPRi System Targeting Photosystem II in the Cyanobacterium *Synechocystis* sp. PCC 6803 70
3.1 Summary 71
3.2 Introduction 72
3.3 Results 75
3.3.1 Repression of *psbD* genes in *Synechocystis* sp. PCC 6803 by CRISPRi 75
3.3.2 Construction of a Chimeric Promoter Optimized the performance of the P_{RhaBAD} Promoter 77
3.3.3 Tightly Controlled Expression of D2 and CP43 by the CRISPRi-$_{RSW}$ system 7118
3.3.4 Release of CRISRPi Repression Allows Recovery of the Expression of D2 and CP43 Proteins 82
3.4 Discussion 87
3.5 Materials and Methods 87
3.5.1 Strains and Culture Conditions 87
3.5.2 Construction of Recombinant Plasmids and Engineered Strains 88
3.5.3 Measurement of EYFP Fluorescence 88
3.5.4 Reverse Transcription-PCR and Quantitative PCR 89
3.5.5 Western Blot Analysis 89
3.5.6 Measurement of Photosynthetic Activity 90
3.5.7 Cell Number Counting 90
3.6 Supporting Information 91
3.7 References 102
Chapter 4: Control of Expression of the PSII Assembly Factor CtpA 106

4.1 Summary 107
4.2 Introduction 107
4.3 Results 110
4.3.1 CRISPRi-RSW CtpA 110
4.3.2 RhaBAD-RSW Inducible CtpA 112
4.3.3 Nickel-Inducible CtpA 114
4.3.4 Pslr0701 CRISPRi-RSW CtpA 116
4.4 Discussion 117
4.5 Materials and Methods 118
4.5.1 Strains and Culture Conditions 118
4.5.2 Strain Generation 118
4.5.3 Western Blot Analysis 121
4.5.4 Measurement of PSII Activity 122
4.6 Supporting Information 123
4.7 References 129
Chapter 5: Psb27 Contributes to Non-Photochemical Quenching During its Participation in the PSII Lifecycle 131
5.1 Summary 132
5.2 Introduction 133
5.3 Results 136
5.4 Discussion 144
5.5 Materials and Methods 148
5.5.1 Culture and Growth of S6803 Strains 148
5.5.2 Mutant Construction and Psb27 Quantification 148
5.5.3 Fluorescence Analysis 149
5.6 Supporting Information 152
5.7 References 154
Chapter 6: Conclusions, Future Directions, and Additional Data 157
6.1 Conclusions 158
6.2 Conclusions and Future Directions from Chapter 2 158
6.3 Conclusions and Future Directions from Chapter 3 163
6.3.1 CRISPRi on PSII Proteins in *Synechococcus elongatus* UTEX 2973 164

6.3.2 CN PAGE of D2-CRISPRi Samples During PSII Recovery 164
6.3.3 Membrane Structure of S6803 During PSII Degradation and Recovery 167
6.4 Conclusions and Future Directions from Chapter 4 167
6.5 Conclusions and Future Directions from Chapter 5 170
6.6 Materials and Methods 171
6.6.1 Cell Culture, PSII Purification, and Protein Analysis 171
6.6.2 Clear Native Polyacrylamide gel electrophoresis 172
6.7 References 173
Appendix 175
A.1 Mass Spectrometry on CN-PAGE bands from Purified His-47 and His-Psb27 PSII 176
A.2 Materials and Methods 183
A.2.1 Clear Native PAGE analysis 183
A.2.2 In-gel digestion and LC-MS/MS analysis 183

List of Figures

Figure 1.1: Schematic of PSII Monomer……...…4

Figure 1.2: Schematic of PSII Lifecycle ……...……..…7

Figure 2.1: Model of PSII Lifecycle Based on Previous Findings…….……...……...…39

Figure 2.2: Isolation and Characterization of a Novel PSII Subcomplex (NRC) …….……..…50

Figure 2.3: CN-PAGE of Isolated PSII Complexes....……...……..…52

Figure 2.4: Major Protein Components of NRC ……...……..…53

Figure 2.5: Mass Spectra of Intact, Low Molecular Mass Subunits in *ΔpsbO*-NRC and *ΔpsbO*-PSII-M…….……...……...…55

Figure 2.6: AUC to Determine the Size of NRC and PSII-M ……...……...……..…56

Figure 2.7: Time-Resolved Fluorescence of *ΔpsbO*-NRC and *ΔpsbO*-PSII-M …….…..……..…58

Figure 2.8: Clear-Native PAGE of High Light Treated PSII Samples …..……...……...…60

Figure 2.9: Scan of CN PAGE in Figure 2.8 …….……...……..……60

Figure 2.10: Schematic of PSII Lifecycle Based on New Findings...……...……...…64

Figure 3.1: Repressing the Expression of the *psbD* gene in S6803 through CRISPRi ….……...…76

Figure 3.2: Adding the Theophylline-Responsive Riboswitch (RSW) Optimizes the Inducible Promoter System …….……...……...……78

Figure 3.3: Repressing the Expression of D2 and CP43 Encoding Genes by the Inducible CRISPRi-RSW System……...…….....……81

Figure 3.4: Recovery of the Expression of D2 and CP43 After Release of Repression by the CRISPRi-RSW System……...……...……84

Figure S3.1: Schematic Map of the Plasmid Containing the CRISPRi System ……...……...91

Figure S3.2: EYFP is Expressed by the P_{RhaBAD} Promoter Even Without Rhamnose …..…….92

Figure S3.3: Expression Levels of EYFP Driven by $P_{RhaBAD\text{-}RSW}$ ……...…93

Figure S3.4: Semiquantitative RT-PCR of Photosystem Genes ……...……..…94

Figure S3.5: Transcriptional Levels of Photosystem Genes Quantified by q-PCR .....……...…95

Figure 4.1: CRISPRi-RSW CtpA Construct …….……..110

Figure 4.2: RRCK Plasmid in ΔCtpA S6803 ……..…….……114

Figure 4.3: PnrsB Construct ……...……...……...…115
Figure 4.4: Pslr0701 CRISPRi-RSW CtpA ……...…...117
Figure S4.1: Plasmid Map of CRISPRi-RSW CtpA ……....…….…..123
Figure S4.2: Plasmid Map of RRCK…….……..….124
Figure S4.3: Plasmid Map of PnrsB CtpA.……..…….……125
Figure S4.4: Plasmid Map of Pslr0701 CRISPRi-RSW CtpA…….…….……126
Figure 5.1: OE27 Growth Outpaces WT S6803 in Fluctuating Light……...……..…..136
Figure 5.2: NPQ is Increased in the Psb27 Overexpression Strain….……...……..…..137
Figure 5.3: OE27 is Resilient to Light Adaptation Over 1000 Flashes..……...……..….139
Figure 5.4: Schematic of the Role of Psb27 in NPQ……..……...……..…145
Figure S5.1: *psbA1* and *psb27* Loci in WT, Del27, OE27, and Com27 Strains……...……152
Figure S5.2: Q_A Reoxidation Fit Residuals……...…….……...……153
Figure 6.1: 4-16% CN PAGE of Purified PSII……...……...……..….160
Figure 6.2: CN PAGE of S6803 Membranes and Purified PSII…….……...……161
Figure 6.3: Clear Native PAGE of CRISPRi-RSW D2 Samples……...……..…165
Figure 6.4: CN-PAGE of H47 PSII from CRISPRi-RSW D2 t=0 Samples……...…....….166
Figure A.1: CN-PAGE bands analyzed by Mass Spectrometry……..……...….....…..176

List of Tables

Table 1.1: PSII Assembly Factors 9

*Table S2.1: Proteins identified in the bands corresponding to Δ*O*-PSII-M, Δ*O*-NRC, and His47-NRC by LC-MS/MS following in-gel digestion of Δ*O*-PSII and His47-PSII samples……...65

*Table S2.2: Proteins identified by LC-MS/MS following in-solution digestion of Δ*O*-PSII-M...65

*Table S2.3: Proteins identified by LC-MS/MS following in-solution digestion of Δ*O*-NRC…...66

*Table S2.4:Inclusion list used to fragment intact LMM proteins in Δ*O*-PSII-M and Δ*O*-NRC during MS analysis 66

*Table S2.5: MS/MS fragment ions observed for intact LMM proteins in Δ*O*-PSII-M…….....66

Table S3.1: Nucleotide Sequences of Promoters and Genes in Chapter 3 96

Table S3.2: Strains and Plasmids Used in Chapter 3.....99

Table S3.3: List of Primers Used in Chapter 3 100

Table S4.1: Strains and Plasmids Used in Chapter 4.....127

Table S4.1: List of Primers Used in Chapter 4 128

Table 5.1: Fluorescence Decay Kinetics after a Single Actinic Flash.....141

Table 5.2: Fluorescence Decay Kinetics After 1000 Actinic Flashes 141

Table S5.1: Primers Used in Chapter 5.....153

*Table S5.2:QA Reoxidation Data for First, Last Flashes……..……..153

Table A.1: PSII related peptides found in H47_D.....177

Table A.2: PSII related peptides found in H47_M.....178

Table A.3: PSII related peptides found in H47_RC47 178

Table A.4: PSII related peptides found in H47_2 179

Table A.5: PSII related peptides found in H47_3 179

Table A.6: PSII related peptides found in H47_4 180

Table A.7: PSII related peptides found in H47_5 181

Table A.8: PSII related peptides found in H27_M.....181

Table A.9: PSII related peptides found in H47_2 182

Table A.10: PSII related peptides found in H47_3 182

Table A.11: Full peptide lists from all samples.....183

*Separate File

Acknowledgments

I would like to thank my research advisor, Professor Himadri Pakrasi, for his support and guidance throughout my graduate studies. Additionally, I would like to thank my committee members: Professors Joe Jez, Hani Zaher, Arpita Bose, Janice Robertson, and Bob Blankenship.

Much of my thesis work was done in collaboration with other members of the Pakrasi Lab. In particular, Dr. Daniel Weisz taught me how to grow cyanobacteria and to purify Photosystem II. He wrote the co-authored paper from which Chapter 2 was adapted. Dr. Deng Liu developed the CRISPR-inhibition system detailed in Chapter 3 and did much of the experimental work presented in that chapter. He is an endless source of wisdom into molecular engineering of cyanobacteria. I would also like to thank all of the Pakrasi Lab members for making the lab such an enjoyable place to come to work every day, and for providing their help, knowledge, and advice whenever asked.

I would like to thank my many collaborators, particularly Dr. Haijun Liu, who has provided indispensable advice and assistance with mass spectrometry experiments and performed much of the experimental work that became part of Chapter 5 and the Appendix.

I thank Professors Josef Komenda, Jian-Ren Shen, Gary Brudvig, Devaki Bhaya, Athina Zouni, Jan Kern, Marc Nowaczyk, Yasuhiro Kashino, and Haijun Liu for collegial discussions on the nomenclature of recently identified PSII assembly factors shown in Table 1.1.

Work in all of the chapters in this thesis was supported by the U.S. Department of Energy, Office of Basic Energy Sciences (Grant DE-FG02-99ER20350 to H.B.P.), and I was personally supported by the Washington University Imaging Sciences Pathway, training grant T32 EB014855 from the National Institute of Biomedical Imaging and Bioengineering, NIH.

Data in Chapter 2 and mass spectrometry data in the Appendix were collected with support from the Photosynthetic Antenna Research Center, an Energy Frontier Research Center funded by the U.S. DOE, Office of Basic Energy Sciences (Grant DE-SC 0001035 to H.B.P., R.E.B., and M.L.G.); NIH Grant P41GM103422 to M.L.G. and NIH Grant GM030498 to T.M.L. In Chapter 5, H.L. was partially supported by DOE grant (DE-FG02-07ER15902).

I would also like to thank my family for all of their support. To my parents for supporting and encouraging me throughout my education. To my mom, for always being there for me. My sister, Betsy, for always having an opinion. And to Nick, for all his support.

This thesis is dedicated to my father, Mark Johnson.

Virginia M. Johnson

Washington University in St. Louis

May 2022

ABSTRACT OF THE DISSERTATION

Assembly and Repair of Photosystem II

by

Virginia Mitchell Johnson

Doctor of Philosophy in Biology and Biomedical Sciences

Plant and Microbial Biology

Washington University in St. Louis, 2022

Himadri Pakrasi, Chair

Photosystem II is a light-driven water-plastoquinone oxidoreductase present in cyanobacteria, plants, and algae. It is the photosynthetic membrane protein complex responsible for oxidizing water into molecular oxygen, which is necessary for life as we know it. As a multi-subunit membrane-protein-pigment complex, Photosystem II undergoes a complex cycle of assembly, damage, and repair called the Photosystem II lifecycle. This cycle must consistently occur to maintain a high level of photosynthetic activity at the cellular level. Cyanobacteria, oxygenic photosynthetic bacteria, are frequently used as model organisms to study oxygenic photosynthetic processes due to their ease of growth and genetic manipulation. Cyanobacterial PSII structure and function have been well-characterized, but its life cycle is under active investigation. In this work, the state of the field is reviewed and various aspects of the PSII lifecycle are investigated in the cyanobacterium *Synechocystis* sp. PCC 6803. New tools for investigating the PSII lifecycle are developed and an outlook for how these tools may be used to better understand the PSII lifecycle is discussed. In Chapter 1, current knowledge and recent advances in studying the PSII lifecycle

in cyanobacteria are reviewed and discussed. Chapter 2 details the discovery and characterization of a chlorophyll-protein complex in the lifecycle of PSII. In Chapter 3, the development of a CRISPR-inhibition system to reversibly halt synthesis of PSII in *Synechocystis* sp. PCC 6803 by inhibiting expression of the PSII reaction center protein D2 is described. Chapter 4 discusses the development of a system to reversibly halt the PSII lifecycle mid-way by controlling expression of the PSII assembly factor CtpA, and Chapter 5 discusses findings about an overexpression strain of the PSII assembly factor Psb27. In Chapter 6, conclusions and future directions from each chapter, as well as additional data, are summarized.

Chapter 1

Introduction: Advances in the understanding of the Photosystem II Lifecycle in Cyanobacteria

This chapter was adapted with permission from an invited review article: Johnson, V.M. and Pakrasi, H.B (2022). Advances in the Understanding of the Lifecycle of Photosystem II. *Microorganisms.*

Chapter contributions: All figures in this chapter were generated by VMJ

1.1 Summary

Photosystem II is a light-driven water-plastoquinone oxidoreductase present in cyanobacteria, algae and plants. It produces the molecular oxygen and reducing equivalents to fix carbon that fuel life on Earth. As a multi-subunit membrane-protein-pigment complex, Photosystem II undergoes a dynamic cycle of synthesis, damage, and repair known as the Photosystem II lifecycle, to maintain a high level of photosynthetic activity at the cellular level. Cyanobacteria, oxygenic photosynthetic bacteria, are frequently used as model organisms to study oxygenic photosynthetic processes due to their ease of growth and genetic manipulation. Cyanobacterial PSII structure and function have been well-characterized, but its life cycle is under active investigation. In this review, advances in studying the life cycle of Photosystem II in cyanobacteria will be discussed, with a particular emphasis on new structural findings enabled by cryo-electron microscopy. These structural findings complement a rich and growing body of biochemical and molecular biology research into Photosystem II assembly and repair.

1.2 Introduction: Photosystem II and Cyanobacteria

Photosystem II (PSII) is a multi-subunit membrane protein complex located in the thylakoid membrane of plants, cyanobacteria, and algae. It is the enzyme responsible for splitting water, providing the oxygen that fuels life on earth as we recognize it. PSII performs this demanding photochemical reaction through sequential oxidation of a catalytic Mn_4CaO_5 cluster, which accumulates four oxidizing equivalents, cycling through five so-called S_n-states of oxidation (1) before oxidizing water in a concerted manner into molecular oxygen, producing four protons and four electrons in the process.

Cyanobacteria, oxygenic photosynthetic prokaryotes, have frequently been used as model organisms to study oxygenic photosynthetic processes due to their relatively fast growth and ease of genetic manipulation as compared with plants. For study of Photosystem II, three organisms have been widely utilized: *Synechocystis* sp. PCC 6803 (S6803), *Thermosynechococcus elongatus, and Thermosynechococcus vulcanus.* The mesophilic S6803 has been utilized for physiological studies and studies that require genetic manipulation of photosynthetic proteins, as it is a facultative heterotroph. The ability to grow S6803 on glucose allows for mutations and deletions to be made in genes necessary for photoautotrophic growth. PSII from either *T. elongatus* or *T. vulcanus,* thermophilic cyanobacterial strains, has been utilized for all high-resolution x-ray diffraction structures of PSII. Proteins from thermophilic organisms are often used for structural studies, as these proteins are more stable than their mesophilic homologs. Currently, due to these structural studies, our 'static' picture of active PSII is quite detailed. Atomic-resolution x-ray diffraction structures are available from *T. elongatus* and *T. vulcanus* (2-4) and x-ray free-electron laser (XFEL) technology and sample preparation have advanced to allow structural determination

of each of the Kok's S-states of the Mn_4CaO_5 cluster up to S_3 (5). Recently cryo-electron microscopy has enabled elucidation of the structure of active PSII from S6803 as well (6).

The biogenesis and repair (PSII life cycle) of this membrane-protein-pigment complex are under active investigation. The assembly of PSII, a 20+ subunit membrane-protein-pigment complex, is an intricate process, involving cellular localization of protein subunits, pigment insertion, subunit assembly and processing, and cofactor assembly. Furthermore, under normal

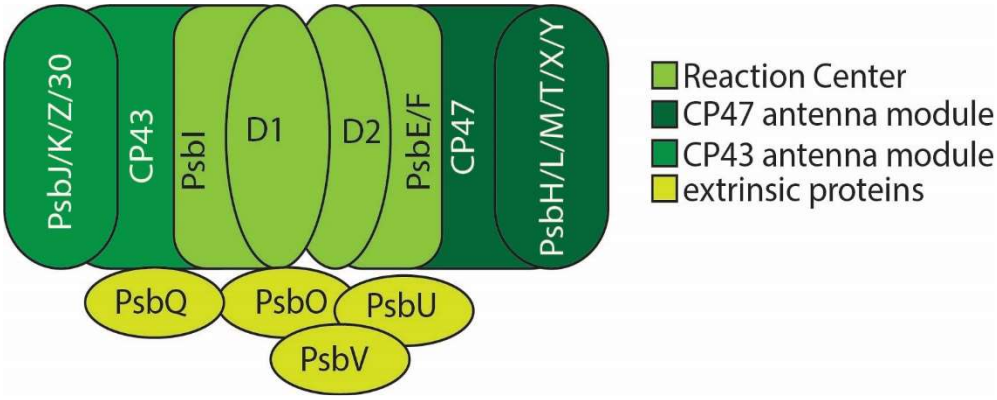

Figure 1.1 Schematic of PSII monomer (PSII forms a dimer *in vivo*). Modules are colored as indicated.

growth conditions, PSII is routinely damaged by reactive oxygen species that form within the protein and in its immediate vicinity (7, 8). To maintain a high level of photosynthetic activity, PSII must be repaired when damage occurs: damaged protein subunits must be replaced while the undamaged ones remain protected, and the biogenesis and repair processes must be coordinated within the cell.

In this review, I will discuss what is known about PSII assembly and repair in cyanobacteria, with an emphasis on new findings since the topic was last reviewed (9-17). Recently, the field has been greatly advanced by high-resolution cryo-electron microcopy (cryo-EM). Cryo-EM has enabled several PSII assembly intermediate structures to be solved, as well as

structures from the mesophilic S6803. These advances, in addition to other progress in the field, warrant a review and discussion.

1.3 PSII structure

Active PSII has a modular architecture, consisting of what can be described as four 'modules' (Figure 1.1). These include the membrane-intrinsic reaction center and chlorophyll-binding antennas, and the membrane-extrinsic thylakoid lumenal proteins. For a thorough discussion of the PSII structure-function relationship, see Müh et. al. (18).

The PSII reaction center (RC) consists of the D1 and D2 protein subunits. These subunits bind the P680 reaction center chlorophyll special pair as well as the primary electron transfer chain, including plastoquinones Q_A and Q_B and the catalytic Mn_4CaO_5 water-oxidizing complex (WOC or OEC for oxygen evolving center). The PsbI subunit and cytochrome b559 (made up of the PsbE and PsbF subunits) complete the reaction center. This reaction center complex has been isolated independently and is the smallest PSII sub-complex capable of charge separation (19-21). It is notable, however, that the CP43 subunit also provides a ligand to the manganese cluster, and so, while capable of charge separation, the reaction center proteins alone are not sufficient to bind the catalytic metal center or perform water-oxidizing chemistry.

The two antenna modules bind chlorophyll to absorb light energy that is funneled into the reaction center. These modules consist of the CP47 and CP43 proteins and their associated low molecular weight subunits (which are also referred to as low-molecular mass or small membrane-intrinsic subunits). PsbH, PsbL, PsbM, PsbT, PsbX, and PsbY bind to CP47. CP43 is associated with the small transmembrane subunits PsbJ, PsbK, and PsbZ and Psb30 (Ycf12). These low-

molecular weight subunits can be individually deleted without a loss of photosynthetic capacity, but stabilize and optimize PSII photochemistry, and some may play a regulatory role in the PSII life cycle.

The last module consists of membrane-extrinsic proteins which bind PSII on the lumenal side of the thylakoid membrane and contribute to PSII stability and optimal performance. This module is the site of greatest variability between and among plants, algae, and cyanobacteria (22-25).

In addition to the active PSII subunits, there are assembly factors and accessory proteins involved in *de novo* biogenesis and repair following photodamage that are not part of the active PSII complex. Knowledge of these is almost certainly not complete, and they number as many if not more than the protein subunits of the active complex. These proteins, especially the Psb27 subunit, have been the focus of much recent research effort.

1.4 PSII assembly

The first step in PSII assembly is the formation of two pre-complexes, one containing pD1 and PsbI (26-28), and one containing D2 and cytochrome b559 (27-31) (Figure 1.2A, cytochrome b559 is composed of PsbE and PsbF). pD1 is a pre-processed form of D1. It has a 16 amino acid c-terminal extension that is cleaved by the protease **CtpA** (see Table 1 for details on bolded proteins) prior to assembly of the Mn_4CaO_5 cofactor (32, 33). The pre-D1 complex consists of the pD1 subunit and the PsbI subunit, as well as numerous translation and assembly chaperones that aid in ribosome binding to the *psbA* (gene coding for D1) transcript, insertion of the nascent peptide into the membrane, and chlorophyll binding to the newly inserted peptide. One such protein, **PratA** is

involved with insertion of pD1 to the membrane and coordination of an initial Mn^{2+} ion to D1 (34-36). It is also thought to be associated with specialized regions of the thylakoid membrane where PSII is synthesized and repaired (34, 37). The deletion of PratA was shown to be deficient in c-terminal processing of D1 (36), leading to the hypothesis that it facilitates access of the c-terminal protease, CtpA, to pD1. The rubredoxin **RubA** (21, 31, 38) also binds to D1 prior to its association with D2 and has been implicated in protection from photodamage to the reaction center during PSII assembly in the green alga *Chlamydomonas reinhardtii* (38).

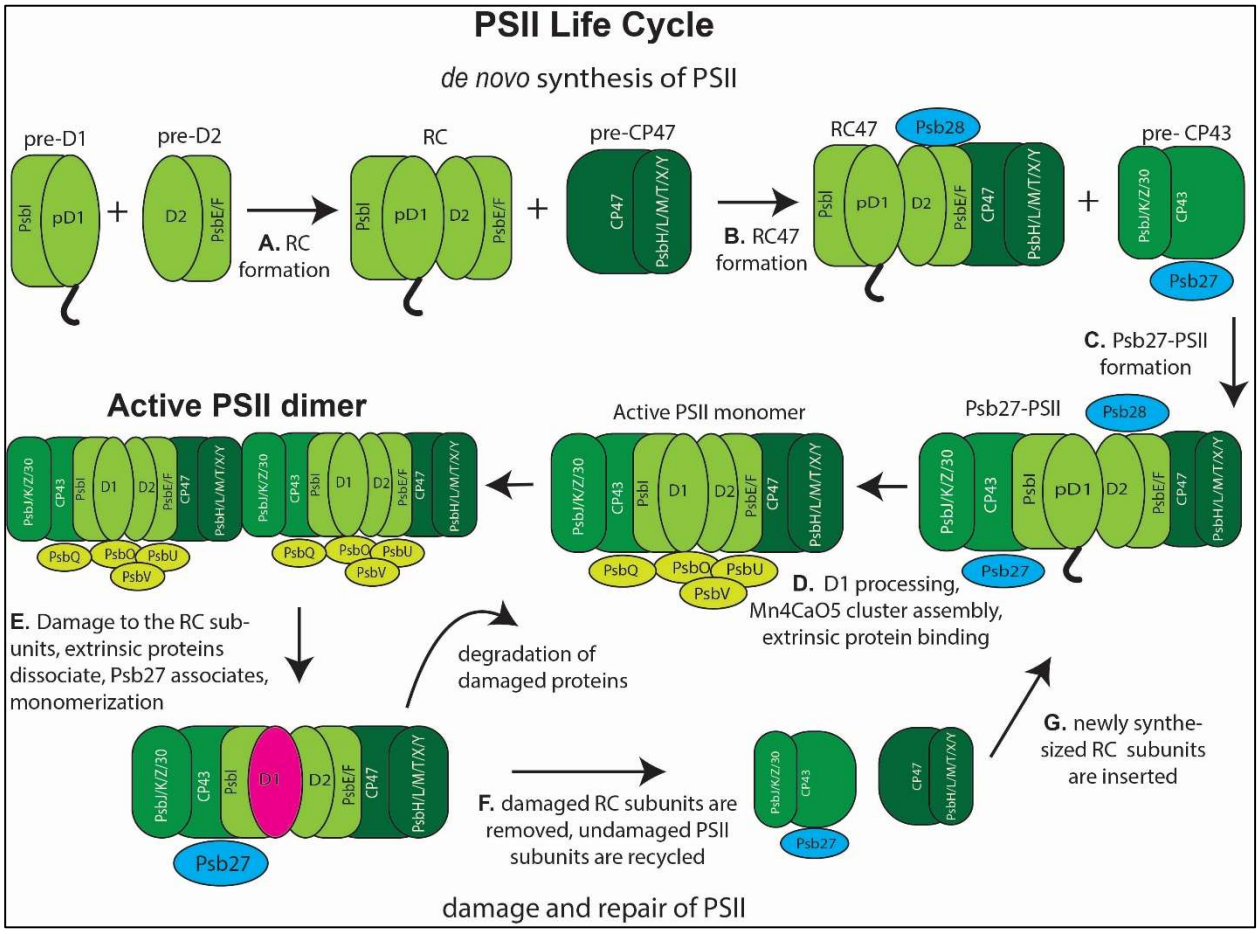

Figure 1.2 Schematic of PSII Life cycle, simplified. Not all accessory assembly chaperones are illustrated. (A)-(D) illustrate *de novo* synthesis, while (D)-(G) illustrate the repair cycle. A) The pre-D1 and pre-D2 complexes come together to form the RC module. B) RC and pre-CP47 modules come together to form the RC47 complex. Psb28 binds at this stage. C) Psb27-PSII forms from pre-CP43 module and RC47. D) Active PSII monomer is formed in a series of steps, which include processing of the D1 c-terminus, photo-assembly of the Mn_4CaO_5 cluster, and binding of extrinsic proteins PsbO, PsbV, PsbU, and PsbQ. The active PSII dimer forms following complete monomer assembly.

E) Following a photodamage event, the extrinsic proteins dissociate, Psb27 binds, and the dimer dissociates into monomers. F) Damaged subunits are removed and proteolytically degraded. G) Newly synthesized PSII subunits are inserted into recycled subunits to form a Psb27-PSII complex and the repair pathway re-joins the *de-novo* synthesis pathway.

Knoppova et al. found that Ycf39 and two HLIP family chlorophyll-binding proteins (39), **HliC** (ScpB) and **HliD** (ScpE), associate with D1 co-translationally (28). The HLIP (high light-inducible) family of proteins is a family of chlorophyll-binding proteins related to the light-harvesting complex family of proteins in eukaryotes. In cyanobacteria, they are known to bind chlorophyll and stabilize the assembly of chlorophyll-binding proteins (39). Ycf39, HliC and HliD form a complex which contains chlorophyll and β-carotene and is necessary for formation of the reaction center. This Ycf39-Hlip complex is also proposed to be involved in the delivery of recycled chlorophyll to newly synthesized D1 and protection from photodamage, as it interacts with the YidC/Alb3 membrane insertase complex as well as chlorophyll synthase (40, 41). **Pam68**, along with **Ycf48** and **Ycf39**, is implicated in co-translational insertion of chlorophyll to the reaction center proteins D1 and D2 (28, 37, 42, 43). Ycf48 is a soluble thylakoid membrane-associated protein associated with the D1 pre-complex and the reaction center complex (21, 27, 31, 44-48), and it contains a conserved arginine patch that mediates its binding to integral membrane proteins (47). These findings, in addition to the finding that apo-D1 does not accumulate (29), provide evidence that chlorophyll is co-translationally inserted into D1 as it is translocated into the membrane.

The reaction center forms (Figure 1.2A) (29, 30, 49, 50) when the D1 and D2 pre-complexes bind together. **PsbP** (CyanoP), which binds to the D2 pre-complex (51), is thought to be involved in RC formation (22, 52, 53). Recently, an RC complex was isolated from a strain of S6803 lacking CP47 that contains **PsbN** as well as the protein products of *slr0575* and *slr1470* (21). This complex is on the *de novo* synthesis pathway, as active PSII does not form in this strain.

However, a pre-D2 complex was also isolated from this strain which was associated with the protease FtsH2/FtsH3. This finding indicates that free-D2 levels are regulated by FtsH2/FtsH3.

The CP47 pre-complex contains PsbH, PsbL, PsbT, and possibly PsbM, PsbX, and PsbY (54, 55). The assembly factor **Psb35** also associates with the CP47 pre-complex and was shown to stabilize it and its association with **HliA** and **HliB** (ScpC and SpcD) (56). Psb35 itself is a homolog of the cyanobacterial one helix domain/HLIP family of proteins, but it is unknown whether it binds chlorophyll. Pam68, in addition to its association with the pre-D1 complex, has been shown to be involved with co-translational insertion of chlorophyll into CP47 prior to PsbH binding (57).

In the next step of PSII assembly, the RC joins together with the CP47 pre-complex to form the RC47 complex (Figure 1.2B). RC47 is bound by HliA/HliB and **Psb28** (55, 58-63). While the deletion mutant of Psb28 is photoautotrophic, it is deficient in recovery from photodamage at high temperature (62) and in light/dark conditions (63), indicating a role in stabilizing PSII intermediate assembly and repair complexes. Recent structural studies are consistent with the role of Psb28 as stabilizing assembly intermediates and protecting them from photodamage as well (discussed below).

Table 1.1 PSII assembly factors. Psb subunits are listed alphabetically, followed by additional assembly factors, listed alphabetically.

name	**function**	**S6803 locus tag**	**homolog in *A. thaliana* or *C. reinhardtii***	**phenotype of inactivation**	**citations**
PsbN	RC formation	smr0009	PsbN	Not significant in cyanobacteria	(21, 48, 64)
PsbP (cyanoP)	RC formation	sll1418	PsbP	Reduced O_2 evolution, severe phenotype in low $CaCl_2$	(22, 51, 53)

Psb27	Binds to CP43 during assembly	slr1645	Psb27	Defective photoactivation, sensitive to high light	(44, 65-73)
Psb28	Binds to CP47/cytochrome b559 in RC complex and Psb27-PSII complex. Alters electron transfer properties to increase photoprotection	sll1398	Psb28	Susceptible to photoinhibition in high light	(45, 55, 58, 59, 62, 63, 70, 72)
Psb29	Accumulation of FtsH2/FtsH3	sll1414	Psb29/Thf1	Impaired growth in high light, lower PSII efficiency	(74, 75)
Psb32	?	sll1390	TLP18.3	Sensitive to photoinhibition	(76-79)
Psb34	Binds to RC47 and PSII-I prior to activation	ssl1498	?	N/A	(60, 61, 80)
Psb35	Pre-CP47	ssl2148	?	Lower CP47 accumulation, faster bleaching in dark	(56)
CtpA	C-terminal processing of D1	slr0008	CtpA	not photosynthetic, no Mn_4CaO_5 cluster formation	(32, 65)
HliA	CP47 formation	ssl2542	?	Inhibited growth in high light	(39)
HliB	CP47 formation	ssr2595	?	Inhibited growth in high light	(39)
HliC/ScpB	Chlorophyll insertion	ssl1633	CAB/HLIP/ELIP family (counterpart of OHP1/OHP2)	Inhibited growth in high light, depleted chlorophyll	(21, 28, 39, 81, 82)
HliD/ScpE	Chlorophyll insertion	ssr1789	CAB/HLIP/ELIP family (counterpart to OHP1/OHP2)	Inhibited growth in high light, depleted chlorophyll	(21, 28, 39, 40, 81)

Pam68	Translation of CP47 and insertion of chlorophyll	sll0933	PAM68	Sensitive to high light, low temperature, fluctuating light	(42, 43, 57)
PratA	Mn^{2+} loading to D1 and D1 processing; thylakoid and plasma membrane connection	slr2048	LPA1	abnormal membranes, reduced PSII accumulation	(34-37)
RubA	D1/D2 assembly	slr2033	RBD1, *At1g54500*	Reduced PSII level and activity	(31, 83)
Slr0144-Slr0152	PSII assembly associated	slr0144-slr0152	?	Slower growth and lower PSII activity	(46, 84, 85)
Ycf39	Pre-D2 stabilization, chlorophyll insertion	slr0399	HCF244	Decrease in thermotolerance	(21, 28, 40, 43)
Ycf48	Insertion of D1, chlorophyll into D1, replacement of damaged D1, RC formation	slr2034	HCF136	Decrease in D1, PSII, increase in susceptibility to photoinhibition	(21, 27, 31, 43, 44, 53, 86)

RC47 binds to the CP43 pre-complex to form Psb27-PSII (Figure 1.2C). The CP43 pre-complex is composed of CP43, the **Psb27** assembly protein, PsbK, Psb30, and possibly PsbZ (54, 69, 71, 87). At this stage, the Psb27-PSII complex consists of most of the intrinsic membrane subunits of the PSII monomer. Sll0606 is involved in RC47 binding to CP43, and its deletion leads to a loss of photoautotrophy (88). **Psb34** (Ssl1498), an HLIP-family protein with no pigment binding site, is also suggested to be involved in RC47 binding to CP43 (60, 61, 80), as it is found in both RC47 and Psb27-PSII. This subunit is suggested to be involved in later stages of PSII assembly following HLIP dissociation, as it seems to compete for binding sites on PSII intermediates, and in its deletion strain HliA/HliB increase (80). It should be noted that, in (89), the subunit name Psb34 is assigned to a PSII subunit from *C. gracilis.* However, the sequence of that subunit was unable to

be determined. Therefore, I defer to more recent publications that have assigned Psb34 to a PSII subunit with a known sequence and gene, Tsl0063 in *T. elongatus* or Ssl1498 in S6803, which is in a different position in the PSII structure from the unknown subunit.

In Figure 1.2D, the Psb27-PSII complex becomes the active PSII monomer. This step is presumably shared between the assembly and repair stages of the PSII lifecycle and requires several events to occur, the order of which are still unclear. These include processing of the D1 c-terminus by CtpA, assembly of the Mn_4CaO_5 cofactor (photoactivation (90)-discussed further below), dissociation of Psb28, dissociation of Psb27 (65, 67, 70), and assembly of the extrinsic proteins PsbO, PsbU, PsbV, and PsbQ (also called cyanoQ) (23, 24, 91).

It is also unclear at what stage some subunits found in the active PSII complex bind. In particular, PsbJ has not been found in intermediate complexes. PsbJ binds near the Q_B site and possibly does not bind until after the formation of Psb27-PSII, when it triggers Psb28 dissociation. The ΔPsbJ mutant retains Psb28 in the active PSII monomer and accumulates more of a Psb27- and Psb28-bound PSII complex (72, 73). This mutant also has a much longer lifetime of reduced Q_A as compared to wild type. Therefore, it was proposed that PsbJ plays a role in forward electron flow from reduced Q_A to the plastoquinone pool (92, 93). This observations lead to the hypothesis that binding of PsbJ is a regulatory step in PSII formation.

In addition to the assembly factors described above, several genes have been implicated in PSII assembly and/or maintenance whose specific interactions with PSII have not been fully elucidated. The operon containing *slr0144-slr0152* (46, 84, 85) is implicated in optimal PSII function. Slr0151, in particular, is involved in D1 association with CP43 (84). Its deletion causes lower PSII levels, impaired D1 replacement, and reordering of the thylakoid membranes. **Psb32** is a transmembrane protein which was shown to minimize photodamage in cyanobacteria (77), but

how it does so is unknown. **Psb29** was shown to contribute to optimal PSII maintenance in both S6803 and *Arabidopsis thaliana* (74) by interacting with the FtsH2/FtsH3 protease, which removes damaged PSII subunits.

Following assembly of the active PSII dimer, higher-level organization of antenna complexes and photosystems into supercomplexes takes place. In cyanobacteria, this involves phycobilisome docking and PSI-PSII-Phycobilisome supercomplex formation (63, 94). These inter-complex molecular interactions are likely to be important for optimal cellular metabolism and highest photosynthetic activity.

1.5 PSII Repair

The repair cycle of Photosystem II is less well studied than PSII synthesis due to the inherently difficult nature of experimentally separating the two spatially and temporally overlapping processes. Deletion mutants of key photosynthetic proteins have been a crucial part of the elucidation of *de novo* PSII synthesis but are halted at certain points in the assembly of active PSII, and so never form active PSII to be damaged and subsequently repaired. What is well-established is that the lifetimes of PSII subunits are not all the same (81, 95). The D1 subunit is turned over most frequently, with a half-life of less than an hour in cyanobacteria. This is followed by D2 with a half-life of about 3 hours, CP43 at 6.5 hours and CP47 around 11 hours. Other proteins, such as Photosystem I subunits, are much more stable under normal conditions. The high turnover rate of D1, and the stark contrast in lifetime between the PSII subunits, is of considerable interest, as it implicates that D1 is removed selectively from PSII and replaced, while other PSII proteins remain stably bound together. How the cell signals that certain subunits are damaged and selectively replaced, or if certain subunits are constitutively replaced at different rates, is not known.

As for how the damaged protein subunits are selectively replaced, the assumption has been, due to the loose(r) association of the CP43 module and the existence of the RC47 complex, that the CP43 module dissociates, allowing for proteolytic degradation of D1 and re-synthesis and insertion at the RC47 level (50, 96). It is then assumed that, following re-insertion of D1 (and D2), that repair follows the same series of steps as *de novo* synthesis (Figure 1.2C-D). However, whether D1 insertion takes place at the dimer or monomer level has yet to be determined. Dimeric Psb27 has been identified (68, 73), and dimeric RC47, has been identified in a ΔCP43 mutant of S6803 (71), indicating that replacement of D1 may happen on the level of an RC47 dimer.

Recently, a complex that was a combination of the CP47 module and CP43 modules, called NRC for No Reaction Center (97), was isolated. Its abundance increased in the absence of protein synthesis and in high light, conditions that enhance PSII repair. This complex was hypothesized to be part of the repair cycle. Whether the CP47 and CP43 pre-complexes form a stable complex is disputed (98), but this is a topic that warrants further investigation.

1.6 Structural Advances in PSII research

Cryo-electron microscopy (cryo-EM) has brought forth some of the most significant advances in our understanding of PSII assembly and function in recent years. An area of intense research focus and progress has been elucidation of PSII structures from S6803 and also intermediate PSII complexes. Cryo-EM has provided an excellent means of studying such membrane protein complexes, as the technique does not require protein crystallization and allows for greater heterogeneity within samples.

Protein crystals of PSII from thermophilic cyanobacteria have been extensively characterized by x-ray crystallography. However, the structure of PSII from the mesophilic S6803, on which many physiological and biophysical studies have been performed, had been elusive. Gisriel et al. (6) solved the cryo-EM structure of a dimeric, active PSII from S6803 to 1.93Å. This structure is an important step in our understanding of PSII function, as many studies that model PSII based on biophysical data from S6803 assume that the structure and function is conserved between cyanobacterial species. However, as the authors note, there are significant differences in sequence between PSII from S6803 and the thermophilic organisms, and membrane proteins generally have different intermolecular interactions in mesophilic and thermophilic organisms. Importantly, this structure definitively shows the binding site of PsbQ, which was known to associate with active PSII in S6803 (76, 91), but had not been captured in any cyanobacterial structure. PsbQ is found associated with the most highly active isolated PSII complexes (91). However, the authors found that PsbQ binding does not affect the conformation of PSII when bound, hypothesizing that PsbQ stabilizes interactions of other membrane-extrinsic proteins with the PSII core, contributing to high activity in isolated complexes. This structure will certainly be of great value as a basis for computational studies to interpret the mechanism of PSII water-splitting, and the impact of point mutants in S6803.

Many intermediate PSII complexes have been isolated and characterized, but until recently, structural details of these complexes and their implications for PSII function were unknown. To better understand the role of Psb27 in the PSII life cycle, Huang et al. (73) isolated a dimeric Psb27-PSII complex from *T. vulcanus* and determined the cryo-EM structure to 3.78 Å. The complex was isolated from a deletion mutant of the PsbV subunit, as increased assembly and repair intermediates are present in that strain. This dimeric Psb27-PSII does not have extrinsic proteins

bound and it does not have an assembled Mn_4CaO_5 cluster. Psb27 binds to the E-loop of CP43, as evidenced previously by mass-spectrometry cross-linking data (69, 71, 87). The authors found that there are limited molecular interactions between Psb27 and CP43, indicating relatively weak binding of the assembly factor. They demonstrate that Psb27 prevents binding of PsbO and PsbV by sterically hindering their association sites, which is consistent with data that report that Psb27 binds to PSII in Psb27-PSII to allow photoassembly of the Mn_4CaO_5 cluster to occur by preventing binding of extrinsic subunits (67). Additionally, the authors did not find electron density corresponding to PsbY or PsbJ. PsbY has frequently been absent in PSII structures, which has been explained by the fact that it may easily dissociate due to its location on the periphery of PSII. PsbJ has been found to be absent in assembly intermediates that include Psb27. The authors suggest that structural perturbations from active PSII amongst subunits in Psb27-PSII may cause dissociation or prevent association of PsbJ.

The dimeric Psb27-PSII in (73) may be the same species previously described by Grasse et al. (68) that was isolated from cyanobacteria grown at low temperature and high light. Because that dimeric Psb27-PSII was proposed to be part of the PSII repair cycle (68), and because the c-terminus of the D1 protein was unable to be modeled beyond Arg334 (the final residue in the mature peptide is Ala344) in the cryo-EM structure, the authors hypothesized that D1 in their sample may be partially proteolytically degraded as part of the first step of PSII repair. To test this hypothesis, they analyzed D1 c-terminal peptides from their sample through mass spectrometry and found that about 1% are proteolytically cleaved prior to the c-terminal Alanine 344 of the mature peptide. This finding confirms that the invisibility of the D1 c-terminus in their structure is due to its flexibility in the absence of a bound manganese cluster and extrinsic proteins, and not because it is degraded. However, the small amount of proteolytically cleaved D1 subunits does not

preclude the possibility that this complex is part of the repair cycle, consisting of damaged PSII that has been partially disassembled. Interestingly, Zabret et al. (60) found that the D1 c-terminus of their monomeric Psb27-PSII structure (detailed below) can be modeled and is bound more closely to CP43 than in mature PSII. This difference may be due to a higher overall resolution of the structure, or to different stages of the complexes in the PSII lifecycle.

Zabret et al. (60) purified a PSII assembly intermediate containing Psb27, Psb28, and Psb34 from the ΔPsbJ mutant of *T. elongatus*, based on the observation from (72) that this mutant contains an increased amount of this intermediate sub-complex. They solved the cryo-EM structure of this complex, which they term PSII-I, to 2.9Å. In the structure, they found that the c-terminus of mature D1 is bound more closely to CP43 than in the active structure. They propose that this is to hold the D1 c-terminus in a conformation that favors photoassembly of the OEC. One cation was modeled at the OEC site, which could either be a Mn^{2+} or a Ca^{2+} cation. In addition to the difference in the D1 c-terminus described above, there is a slight discrepancy with the finding in the Huang Psb27-PSII structure in that they do not find a direct steric conflict with PsbO binding. PsbO has been found associated with Psb27-PSII in (69), so perhaps this also a difference between the dimeric, repair intermediate and the monomeric, Psb-28 bound complex which may be the state of PSII just prior to photoactivation on the assembly pathway. On the acceptor side of PSII, they find that the D1 DE loop interaction with CP47 in active PSII is disturbed by Psb28 binding and that the CP47 c-terminus forms a β-sheet with Psb28. In addition, the Q_B binding site and the non-heme iron hydrogen bond network are altered from the active PSII structure, resulting in the absence of the bicarbonate ion and Q_B. They found that these changes lead to changes in the PSII electron transfer pathway that reduce singlet O_2 formation. These findings suggest that Psb28 binds to PSII during its assembly to protect PSII from photodamage. Interestingly, Eaton-Rye found that

PsbT interacts with the D1 DE loop in active PSII, and PsbT deletion causes increased photodamage (99-101), indicating a regulatory role of this loop in the repair cycle.

Xiao et al. also solved the structure of a Psb28 bound-PSII, as well as a Psb28-bound RC47 (61), to 3.14 Å resolution. They used a His-tagged Psb28 to isolate PSII intermediate complexes from both a ΔPsbV mutant and WT strain of *T. vulcanus*. Both the 28-PSII and the RC47 structure have Psb28, Psb34, and an unknown subunit bound that they were not able to model. This additional subunit was not found in the similar PSII-I structure in (60), but may be a second Psb34 copy. The authors found that Psb28 and Psb34 associate similarly to in the PSII-I structure, and consistent with the Zabret paper, there are changes in the quinone binding sites and H-bond network around the non-heme iron, with absence of the bicarbonate. They also observed a similar shift of the D1 c-terminus and increased flexibility. CP43, and the CP43 module as a whole is also shifted relative to its position in active PSII, consistent with (60, 102), which the authors describe as a looser attachment. Additionally, alpha helices in D1, D2, and CP47 are changed to loops near Psb28 binding on cytoplasmic side. Overall, the PSII-I and Psb28-PSII structures are consistent with the binding position of Psb28 determined by Weisz et al. (58), although the precise attachment is slightly altered. Intriguingly, the WT 28-PSII structure has Psb27 bound, but ΔPsbV does not. This finding led the authors to propose that Psb27 associates following Psb28 dissociation. However, it is not consistent with multiple findings that CP43 and Psb27 associate with one another prior to joining with RC47. PsbJ and PsbY were not found in either structure.

Xiao (61) and Zabret (60) both observed a distorted Q_B binding pocket and bicarbonate and heme iron binding site in the Psb28-bound PSII. These structures are consistent with the position of Psb28 that was identified by (58), and they find that, as proposed by Weisz et. al., the donor side of PSII is perturbed by the presence of Psb28. Discrepancies between the crosslinking

data and the structure could also have resulted from the fact that the location in the crosslinking paper was modeled off the active structure, while it was found that Psb28 binding causes significant structural changes in the acceptor (cytoplasmic) side of PSII. These structural alterations may slow electron transfer to the plastoquinone pool and change the midpoint redox potential of $Q_A/Q_A^{-\bullet}$, as proposed by Brinkert et al. (103), who showed that bicarbonate loss alters the *Em* of $Q_A/Q_A^{-\bullet}$ to a more positive value. This positive shift is predicted to increase the potential between $P_{680}^{+\bullet}/Q_A^{-\bullet}$ and $P_{680}^{+\bullet}/Pheo^{-\bullet}$, which may favor direct recombination between $P_{680}^{+\bullet}/Q_A^{-\bullet}$ decrease back-reactions through $P_{680}^{+\bullet}/Pheo^{-\bullet}$ recombination, reducing the probability of the formation of an RC triplet state. Overall, this may lead to a decrease in the production of singlet O_2, consistent with the findings in Zabret et. al. Additionally, photoactivation is also thought to decrease the potential of $Q_A/Q_A^{-\bullet}$ (104), so intermediate complexes such as the Psb28-bound PSII structures lacking OEC would also be protected by a similar mechanism.

Higher levels of Psb27-PSII are also associated with higher NPQ (105). This finding would be consistent with an overall model where Psb27 and Psb28 binding to PSII intermediates induces structural perturbations that protect the not-fully-assembled PSII from photodamage. An unanswered question in the role of Psb27 is that of Psb27 N-terminal lipidation and how it relates to the interaction between PSII and Psb27. Nowaczyk and coworkers initially suggested that Psb27 had an n-terminal lipid modification based on the presence of a lipobox motif next to the N-terminal cysteine of the mature peptide and confirmed a lipid attachment through mass spectrometry (66). Recently, more focused mass spectrometry has provided a more detailed picture of the lipid attachment (106). However, this lipid attachment was not resolved in the recent structures of Psb27-PSII, so how it mediates attachment of Psb27 to the thylakoid membrane and/or to PSII remains unclear.

1.7 Advances in Photoactivation

Assembly of the Mn_4CaO_5 cluster takes place through sequential binding and oxidation of Mn^{2+} ions, as well as binding of Ca^{2+} and protonation of water, using the same photochemical machinery for charge separation as active PSII. Photoactivation must take place during both *de novo* PSII assembly and repair, when the D1 subunit is replaced. This phenomenon has long been known and studied (12, 90, 104, 107-110), but its exact mechanism is unclear. Recent PSII structures and studies have begun to describe this process in greater detail.

In one such structural study, Zhang et al. (111) solved the structure of apo-PSII (PSII without an intact Mn_4CaO_5 cluster) from *T. elongatus* using x-ray crystallography and found that it aligned closely to the active PSII structure, but without electron density corresponding to the OEC. The authors in this study intentionally removed the Mn_4CaO_5 cluster by treating crystals with ammonium hydroxide and EDTA, but the extrinsic PSII subunits were maintained. They propose that the lack of structural alteration of the OEC ligands in its absence means that the protein scaffold is already 'pre-organized' prior to Mn_4CaO_5 cluster assembly, and significant rearrangement does not need to take place for it to form. However, in another study, Gisriel et al. solved a structure of apo-PSII from S6803 (112) using cryo-EM and did find structural differences in the soluble domain of CP43 and the D1 c-terminus between their structure and that of active PSII. It is likely that this structure from S6803 lost the Mn_4CaO_5 cluster during sample preparation, unlike the Psb28-and Psb27-PSII structures described above, which are most likely assembly complexes. However, the study does provide insight into photoactivation, as the S6803 apo-PSII lacks the OEC and extrinsic PSII subunits and CP43 is shifted as in (60, 61, 73). These features suggest that the donor side of PSII does have some structural flexibility prior to photoactivation,

and that rearrangement needs to take place during the assembly of the OEC. The S6803 apo-PSII structure is also lacking PsbY, PsbJ, and PsbZ, although whether they were lost in sample preparation is unknown. It is possible that the flexibility observed in the S6803 apo-PSII is not observed in the apo-PSII crystal structure due to the constraints of the crystals, as the OEC was removed after crystallization.

Computational modeling can complement structural studies and provide insight into structural perturbations and dynamics. Narzi et al. used molecular dynamics simulation to find that structural rearrangements do need to occur after the first Mn^{2+} oxidation (113) for the manganese binding sites to form in apo-PSII. Their results are in agreement with the flexible nature of the D1 c-terminus found in (60, 73, 112), and they propose that alternate protonation of OEC-liganding residues contributes to flexibility in D1 c-terminus as well. These results, together with Gisriel et al., also suggest that the structure solved by Zhang et al. was constrained by crystal contacts and does not represent the native structure of PSII prior to photoactivation. This study also agrees with a wealth of biophysical data that suggests a structural rearrangement of OEC ligands takes place during photoactivation (90, 104, 107-110, 114).

The conditions necessary for optimal photoassembly, or photoactivation, of the manganese cluster have been the focus of recent work (114-116). Photoactivation requires Ca^{2+} and is known to have a much lower quantum efficiency than photochemistry in active PSII leading to O_2 evolution. Low quantum efficiency of photoactivation has been explained by need for rearrangement of the ligand shell after the first Mn^{2+} oxidation, but also the need for acceptor side rearrangement to downshift $Q_A/Q_A^{-\bullet}$ potential (104). Cl^- is necessary for photoactivation as well. Vinyard and coworkers found, by tracking photoactivation using EPR, that it tunes the pK_a of residues around the OEC site, allowing for necessary deprotonation (115). In another recent study,

Avramov et. al. examined an over-expression strain of the Psb27 protein (OE27), as well as a deletion mutant of the PsbO protein for photoactivation. They found that, while both the ΔPsbO and OE27 strains had an increased optimal ratio of Ca^{2+}/Mn^{2+}, the quantum efficiency of photoactivation also increased in OE27, implicating a role for Psb27 beyond just blocking binding of extrinsic proteins as previously proposed (67). The authors suggest Psb27 has a role in maintaining an optimal ligand configuration for photoassembly, in agreement with the altered CP43/D1 c-terminal conformation in (60, 61). How these results relate to the findings that Psb28- and Psb27- bound PSII have altered photochemistry, and when these subunits dissociate during the process, is yet to be determined.

1.8 Use of CRISPR and CRISPR inhibition for study of photosynthetic protein complexes

CRISPR and its associated techniques have emerged as powerful tools to manipulate genes and gene expression in cyanobacteria (117-121). Specifically in cyanobacteria, the nucleases Cas9 and Cas12a (Cpf1), and their DNase-dead counterparts have been used to great effect to efficiently make modifications. While these techniques are of great interest for metabolic engineering of cyanobacteria, they also have potential to expedite and enable basic photosynthesis research. One advantage of CRISPR editing over more traditional genetic manipulation is that it is markerless, enabling successive mutations to be made without the need for multiple antibiotic resistance cassettes to be stacked or cells to be maintained on multiple antibiotics. Additionally, CRISPR editing allows for an expedited segregation process, which is an important consideration in an organism that has multiple genome copies.

Of recent interest in terms of Photosystem II research is CRISPR-inhibition, whereby a DNase-dead CRISPR-associated protein is targeted to a specific genomic locus (or loci) to block transcription. CRISPRi has emerged as a strategy to selectively inhibit photosynthetic genes. CRISPRi enables a particularly intriguing strategy for manipulation of photosynthetic proteins due to its reversibility and its potential to multiplex targets through incorporation of multiple guide RNAs (122, 123). In one example of this type of strategy, DNase-dead Cpf1 was introduced into *S. elongatus* UTEX 2973 as part of a CRISPRi system to target Photosystem I for inhibition (124). Additionally, a plasmid-based CRISPRi system was introduced into S6803 (125) to inhibit expression of the D1 protein of photosystem II and Liu et al. (126) introduced a reversible CRISPRi system into S6803 by using a Rhamnose-theophylline inducible promoter system. This CRISPRi system was able to almost completely knock out PSII by targeting the D2 (*psbD* gene) protein, and it was fully reversible. These inhibition strategies introduce a new paradigm for study of membrane protein complexes, in particular PSII, whereby its assembly can be reversibly halted at varying stages, depending on the gene targeted for inhibition.

1.9 Conclusions

A common point that has been further emphasized in recent studies is that subtle perturbations in PSII structure by either assembly factors or low-molecular-weight peripheral subunits have a significant impact on photochemistry. These perturbations can lead to overall efficiencies on a cellular level by protecting assembly intermediates from photodamage when necessary and optimizing photochemistry in active PSII. Along that theme, the impact of detergent solubilization on our current understanding of PSII function is not well described. A few alternate solubilization techniques that may preserve a more native membrane lipid arrangement, including lipid/protein

nanodiscs (127-129) and SMALPs (130, 131) have been explored, but it is an area that warrants more attention.

A more complete structural and functional picture of the lifecycle of PSII is coming into focus, but there are most likely PSII assembly and repair factors that have not yet been identified. Open questions remain about several aspects of the lifecycle. These aspects include the mechanism of cofactor insertion into nascent PSII subunits and what signals that PSII is damaged and should be repaired (132, 133). Additionally, some PSII assembly factors have been identified whose function has yet to be fully determined. Study of these questions will lend insight into PSII function and membrane protein complex assembly more broadly.

While knowledge about structures of isolated PSII intermediates has been expanded in recent studies, an open area of investigation is cellular localization of PSII biogenesis and repair in cyanobacteria. The topic of localization of PSII biogenesis and repair is related to the question of the structure of the cyanobacterial membrane system. Liberton et al. (134) found through serial sectioning and electron tomography that the thylakoids form a completely independent membrane system from the plasma membrane. However, the thylakoid sheets do converge at certain cellular locations near the plasma membrane (135-138). Whether these convergence zones are connected to the plasma membrane is debated, but they have been proposed to be the site of PSII biogenesis and/or repair (34). An earlier study determined that reaction center proteins were localized to the plasma membrane of cyanobacteria, indicating that certain PSII proteins are inserted to the plasma membrane and then trafficked to the thylakoid to regulate PSII assembly, but that has since been disputed (139, 140). In plants, damaged PSII migrates to the thylakoid stroma lamellae from the grana stacks to be repaired (13), and the 'thylakoid convergence zones' are thought to be the location of an analogous process. Supporting this hypothesis is the fact that ribosomes are found

at these sites, while phycobilisomes are not (138). PratA, which binds to pD1, is found to be associated with an intermediate density membrane fraction between the plasma membrane and the thylakoid membrane (34-37). The membrane fraction which contains PratA was proposed to be the site of the 'thylakoid convergence zones' (also called variously biogenesis centers, thylakoid centers, or thylapses (138)), as it also contained other PSII and chlorophyll biogenesis proteins. These studies were performed by separating membrane fractions by density, but an alternative approach was recently taken by Dahlgren et al. (141), which is a promising avenue for this type of investigation. The authors of that study utilized a proximity-based proteomics approach to identify components of different intracellular compartments. In this case, they used the APEX2 protein, a modified ascorbate peroxidase that catalyzes a reaction between biotin-phenol (BP) and hydrogen peroxide (H_2O_2) to create a BP radical that covalently attaches to proteins, fused to a known thylakoid lumen protein, PsbU, to selectively biotinylate proteins localized in the thylakoid lumen of *Synechococcus* sp. PCC 7002. Approaches such as this have great potential for answering questions of cellular localization and reinforcing findings by other methods.

Atomic force microscopy and hyperspectral confocal (142) studies of thylakoid fragments from *Thermosynechococcus elongatus*, *Synechococcus* sp. PCC 7002, and *Synechocystis* sp PCC 6803 suggest that there are defined regions of the thylakoids that are differentiated by the arrangement of photosynthetic and respiratory complexes in cyanobacteria. This finding is corroborated by Casella et al. (143) in *Synechococcus elongatus* PCC 7942. The purpose of these differentiated membrane regions is yet to be determined, but the arrangement certainly has an impact on diffusion of photosynthetic reactants and intermediates, such as quinones, as well as the spatial organization of PSII biogenesis and repair. However, it should also be noted that thylakoid arrangement varies drastically among cyanobacterial species (144), and so if and how these

findings apply generally to other cyanobacteria is also unclear. Understanding the relative mobility of protein complexes and supercomplexes and assembly intermediates and their coordination will be key to understanding the purpose of these processes. Further advances in imaging, specifically electron microscopy correlated with light microscopy, and cryo-electron tomography or cryo-TEM on sections of cells, will shed light on this issue. One example of the potential of this kind of study is the *in-situ* structure of a phycobilisome-PSII supercomplex from red algae (145). New technologies, and new applications of technologies, will shed insight into our knowledge of PSII assembly, the process of membrane protein complex assembly more generally, and photosynthetic organisms on a systems level.

1.10 References

1. Kok B, Forbush B, & McGloin M (1970) Cooperation of charges in photosynthetic O2 evolution-I. A linear four step mechanism. *Photochem Photobiol* 11(6):457-475.
2. Umena Y, Kawakami K, Shen J-R, & Kamiya N (2011) Crystal structure of oxygen-evolving photosystem II at a resolution of 1.9 Å. *Nature* 473(7345):55-60.
3. Suga M*, et al.* (2015) Native structure of photosystem II at 1.95 A resolution viewed by femtosecond X-ray pulses. *Nature* 517(7532):99-103.
4. Young ID*, et al.* (2016) Structure of photosystem II and substrate binding at room temperature. *Nature* 540(7633):453-457.
5. Kern J*, et al.* (2018) Structures of the intermediates of Kok's photosynthetic water oxidation clock. *Nature* 563(7731):421-425.
6. Gisriel CJ*, et al.* (2022) High-resolution cryo-electron microscopy structure of photosystem II from the mesophilic cyanobacterium, Synechocystis sp. PCC 6803. *Proc Natl Acad Sci U S A* 119(1).
7. Vass I (2012) Molecular mechanisms of photodamage in the Photosystem II complex. *Biochim Biophys Acta* 1817(1):209-217.
8. Zavafer A (2021) A theoretical framework of the hybrid mechanism of photosystem II photodamage. *Photosynth Res* 149(1-2):107-120.
9. Nixon PJ, Michoux F, Yu J, Boehm M, & Komenda J (2010) Recent advances in understanding the assembly and repair of photosystem II. *Ann Bot* 106(1):1-16.
10. Komenda J, Sobotka R, & Nixon PJ (2012) Assembling and maintaining the Photosystem II complex in chloroplasts and cyanobacteria. *Curr Opin Plant Biol* 15(3):245-251.

11. Nickelsen J & Rengstl B (2013) Photosystem II assembly: from cyanobacteria to plants. *Annu Rev Plant Biol* 64:609-635.

12. Vinyard DJ, Ananyev GM, & Dismukes GC (2013) Photosystem II: the reaction center of oxygenic photosynthesis. *Annu Rev Biochem* 82:577-606.

13. Jarvi S, Suorsa M, & Aro EM (2015) Photosystem II repair in plant chloroplasts--Regulation, assisting proteins and shared components with photosystem II biogenesis. *Biochim Biophys Acta* 1847(9):900-909.

14. Weisz DA, Gross ML, & Pakrasi HB (2016) The Use of Advanced Mass Spectrometry to Dissect the Life-Cycle of Photosystem II. *Front Plant Sci* 7:617.

15. Heinz S, Liauw P, Nickelsen J, & Nowaczyk M (2016) Analysis of photosystem II biogenesis in cyanobacteria. *Biochim Biophys Acta* 1857(3):274-287.

16. Theis J & Schroda M (2016) Revisiting the photosystem II repair cycle. *Plant Signal Behav* 11(9):e1218587.

17. Barber J (2016) 'Photosystem II: the water splitting enzyme of photosynthesis and the origin of oxygen in our atmosphere'. *Q Rev Biophys* 49:e14.

18. Muh F & Zouni A (2020) Structural basis of light-harvesting in the photosystem II core complex. *Protein Sci* 29(5):1090-1119.

19. Nanba O & Satoh K (1987) Isolation of a photosystem II reaction center consisting of D-1 and D-2 polypeptides and cytochrome b-559. *Proc Natl Acad Sci U S A* 84(1):109-112.

20. Ikeuchi M & Inoue Y (1988) A new photosystem II reaction center component (4.8 kDa protein) encoded by chloroplast genome. *FEBS Lett* 241(1-2):99-104.

21. Knoppova J*, et al.* (2022) Assembly of D1/D2 complexes of photosystem II: binding of pigments and a network of auxiliary proteins. *Plant Physiol*.

22. Thornton LE*, et al.* (2004) Homologs of plant PsbP and PsbQ proteins are necessary for regulation of photosystem ii activity in the cyanobacterium Synechocystis 6803. *Plant Cell* 16(8):2164-2175.

23. Roose JL, Wegener KM, & Pakrasi HB (2007) The extrinsic proteins of Photosystem II. *Photosynth Res* 92(3):369-387.

24. Bricker TM, Roose JL, Fagerlund RD, Frankel LK, & Eaton-Rye JJ (2012) The extrinsic proteins of Photosystem II. *Biochim Biophys Acta* 1817(1):121-142.

25. Gisriel CJ & Brudvig GW (2022) Comparison of PsbQ and Psb27 in photosystem II provides insight into their roles. *Photosynth Res*.

26. Dobakova M, Tichy M, & Komenda J (2007) Role of the PsbI protein in photosystem II assembly and repair in the cyanobacterium Synechocystis sp. PCC 6803. *Plant Physiol* 145(4):1681-1691.

27. Komenda J*, et al.* (2008) The cyanobacterial homologue of HCF136/YCF48 is a component of an early photosystem II assembly complex and is important for both the efficient assembly and repair of photosystem II in Synechocystis sp. PCC 6803. *J Biol Chem* 283(33):22390-22399.

28. Knoppova J*, et al.* (2014) Discovery of a chlorophyll binding protein complex involved in the early steps of photosystem II assembly in Synechocystis. *Plant Cell* 26(3):1200-1212.

29. Muller B & Eichacker LA (1999) Assembly of the D1 precursor in monomeric photosystem II reaction center precomplexes precedes chlorophyll a-triggered accumulation of reaction center II in barley etioplasts. *Plant Cell* 11(12):2365-2377.

30. Komenda J*, et al.* (2004) Accumulation of the D2 protein is a key regulatory step for assembly of the photosystem II reaction center complex in Synechocystis PCC 6803. *J Biol Chem* 279(47):48620-48629.

31. Kiss E*, et al.* (2019) A Photosynthesis-Specific Rubredoxin-Like Protein Is Required for Efficient Association of the D1 and D2 Proteins during the Initial Steps of Photosystem II Assembly. *Plant Cell* 31(9):2241-2258.

32. Anbudurai PR, Mor TS, Ohad I, Shestakov SV, & Pakrasi HB (1994) The ctpA gene encodes the C-terminal processing protease for the D1 protein of the photosystem II reaction center complex. *Proc Natl Acad Sci U S A* 91(17):8082-8086.

33. Komenda J*, et al.* (2007) Cleavage after residue Ala352 in the C-terminal extension is an early step in the maturation of the D1 subunit of Photosystem II in Synechocystis PCC 6803. *Biochim Biophys Acta* 1767(6):829-837.

34. Stengel A*, et al.* (2012) Initial steps of photosystem II de novo assembly and preloading with manganese take place in biogenesis centers in Synechocystis. *Plant Cell* 24(2):660-675.

35. Schottkowski M*, et al.* (2009) Interaction of the periplasmic PratA factor and the PsbA (D1) protein during biogenesis of photosystem II in Synechocystis sp. PCC 6803. *J Biol Chem* 284(3):1813-1819.

36. Klinkert B*, et al.* (2004) PratA, a periplasmic tetratricopeptide repeat protein involved in biogenesis of photosystem II in Synechocystis sp. PCC 6803. *J Biol Chem* 279(43):44639-44644.

37. Rengstl B, Oster U, Stengel A, & Nickelsen J (2011) An intermediate membrane subfraction in cyanobacteria is involved in an assembly network for Photosystem II biogenesis. *J Biol Chem* 286(24):21944-21951.

38. Garcia-Cerdan JG*, et al.* (2019) A thylakoid membrane-bound and redox-active rubredoxin (RBD1) functions in de novo assembly and repair of photosystem II. *Proc Natl Acad Sci U S A* 116(33):16631-16640.

39. Komenda J & Sobotka R (2016) Cyanobacterial high-light-inducible proteins--Protectors of chlorophyll-protein synthesis and assembly. *Biochim Biophys Acta* 1857(3):288-295.

40. Chidgey JW*, et al.* (2014) A cyanobacterial chlorophyll synthase-HliD complex associates with the Ycf39 protein and the YidC/Alb3 insertase. *Plant Cell* 26(3):1267-1279.

41. Ossenbuhl F, Inaba-Sulpice M, Meurer J, Soll J, & Eichacker LA (2006) The synechocystis sp PCC 6803 oxa1 homolog is essential for membrane integration of reaction center precursor protein pD1. *Plant Cell* 18(9):2236-2246.

42. Armbruster U*, et al.* (2010) The Arabidopsis thylakoid protein PAM68 is required for efficient D1 biogenesis and photosystem II assembly. *Plant Cell* 22(10):3439-3460.

43. Knoppova J & Komenda J (2019) Sequential deletions of photosystem II assembly factors Ycf48, Ycf39 and Pam68 result in progressive loss of autotrophy in the cyanobacterium Synechocystis PCC 6803. *Folia Microbiol (Praha)* 64(5):683-689.

44. Jackson SA, Hervey JR, Dale AJ, & Eaton-Rye JJ (2014) Removal of both Ycf48 and Psb27 in Synechocystis sp. PCC 6803 disrupts Photosystem II assembly and alters Q(A)(-) oxidation in the mature complex. *FEBS Lett* 588(20):3751-3760.

45. Mabbitt PD, Wilbanks SM, & Eaton-Rye JJ (2014) Structure and function of the hydrophilic Photosystem II assembly proteins: Psb27, Psb28 and Ycf48. *Plant Physiol Biochem* 81:96-107.

46. Rast A, Rengstl B, Heinz S, Klingl A, & Nickelsen J (2016) The Role of Slr0151, a Tetratricopeptide Repeat Protein from Synechocystis sp. PCC 6803, during Photosystem II Assembly and Repair. *Front Plant Sci* 7:605.

47. Yu J*, et al.* (2018) Ycf48 involved in the biogenesis of the oxygen-evolving photosystem II complex is a seven-bladed beta-propeller protein. *Proc Natl Acad Sci U S A* 115(33):E7824-E7833.

48. Plochinger M, Schwenkert S, von Sydow L, Schroder WP, & Meurer J (2016) Functional Update of the Auxiliary Proteins PsbW, PsbY, HCF136, PsbN, TerC and ALB3 in Maintenance and Assembly of PSII. *Front Plant Sci* 7:423.

49. Vermaas WF, Ikeuchi M, & Inoue Y (1988) Protein composition of the photosystem II core complex in genetically engineered mutants of the cyanobacterium Synechocystis sp. PCC 6803. *Photosynth Res* 17(1-2):97-113.

50. van Wijk KJ, Roobol-Boza M, Kettunen R, Andersson B, & Aro EM (1997) Synthesis and assembly of the D1 protein into photosystem II: processing of the C-terminus and identification of the initial assembly partners and complexes during photosystem II repair. *Biochemistry* 36(20):6178-6186.

51. Knoppova J, Yu J, Konik P, Nixon PJ, & Komenda J (2016) CyanoP is Involved in the Early Steps of Photosystem II Assembly in the Cyanobacterium Synechocystis sp. PCC 6803. *Plant Cell Physiol* 57(9):1921-1931.

52. Suorsa M*, et al.* (2004) Protein assembly of photosystem II and accumulation of subcomplexes in the absence of low molecular mass subunits PsbL and PsbJ. *Eur J Biochem* 271(1):96-107.

53. Jackson SA & Eaton-Rye JJ (2015) Characterization of a Synechocystis sp. PCC 6803 double mutant lacking the CyanoP and Ycf48 proteins of Photosystem II. *Photosynth Res* 124(2):217-229.

54. Boehm M*, et al.* (2011) Investigating the early stages of photosystem II assembly in Synechocystis sp. PCC 6803: isolation of CP47 and CP43 complexes. *J Biol Chem* 286(17):14812-14819.

55. Boehm M*, et al.* (2012) Subunit composition of CP43-less photosystem II complexes of Synechocystis sp. PCC 6803: implications for the assembly and repair of photosystem II. *Philos Trans R Soc Lond B Biol Sci* 367(1608):3444-3454.

56. Pascual-Aznar G*, et al.* (2021) Psb35 Protein Stabilizes the CP47 Assembly Module and Associated High-Light Inducible Proteins during the Biogenesis of Photosystem II in the Cyanobacterium Synechocystis sp. PCC6803. *Plant Cell Physiol* 62(1):178-190.

57. Bucinska L*, et al.* (2018) The Ribosome-Bound Protein Pam68 Promotes Insertion of Chlorophyll into the CP47 Subunit of Photosystem II. *Plant Physiol* 176(4):2931-2942.

58. Weisz DA, *et al.* (2017) Mass spectrometry-based cross-linking study shows that the Psb28 protein binds to cytochrome b559 in Photosystem II. *Proc Natl Acad Sci U S A* 114(9):2224-2229.

59. Dobakova M, Sobotka R, Tichy M, & Komenda J (2009) Psb28 protein is involved in the biogenesis of the photosystem II inner antenna CP47 (PsbB) in the cyanobacterium Synechocystis sp. PCC 6803. *Plant Physiol* 149(2):1076-1086.

60. Zabret J, *et al.* (2021) Structural insights into photosystem II assembly. *Nat Plants* 7(4):524-538.

61. Xiao Y, *et al.* (2021) Structural insights into cyanobacterial photosystem II intermediates associated with Psb28 and Tsl0063. *Nat Plants* 7(8):1132-1142.

62. Sakata S, Mizusawa N, Kubota-Kawai H, Sakurai I, & Wada H (2013) Psb28 is involved in recovery of photosystem II at high temperature in Synechocystis sp. PCC 6803. *Biochim Biophys Acta* 1827(1):50-59.

63. Beckova M, *et al.* (2017) Association of Psb28 and Psb27 Proteins with PSII-PSI Supercomplexes upon Exposure of Synechocystis sp. PCC 6803 to High Light. *Mol Plant* 10(1):62-72.

64. Kashino Y, *et al.* (2002) Low-molecular-mass polypeptide components of a photosystem II preparation from the thermophilic cyanobacterium Thermosynechococcus vulcanus. *Plant Cell Physiol* 43(11):1366-1373.

65. Roose JL & Pakrasi HB (2004) Evidence that D1 processing is required for manganese binding and extrinsic protein assembly into photosystem II. *J Biol Chem* 279(44):45417-45422.

66. Nowaczyk MM, *et al.* (2006) Psb27, a cyanobacterial lipoprotein, is involved in the repair cycle of photosystem II. *Plant Cell* 18(11):3121-3131.

67. Roose JL & Pakrasi HB (2008) The Psb27 protein facilitates manganese cluster assembly in photosystem II. *J Biol Chem* 283(7):4044-4050.

68. Grasse N, *et al.* (2011) Role of novel dimeric Photosystem II (PSII)-Psb27 protein complex in PSII repair. *J Biol Chem* 286(34):29548-29555.

69. Liu H, Huang RY, Chen J, Gross ML, & Pakrasi HB (2011) Psb27, a transiently associated protein, binds to the chlorophyll binding protein CP43 in photosystem II assembly intermediates. *Proc Natl Acad Sci U S A* 108(45):18536-18541.

70. Liu H, Roose JL, Cameron JC, & Pakrasi HB (2011) A genetically tagged Psb27 protein allows purification of two consecutive photosystem II (PSII) assembly intermediates in Synechocystis 6803, a cyanobacterium. *J Biol Chem* 286(28):24865-24871.

71. Komenda J, *et al.* (2012) The Psb27 assembly factor binds to the CP43 complex of photosystem II in the cyanobacterium Synechocystis sp. PCC 6803. *Plant Physiol* 158(1):476-486.

72. Nowaczyk MM, *et al.* (2012) Deletion of psbJ leads to accumulation of Psb27-Psb28 photosystem II complexes in Thermosynechococcus elongatus. *Biochim Biophys Acta* 1817(8):1339-1345.

73. Huang G, *et al.* (2021) Structural insights into a dimeric Psb27-photosystem II complex from a cyanobacterium Thermosynechococcus vulcanus. *Proc Natl Acad Sci U S A* 118(5).

74. Keren N, Ohkawa H, Welsh EA, Liberton M, & Pakrasi HB (2005) Psb29, a conserved 22-kD protein, functions in the biogenesis of Photosystem II complexes in Synechocystis and Arabidopsis. *Plant Cell* 17(10):2768-2781.

75. Bec Kova M*, et al.* (2017) Structure of Psb29/Thf1 and its association with the FtsH protease complex involved in photosystem II repair in cyanobacteria. *Philos Trans R Soc Lond B Biol Sci* 372(1730).

76. Kashino Y*, et al.* (2002) Proteomic analysis of a highly active photosystem II preparation from the cyanobacterium Synechocystis sp. PCC 6803 reveals the presence of novel polypeptides. *Biochemistry* 41(25):8004-8012.

77. Wegener KM, Bennewitz S, Oelmuller R, & Pakrasi HB (2011) The Psb32 protein aids in repairing photodamaged photosystem II in the cyanobacterium Synechocystis 6803. *Mol Plant* 4(6):1052-1061.

78. Sirpio S*, et al.* (2007) TLP18.3, a novel thylakoid lumen protein regulating photosystem II repair cycle. *Biochem J* 406(3):415-425.

79. Jarvi S*, et al.* (2016) Photosystem II Repair and Plant Immunity: Lessons Learned from Arabidopsis Mutant Lacking the THYLAKOID LUMEN PROTEIN 18.3. *Front Plant Sci* 7:405.

80. Rahimzadeh-Karvansara P, Pascual-Aznar G, Beckova M, & Komenda J (2022) Psb34 protein modulates binding of high-light-inducible proteins to CP47-containing photosystem II assembly intermediates in the cyanobacterium Synechocystis sp. PCC 6803. *Photosynth Res*.

81. Yao DC, Brune DC, Vavilin D, & Vermaas WF (2012) Photosystem II component lifetimes in the cyanobacterium Synechocystis sp. strain PCC 6803: small Cab-like proteins stabilize biosynthesis intermediates and affect early steps in chlorophyll synthesis. *J Biol Chem* 287(1):682-692.

82. Kufryk G*, et al.* (2008) Association of small CAB-like proteins (SCPs) of Synechocystis sp. PCC 6803 with Photosystem II. *Photosynth Res* 95(2-3):135-145.

83. Calderon RH*, et al.* (2013) A conserved rubredoxin is necessary for photosystem II accumulation in diverse oxygenic photoautotrophs. *J Biol Chem* 288(37):26688-26696.

84. Yang H*, et al.* (2014) Slr0151 in Synechocystis sp. PCC 6803 is required for efficient repair of photosystem II under high-light condition. *J Integr Plant Biol* 56(12):1136-1150.

85. Wegener KM*, et al.* (2008) High sensitivity proteomics assisted discovery of a novel operon involved in the assembly of photosystem II, a membrane protein complex. *J Biol Chem* 283(41):27829-27837.

86. Knoppova J*, et al.* (2021) The Photosystem II Assembly Factor Ycf48 from the Cyanobacterium Synechocystis sp. PCC 6803 Is Lipidated Using an Atypical Lipobox Sequence. *Int J Mol Sci* 22(7).

87. Liu H*, et al.* (2013) Mass spectrometry-based footprinting reveals structural dynamics of loop E of the chlorophyll-binding protein CP43 during photosystem II assembly in the cyanobacterium Synechocystis 6803. *J Biol Chem* 288(20):14212-14220.

88. Zhang S, Frankel LK, & Bricker TM (2010) The Sll0606 protein is required for photosystem II assembly/stability in the cyanobacterium Synechocystis sp. PCC 6803. *J Biol Chem* 285(42):32047-32054.

89. Pi X*, et al.* (2019) The pigment-protein network of a diatom photosystem II-light-harvesting antenna supercomplex. *Science* 365(6452).

90. Bao H & Burnap RL (2016) Photoactivation: The Light-Driven Assembly of the Water Oxidation Complex of Photosystem II. *Front Plant Sci* 7:578.

91. Roose JL, Kashino Y, & Pakrasi HB (2007) The PsbQ protein defines cyanobacterial Photosystem II complexes with highest activity and stability. *Proc Natl Acad Sci U S A* 104(7):2548-2553.

92. Shi LX, Hall M, Funk C, & Schroder WP (2012) Photosystem II, a growing complex: updates on newly discovered components and low molecular mass proteins. *Biochim Biophys Acta* 1817(1):13-25.

93. Ohad I, Dal Bosco C, Herrmann RG, & Meurer J (2004) Photosystem II proteins PsbL and PsbJ regulate electron flow to the plastoquinone pool. *Biochemistry* 43(8):2297-2308.

94. Liu H*, et al.* (2013) Phycobilisomes supply excitations to both photosystems in a megacomplex in cyanobacteria. *Science* 342(6162):1104-1107.

95. Yao DC, Brune DC, & Vermaas WF (2012) Lifetimes of photosystem I and II proteins in the cyanobacterium Synechocystis sp. PCC 6803. *FEBS Lett* 586(2):169-173.

96. Krynicka V, Shao S, Nixon PJ, & Komenda J (2015) Accessibility controls selective degradation of photosystem II subunits by FtsH protease. *Nat Plants* 1:15168.

97. Weisz DA*, et al.* (2019) A novel chlorophyll protein complex in the repair cycle of photosystem II. *Proc Natl Acad Sci U S A* 116(43):21907-21913.

98. Beckova M, Sobotka R, & Komenda J (2022) Photosystem II antenna modules CP43 and CP47 do not form a stable 'no reaction centre complex' in the cyanobacterium Synechocystis sp. PCC 6803. *Photosynth Res*.

99. Bentley FK, Luo H, Dilbeck P, Burnap RL, & Eaton-Rye JJ (2008) Effects of inactivating psbM and psbT on photodamage and assembly of photosystem II in Synechocystis sp. PCC 6803. *Biochemistry* 47(44):11637-11646.

100. Fagerlund RD*, et al.* (2020) Stabilization of Photosystem II by the PsbT protein impacts photodamage, repair and biogenesis. *Biochim Biophys Acta Bioenerg* 1861(10):148234.

101. Forsman JA & Eaton-Rye JJ (2021) The Interaction between PsbT and the DE Loop of D1 in Photosystem II Stabilizes the Quinone-Iron Electron Acceptor Complex. *Biochemistry* 60(1):53-63.

102. Tokano T, Kato Y, Sugiyama S, Uchihashi T, & Noguchi T (2020) Structural Dynamics of a Protein Domain Relevant to the Water-Oxidizing Complex in Photosystem II as Visualized by High-Speed Atomic Force Microscopy. *J Phys Chem B* 124(28):5847-5857.

103. Brinkert K, De Causmaecker S, Krieger-Liszkay A, Fantuzzi A, & Rutherford AW (2016) Bicarbonate-induced redox tuning in Photosystem II for regulation and protection. *Proc Natl Acad Sci U S A* 113(43):12144-12149.

104. Johnson GN, Rutherford AW, & Krieger A (1995) A change in the midpoint potential of the quinone QA in Photosystem II associated with photoactivation of oxygen evolution. *Biochimica et Biophysica Acta (BBA) - Bioenergetics* 1229(2):202-207.

105. Johnson VM, Biswas S, Roose JL, Pakrasi HB, & Liu H (2022) Psb27, a photosystem II assembly protein, enables quenching of excess light energy during its participation in the PSII lifecycle. *Photosynth Res*.

106. Lambertz J, Liauw P, Whitelegge JP, & Nowaczyk MM (2021) Mass spectrometry analysis of the photosystem II assembly factor Psb27 revealed variations in its lipid modification. *Photosynth Res*.

107. Dasgupta J, Ananyev GM, & Dismukes GC (2008) Photoassembly of the Water-Oxidizing Complex in Photosystem II. *Coord Chem Rev* 252(3-4):347-360.

108. Hwang HJ, Nagarajan A, McLain A, & Burnap RL (2008) Assembly and disassembly of the photosystem II manganese cluster reversibly alters the coupling of the reaction center with the light-harvesting phycobilisome. *Biochemistry* 47(37):9747-9755.

109. Radmer R & Cheniae GM (1971) Photoactivation of the manganese catalyst of 0 2 evolution II. A two-guantum mechanism. *Biochim Biophys Acta* 253(1):182-186.

110. Cheniae GM & Martin IF (1971) Photoactivation of the manganese catalyst of O 2 evolution. I. Biochemical and kinetic aspects. *Biochim Biophys Acta* 253(1):167-181.

111. Zhang M*, et al.* (2017) Structural insights into the light-driven auto-assembly process of the water-oxidizing Mn4CaO5-cluster in photosystem II. *Elife* 6.

112. Gisriel CJ*, et al.* (2020) Cryo-EM Structure of Monomeric Photosystem II from Synechocystis sp. PCC 6803 Lacking the Water-Oxidation Complex. *Joule* 4(10):2131-2148.

113. Narzi D & Guidoni L (2021) Structural and dynamic insights into Mn4Ca cluster-depleted Photosystem II. *Phys Chem Chem Phys* 23(48):27428-27436.

114. Avramov AP, Hwang HJ, & Burnap RL (2020) The role of Ca(2+) and protein scaffolding in the formation of nature's water oxidizing complex. *Proc Natl Acad Sci U S A* 117(45):28036-28045.

115. Russell BP & Vinyard DJ (2021) Chloride facilitates Mn(III) formation during photoassembly of the Photosystem II oxygen-evolving complex. *Photosynth Res*.

116. Vinyard DJ*, et al.* (2019) Photosystem II oxygen-evolving complex photoassembly displays an inverse H/D solvent isotope effect under chloride-limiting conditions. *Proc Natl Acad Sci U S A* 116(38):18917-18922.

117. Ungerer J & Pakrasi HB (2016) Cpf1 is a versatile tool for CRISPR genome editing across diverse species of Cyanobacteria. *Scientific Reports* 6:39681-39681.

118. Yao L, Cengic I, Anfelt J, & Hudson EP (2016) Multiple Gene Repression in Cyanobacteria Using CRISPRi. *ACS Synth Biol* 5(3):207-212.

119. Behler J, Vijay D, Hess WR, & Akhtar MK (2018) CRISPR-Based Technologies for Metabolic Engineering in Cyanobacteria. *Trends Biotechnol* 36(10):996-1010.

120. Santos-Merino M, Singh AK, & Ducat DC (2019) New Applications of Synthetic Biology Tools for Cyanobacterial Metabolic Engineering. *Front Bioeng Biotechnol* 7:33.

121. Naduthodi MIS, Barbosa MJ, & van der Oost J (2018) Progress of CRISPR-Cas Based Genome Editing in Photosynthetic Microbes. *Biotechnol J* 13(9):e1700591.

122. Yao L*, et al.* (2020) Pooled CRISPRi screening of the cyanobacterium Synechocystis sp PCC 6803 for enhanced industrial phenotypes. *Nat Commun* 11(1):1666.

123. Santos M, Pacheco CC, Yao L, Hudson EP, & Tamagnini P (2021) CRISPRi as a Tool to Repress Multiple Copies of Extracellular Polymeric Substances (EPS)-Related Genes in the Cyanobacterium Synechocystis sp. PCC 6803. *Life (Basel)* 11(11).

124. Knoot CJ, Biswas S, & Pakrasi HB (2020) Tunable repression of key photosynthetic processes using Cas12a CRISPR Interference in the fast-growing cyanobacterium Synechococcus sp. UTEX 2973. *ACS Synthetic Biology* 9(1):132-143.

125. Kirtania P*, et al.* (2019) A single plasmid based CRISPR interference in Synechocystis 6803 - A proof of concept. *PLoS One* 14(11):e0225375.

126. Liu D, Johnson VM, & Pakrasi HB (2020) A Reversibly Induced CRISPRi System Targeting Photosystem II in the Cyanobacterium Synechocystis sp. PCC 6803. *ACS Synthetic Biology* 9(6):1441-1449.

127. Lu Y*, et al.* (2016) Fast Photochemical Oxidation of Proteins Maps the Topology of Intrinsic Membrane Proteins: Light-Harvesting Complex 2 in a Nanodisc. *Anal Chem* 88(17):8827-8834.

128. Denisov IG & Sligar SG (2016) Nanodiscs for structural and functional studies of membrane proteins. *Nat Struct Mol Biol* 23(6):481-486.

129. Marty MT (2020) Nanodiscs and Mass Spectrometry: Making Membranes Fly. *Int J Mass Spectrom* 458.

130. Korotych OI, Nguyen TT, Reagan BC, Burch-Smith TM, & Bruce BD (2021) Poly(styrene-co-maleic acid)-mediated isolation of supramolecular membrane protein complexes from plant thylakoids. *Biochim Biophys Acta Bioenerg* 1862(3):148347.

131. Brady NG, Workman CE, Cawthon B, Bruce BD, & Long BK (2021) Protein Extraction Efficiency and Selectivity of Esterified Styrene-Maleic Acid Copolymers in Thylakoid Membranes. *Biomacromolecules* 22(6):2544-2553.

132. He Q & Vermaas W (1998) Chlorophyll a availability affects psbA translation and D1 precursor processing in vivo in Synechocystis sp. PCC 6803. *Proc Natl Acad Sci U S A* 95(10):5830-5835.

133. Chotewutmontri P, Williams-Carrier R, & Barkan A (2020) Exploring the Link between Photosystem II Assembly and Translation of the Chloroplast psbA mRNA. *Plants (Basel)* 9(2).

134. Liberton M, Howard Berg R, Heuser J, Roth R, & Pakrasi HB (2006) Ultrastructure of the membrane systems in the unicellular cyanobacterium Synechocystis sp. strain PCC 6803. *Protoplasma* 227(2-4):129-138.

135. van de Meene AM, Hohmann-Marriott MF, Vermaas WF, & Roberson RW (2006) The three-dimensional structure of the cyanobacterium Synechocystis sp. PCC 6803. *Arch Microbiol* 184(5):259-270.

136. Nevo R*, et al.* (2007) Thylakoid membrane perforations and connectivity enable intracellular traffic in cyanobacteria. *EMBO J* 26(5):1467-1473.

137. Huokko T*, et al.* (2021) Probing the biogenesis pathway and dynamics of thylakoid membranes. *Nat Commun* 12(1):3475.

138. Rast A*, et al.* (2019) Biogenic regions of cyanobacterial thylakoids form contact sites with the plasma membrane. *Nat Plants* 5(4):436-446.

139. Selao TT, Zhang L, Knoppovaa J, Komenda J, & Norling B (2016) Photosystem II Assembly Steps Take Place in the Thylakoid Membrane of the Cyanobacterium Synechocystis sp. PCC6803. *Plant Cell Physiol* 57(4):878.

140. Zak E, Norling B, Andersson B, & Pakrasi HB (1999) Subcellular localization of the BtpA protein in the cyanobacterium Synechocystis sp. PCC 6803. *European Journal of Biochemistry* 261(1):311-316.

141. Dahlgren KK, Gates C, Lee T, & Cameron JC (2021) Proximity-based proteomics reveals the thylakoid lumen proteome in the cyanobacterium Synechococcus sp. PCC 7002. *Photosynth Res* 147(2):177-195.

142. MacGregor-Chatwin C*, et al.* (2017) Lateral Segregation of Photosystem I in Cyanobacterial Thylakoids. *Plant Cell* 29(5):1119-1136.

143. Casella S*, et al.* (2017) Dissecting the Native Architecture and Dynamics of Cyanobacterial Photosynthetic Machinery. *Mol Plant* 10(11):1434-1448.

144. Mares J, Strunecky O, Bucinska L, & Wiedermannova J (2019) Evolutionary Patterns of Thylakoid Architecture in Cyanobacteria. *Front Microbiol* 10:277.

145. Li M, Ma J, Li X, & Sui SF (2021) In situ cryo-ET structure of phycobilisome-photosystem II supercomplex from red alga. *Elife* 10.

Chapter 2

A Novel Antenna Protein Complex in the Life Cycle of Cyanobacterial Photosystem II

This chapter is adapted, with permission, from:

Daniel A. Weisz*, Virginia M. Johnson*, Dariusz M. Niedzwiedzki, Min Kyung Shinn, Haijun Liu, Clécio F. Klitzke, Michael L. Gross, Robert E. Blankenship, Timothy M. Lohman, Himadri B. Pakrasi (2019) A novel chlorophyll protein complex in the repair cycle of photosystem II. *Proc. Natl. Acad. Sci*.116 (43) 21907-21913; DOI: 10.1073/pnas.1909644116.

*co-first authors

Chapter Contributions: Data presented in Figures 2.2A,B, 2.3, 2.8, and 2.9 were generated by VMJ.

2.1 Summary

In oxygenic photosynthetic organisms, Photosystem II (PSII) is a unique membrane protein complex that catalyzes light–driven oxidation of water. PSII undergoes frequent damage due to its demanding photochemistry. It must undergo a repair and reassembly process following photodamage, many facets of which remain unknown. We have discovered a novel PSII subcomplex that lacks five key PSII core reaction center polypeptides: D1, D2, PsbE, PsbF, and PsbI. This pigment–protein complex does contain the PSII core antenna proteins CP47 and CP43, as well as most of their associated low–molecular–mass subunits, and the assembly factor Psb27. Immunoblotting, mass spectrometry, and ultrafast spectroscopic results support the absence of a functional reaction center in this complex, which we call the 'no reaction center' complex (NRC). Analytical ultracentrifugation and clear native PAGE analysis show that NRC is a stable pigment–protein complex and not a mixture of free CP47 and CP43 proteins. NRC appears in higher abundance in cells exposed to high light and impaired protein synthesis, and genetic deletion of PsbO on the PSII lumenal side results in an increased NRC population, indicative that NRC forms in response to photodamage as part of the PSII repair process. Our finding challenges the current model of the PSII repair cycle and implies an alternative PSII repair strategy. Formation of this complex may maximize PSII repair economy by preserving intact PSII core antennas in a single complex available for PSII reassembly, minimizing the risk of randomly diluting multiple recycled components in the thylakoid membrane following a photodamage event.

2.2 Introduction

Photosystem II (PSII) is a large pigment-protein complex embedded in the thylakoid membrane of all oxygenic photosynthetic organisms: cyanobacteria, algae, and plants. PSII plays a central role in energy flow in the biosphere by harnessing sunlight to split water molecules into protons, electrons, and molecular oxygen, ultimately yielding the vital high-energy molecules ATP and NADPH. This conversion of solar energy to chemical energy powers nearly all life on Earth, while simultaneously producing the oxygen we breathe.

Crystal structures of functional PSII (1-6) have revealed that the water-splitting reaction is catalyzed by a Mn_4CaO_5 (Mn) cluster bound to the lumenal surface of PSII. D1 and D2, two ~30 kDa transmembrane proteins, form a heterodimer at the center of PSII. They coordinate the primary electron transport chain cofactors and contribute most of the Mn-cluster ligands. D1 and D2 associate with the smaller (<10 kDa) subunits PsbE and PsbF (α- and β-subunits of cytochrome b_{559}) and PsbI. Together, these five proteins comprise the core "reaction center" (RC) complex, the smallest PSII subcomplex capable of light-induced charge separation (7). Surrounding the RC subunits are CP47 and CP43, two ~50 kDa proteins that bind chlorophyll *a* (Chl *a*) molecules and serve as antennas, harvesting and funneling light energy towards the RC to drive PSII photochemistry. Around 10 additional low-molecular mass (LMM) subunits bind to fully assembled PSII, contributing to the structural and functional optimization of the complex (8). Finally, functional PSII contains several membrane-extrinsic hydrophilic proteins (PsbO, PsbU, PsbV, and PsbQ in cyanobacteria) (9, 10), bound at the lumenal surface of the complex, that stabilize the Mn cluster.

PSII undergoes frequent oxidative damage owing to the demanding electron-transfer chemistry it performs (11-13). D1, closely followed by D2, is damaged and replaced most frequently of all proteins in the complex (14-18). CP47 and CP43 are, however, more long lived (15, 17). This damage leads to partial disassembly of PSII, replacement of each damaged subunit with a new copy, and reassembly of PSII, in an intricate process known as the PSII repair cycle (14, 19, 20) (Fig. 2.1).

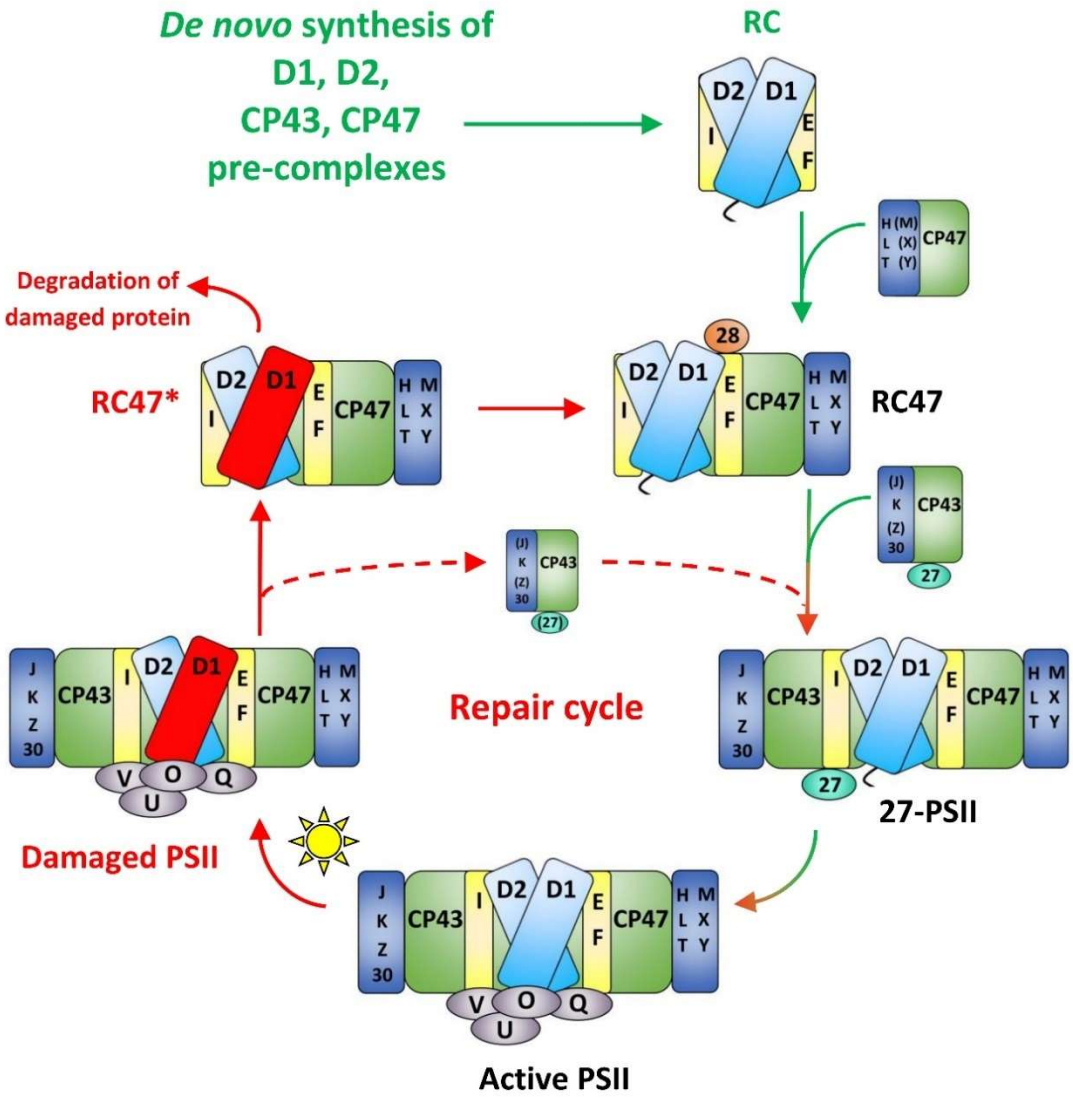

Figure 2.1 Model of the PSII life cycle based on previous findings [reviewed in (14, 19, 21, 22)]. Several intermediary stages in the life cycle are omitted for clarity (steps 1-3 in the Discussion section): dimerization of active PSII; and after damage, dissociation of PsbO, PsbU, PsbV, and PsbQ (22), Psb27 rebinding (23), and monomerization of the complex (22) before the RC47 formation step. In this model, the damaged RC47 complex serves as the site of D1

replacement. Red D1, damaged D1; RC47*, damaged RC47. Green arrows and text represent *de novo* synthesis steps; red arrows and text represent repair cycle steps. Black text and the red-green arrow represent steps common to both processes.

This cycle operates concurrently with *de novo* PSII synthesis. Synthesis of PSII occurs through stepwise assembly of PSII from component subcomplexes, in which the 'RC' complex is joined with the CP47 pre-complex first, followed by addition of the CP43 pre-complex, and finally addition of membrane-extrinsic proteins (Fig. 2.1). Current understanding is that repair occurs in much the same fashion, with removal of the extrinsic subunits, followed by the CP43 pre-complex, replacement of D1 and/or D2 at the RC47 level, and reassembly of PSII (14, 19, 20) (Fig. 2.1). Many accessory proteins, such as Psb27 and Psb28 (23-27), bind exclusively to particular PSII subcomplexes to aid in a specific aspect of assembly. Despite this working model, our understanding is still evolving. Subcomplexes are low in abundance and transient in nature, and a complete characterization of all is far from complete. The steps that occur following photodamage are particularly uncertain, as repair subcomplexes are typically less amenable to targeted accumulation using PSII mutant strains than are intermediates of *de novo* assembly.

In this study, we describe the identification of a novel PSII subcomplex from the cyanobacterium *Synechocystis* sp. PCC 6803 (*Synechocystis* 6803). This subcomplex specifically lacks the five RC subunits, and therefore, we refer to it as the 'no-RC' (NRC) complex. It accumulates to higher abundance in conditions of elevated PSII damage and impaired protein synthesis, leading us to conclude that NRC is an intermediate in the repair cycle of PSII. A revised model of the repair steps following PSII photodamage is presented in light of our findings. We propose that NRC formation maximizes the efficiency of PSII repair and minimizes collateral damage to components of PSII that were unharmed following an initial photodamage event.

2.3 Materials and Methods

2.3.1 Cell culture, PSII purification, and protein analysis

Generation of the Δ*psb*O-His47 strain was reported previously (10). The HT3 (His47) strain was a kind gift from Dr. Terry Bricker (Louisiana State University, Baton Rouge, LA) (28). Cyanobacterial strains were grown in BG11 medium at 30 °C under 40 μmol photons m^{-2} s^{-1}. The growth media were supplemented with 10 μg/mL spectinomycin and 5 μg/mL gentamicin (Δ*psb*O-His47 strain) or 5 μg/mL gentamicin (His47 strain). Histidine-tagged PSII complexes were purified by FPLC, as described previously (29), with minor modifications, and were stored in 25% glycerol (wt/vol), 10 mM $MgCl_2$, 5 mM $CaCl_2$, 50 mM MES buffer pH 6.0. Following FPLC purification, PSII complexes were purified further by glycerol gradient ultracentrifugation, performed as described previously (27). Protein electrophoresis was performed as described previously (30, 31). For immunoblotting, gels were transferred onto a PVDF membrane (MilliporeSigma, Burlington, MA, USA) followed by probing with specific antisera. Immunoblot imaging was performed with chemiluminescence reagents (MilliporeSigma, Burlington, MA, USA) on a LI-COR Odyssey Fc (LI-COR Biotechnology, Lincoln, NE, USA).

2.3.2 Clear native polyacrylamide gel electrophoresis

High resolution clear native PAGE was performed as described in (32). 1.5x160x160 mm clear native polyacrylamide gel, 4-13%, was prepared using a gradient maker. Protein samples containing 10 μg of Chl *a* were loaded in each lane. Gel was run at 4mA for 16 hours at 4° C. Gels were imaged using a Li-COR Odyssey Fc (LI-COR Biotechnology, Lincoln, NE) using the 700 nm channel to visualize chlorophyll fluorescence.

2.3.3 In-gel digestion and LC-MS/MS analysis

Protein samples were excised from the clear native polyacrylamide gel, destained and dehydrated with (1:1) 100mM ammonium bicarbonate:acetonitrile and digested in-gel with 13 ng/uL trypsin (Sigma, St. Louis, MO, USA) in 1mM TEABC. Following digestion, sample was extracted in 1% formic acid and subjected to LC-MS/MS.

Aliquots (5 µL, ~100 pmoles) of the peptide samples were separated online using a Dionex Ulimate 3000 RSLCnano pump and autosampler (Thermo Fisher Scientific, Waltham, MA, USA) and a column packed in-house utilizing ProntoSIL C18AQ, 3 µm particle size, 120 Å pore size (Bischoff, Stuttgart, Germany), in a 75 µm X 15 cm capillary. The mobile phase consisted of A: 0.1% formic acid in water and B: 0.1% formic acid in 80% acetonitrile/20% water (Thermo Fisher Scientific, Waltham, MA, USA). At a flow rate of 500 nL/min, the gradient was held for 5 min at 2% B and slowly ramped to 17% B over the next 30 min, increasing to 47% B over the next 30 min and then finally increasing to 90% B over 30 min and held at 90% for 10 min. The column was then allowed to re-equilibrate for 60 min with a flow of 2% B in preparation for the next injection.

The separated peptides were analyzed on-line by using a Q-Exactive Plus mass spectrometer (Thermo Fisher Scientific, Waltham, MA, USA) operated in standard data-dependent acquisition mode controlled by Xcalibur version 4.0.27.19. Precursor-ion activation was set with an isolation width of *m/z* 1.0 and with two collision energies toggled between 25 and 30%. The mass resolving power was 70,000 for precursor ions and 17,500 for product ions (MS2).

The raw data were analyzed using PEAKS Studio X (version 10.0, Bioinformatics Solution Inc., Waterloo, ON, Canada, www.bioinfor.com) and Protein Metrics Byonic and Byologic (Protein Metrics Inc., Cupertino, CA, www.proteinmetrics.com) (33). PEAKS was used in the *de novo*

mode followed by DB, PTM, and SPIDER modes. Search parameters included a precursor-ion mass tolerance of 10.0 ppm and a fragment-ion mass tolerance of 0.02 Da. Variable modifications included all built-in PTMs. The maximum allowed modifications per peptide were 3; and the maximum missed cleavages were 2; false discovery rate, 0.1%. SPIDER (function) was used to identify unknown spectra by considering homology searches, sequence errors, and residue substitutions to yield a more confident identification.

Byonic searches employed the same database but used a precursor ion mass tolerance of 20 ppm and a fragment ion mass tolerance of 60 ppm with a maximum of 2 missed cleavages. Wildcard searches of ± 200 Da were employed to look for modifications in addition to regular PTM analysis. Protein false discovery rate threshold was determined by the score of the highest ranked decoy protein identified. All of the search results were combined in Byologic for validation.

2.3.4 In-solution digestion and LC-MS/MS analysis

Samples each containing 2 μg Chl *a* of Δ*psbO*-PSII-M and Δ*psbO*-NRC were precipitated using the 2D Cleanup Kit (GE Healthcare, Chicago, IL) according to the manufacturer's instructions. The pellets were resuspended in 20 μL 8M urea, 50 mM ammonium bicarbonate (ABC). Lys C was added at a 1:50 w/w protease:sample ratio and incubated at 37 °C for 2 hours. Samples were diluted to 1M urea with 50 mM ABC and trypsin was added at a 1:50 w/w protease:sample ratio. The samples were incubated overnight at 37 °C, then acidified to 1% formic acid and centrifuged to remove any insoluble material.

Aliquots (5 μL) of the digests were analyzed by LC-MS/MS as described in (27). For detailed methods, see SI Appendix, SI methods. with the following modifications: the LC gradient ran from 2-90% Solvent B with the following steps- 12 min at 2% B, 33 min linear increase to 15% B, 30

min linear increase to 50% B, 15 min linear increase to 90% B, 9 min hold at 90% B, 1 min linear decrease to 2% B, and 30 min hold at 2% B; scan range was m/z 380-2200; for data-dependent MS/MS scans, resolution was 35,000 for ions at m/z 200 and AGC target was set at 2 x 10^5 ions; and the top 10 ions were fragmented by HCD.

The raw data were loaded into PEAKS (version 8.5, Bioinformatics Solution Inc., Waterloo, ON) for protein identification. The data were searched against a database of the *Synechocystis* 6803 proteome using the built-in fusion decoy database for false discovery rate calculation (34). Search parameters were as follows: precursor-ion mass tolerance, 10.0 ppm; fragment-ion mass tolerance, 0.02 Da; variable modifications, all built-in modifications; maximum variable modifications per peptide, 3; maximum missed cleavages, 2; maximum nonspecific cleavages, 0; false discovery rate, 0.1%. The mass spectrometry proteomics data have been deposited to the ProteomeXchange Consortium via the PRIDE partner repository with the dataset identifier PXD013406 and 10.6019/PXD013406.

2.3.5 Mass Spectrometry of Intact Proteins

Δ*O*-M and Δ*O*-NRC samples, each containing 1.4 μg Chl *a*, were precipitated using the 2D Clean-up kit (GE Healthcare, Chicago, IL), following the manufacturer's instructions. The pellets were resuspended in 100 μL 70% acetone, 19% water, 10% isopropanol, 1% formic acid v/v (35), diluted 1:3 in the resuspension solution, and infused directly into a Synapt G2 HDMS mass spectrometer (Waters, Milford, MA). For detailed methods, see SI Appendix, SI methods. at a flow rate of 500 nL/min by means of a syringe pump PHD Ultra (Harvard Apparatus, Holliston, MA). The mass spectrometer, equipped with a nanoelectrospray ionization source, was operated in sensitive 'V' mode with 10,000 mass resolving power (full-width at half-

maximum). Positive-ion formation was achieved by applying a capillary voltage of 2.6 kV. The sampling and extraction cone voltages were 40 and 2 V, respectively, and the source temperature was 30 °C. Mass spectra were acquired between *m/z* 100 and 4,000 with an acquisition rate of one spectrum per sec. Data processing was with MassLynx 4.1 (Waters, Milford, MA). Final spectra were the average of 300 spectra collected in profile mode and converted to centroid data.

For LC-MS/MS analysis, ΔO-M and ΔO-NRC samples were prepared as described above for direct infusion. An aliquot (5 µL, ~1-2 pmol of intact proteins) was loaded onto a trap column (180 µm x 2 cm, C18 Symmetry, 5 µm, 100Å, Waters, Milford, MA) using solvent A (water with 0.1% formic acid). Peptides were eluted from a reverse phase C18 column (ProntonSIL 3µm, 120Å) 75 µm x 150 mm by increasing the fraction of solvent B (80% acetone, 20% water, and 0.1% formic acid). The gradient was supplied by a Dionex Ultimate 3000 instrument (Thermo Scientific, Inc., Sunnyvale, CA) and run from 2 to 17% solvent B over 65 min and then to 40% solvent B for 15 min, and then to 90% solvent B for 15 min at a rate of 500 nL/min followed by 15 min re-equilibration step with 98% solvent A. The Q-Exactive Plus spectrometer (Thermo Fisher Scientific, Waltham, MA, USA) was operated in standard mode with an inclusion list of all the LMM subunits observed by direct infusion on the Synapt G2 (Table S4). Peptide mass spectra (*m/z* range of 350-2000) were acquired at a high mass resolving power (7000 for ions at *m/z* 200) with the Fourier transform (FT) mass spectrometer. Precursor activation in HCD was performed with an isolation width of *m/z* 1.0 and a normalized collision energy of 30%. Default charge state was 3+ with charge exclusion of 1 and >8.

The LC-MS/MS raw data were submitted to the Protein Metrics (PMI) software package for analysis (33). Database searching was performed by the Byonic software using the *Synechocystis* 6803 phycobilisome and reaction centers protein database and a decoy database

containing reversed protein sequences. Search parameters were: precursor ion mass tolerance 20 ppm, fragment ion mass tolerance 60 ppm, 0 cleavage sites, common post-translational modifications, and automatic peptide score cut. Protein false discovery rate threshold was determined by the score of the highest ranked decoy protein identified. The search results were combined in the Byologic software for validation and extraction of ion chromatograms with a mass window of 20 ppm. Manual quality control was performed using XCalibur Qual Browser assisted by the Protein Prospector package (http://prospector.ucsf.edu/prospector/mshome.htm) and Magtran (36).

2.3.6 Ultrafast time-resolved fluorescence spectroscopy

All spectroscopic measurements were carried out at 77 K, using a VNF-100 liquid nitrogen cryostat (Janis, USA). The samples (ΔO-M and ΔO-NRC) were diluted in 60:40 v/v glycerol:RB buffer with 0.04% DM, that after cooling, formed fully transparent glass. Steady-state absorption spectra were recorded on a UV-1800 spectrophotometer (Shimadzu). Time-resolved fluorescence (TRF) imaging was performed using a universal streak camera system (Hamamatsu Corporation, Japan) based on N51716-04 streak tube and A6365-01 spectrograph from Bruker Corporation (Billerica, MA) coupled to an ultrafast laser system, described previously (37). The repetition rate of the exciting laser was 4 MHz, corresponding to ~250 ns between subsequent pulses. The excitation beam was depolarized, focused on the sample in a circular spot of ~1 mm diameter and set to a wavelength of 625 nm and very low photon flux of ~10^{10} photons/cm^2 per pulse. The emission was measured at a right angle to the excitation beam with a long-pass 645-nm filter placed at the entrance slit of the spectrograph. The integrity of the samples was examined by observing the photon counts in real-time over the time course of the experiment. These were constant,

indicating no detectable sample photodegradation. Prior to further analysis, all TRF datasets were subjected to singular value decomposition (SVD), a least-squares estimator of the original data leading to significant noise reduction (38).

The data were globally fitted with application of a simple fitting model that assumes irreversible direction of excitation decay from fastest to slowest decaying states. It is commonly called a sequential model, and spectro-kinetic components obtained from this fitting are typically called evolution-associated spectra (EAS). This nomenclature was adopted for the TRF analysis and the fitting results of those data are called evolution associated fluorescence spectra (EAFS) (39).

2.3.7 Glycerol gradient ultracentrifugation

Following FPLC purification, PSII complexes were purified further by glycerol gradient ultracentrifugation, performed as described previously (27) . To prepare one centrifuge tube, 0.6 mL 50% glycerol in RB buffer pH 6.5 was layered onto the bottom of the tube. The gradient was made from 6 mL each of stock solutions of 5% and 30% glycerol in RB buffer pH 6.5 containing 0.04% β-dodecyl maltoside. The stock solutions were added into the two chambers of a gradient maker connected to a peristaltic pump and were allowed to mix gradually as the pump delivered the mixture into the tube just below the top of the 50% glycerol layer. PSII sample containing 100 μg Chl *a* was diluted 1:5 into RB buffer pH 6.5 (final concentration 5% glycerol), then loaded onto the top of the gradient. Ultracentrifugation was performed at 180,000 *g* overnight at 4 °C. After centrifugation, the bands were harvested and concentrated by using Vivaspin 500 centrifugal

concentrators (50 kDa cutoff) (Vivaproducts, Littleton, MA, USA). The NRC complex was obtained in this manner consistently from numerous distinct biological preparations.

2.3.8 Analytical sedimentation

After sample concentration following glycerol gradient ultracentrifugation (see above), Δ*O*-M and Δ*O*-NRC samples were buffer exchanged into RB buffer pH 6.5 containing 5% glycerol. Sedimentation velocity experiments were performed with an Optima XL-A analytical ultracentrifuge and An50Ti rotor (Beckman Instruments, Fullerton, CA) at 42,000 rpm (25 °C) as described previously (40). The experiment was performed at 4 and 13 μg/mL Chl *a*, while monitoring absorbance at 437 nm, with the results consistent at both concentrations. Data were analyzed using SEDFIT (41), to obtain c(s) distributions. The c(s) distribution function defines the populations of species with different sedimentation rates (sizes) and represents a variant of the distribution of Lamm equation solutions (41). The density and viscosity of the RB buffer at 25° C were determined using SEDNTERP. 0.76 mL/g was used as the partial specific volume (42). Sedimentation equilibrium experiments were performed with NRC sample at the three indicated speeds (25 °C) starting at the lowest and finishing at the highest speed as described previously (43). 110 μL of the NRC sample at the same concentration used for the sedimentation velocity experiments and 120 μL of the buffer were loaded to an Epon charcoal-filled six-channel centerpiece. Absorbance data were collected at intervals of 0.003 cm in the step mode with five averages per step. Data were edited using SEDFIT to extract concentration profiles from each chamber and analyzed using SEDPHAT with the Species Analysis with Mass Conservation model (44).

2.3.9 PSII damage induction

His47 cells were grown to late log phase under conditions described above, and then divided and allowed to grow for 3 hours before being subjected to either high light and lincomycin (400 µmol photons/m^2*s and 20 µg/mL lincomycin), high light without lincomycin, low light and lincomycin (40 µmol photons/m^2*s and 20 µg/mL lincomycin) or low light without lincomycin. After 5 hours under these conditions, when photosynthetic efficiency decreased to 50% for the high light and lincomycin treatment, cells were harvested and PSII was isolated as described above. Photosynthetic efficiency (F_v/F_m) was monitored using an FL-200 fluorometer (PSI, Brno, Czech Republic).

2.4 Results

2.4.1 Isolation of a novel PSII subcomplex

We purified PSII complexes from the His47 and Δ*psb*O-His47 strains of *Synechocystis* 6803 by FPLC using a nickel affinity column. His47 has a 6xHis-tag on the CP47 subunit of PSII, and Δ*psb*O-His47 is the same strain with an insertional deletion of the *psbO* gene. These complexes were then analyzed by high resolution clear native acrylamide gel electrophoresis (Fig. 2.2A).

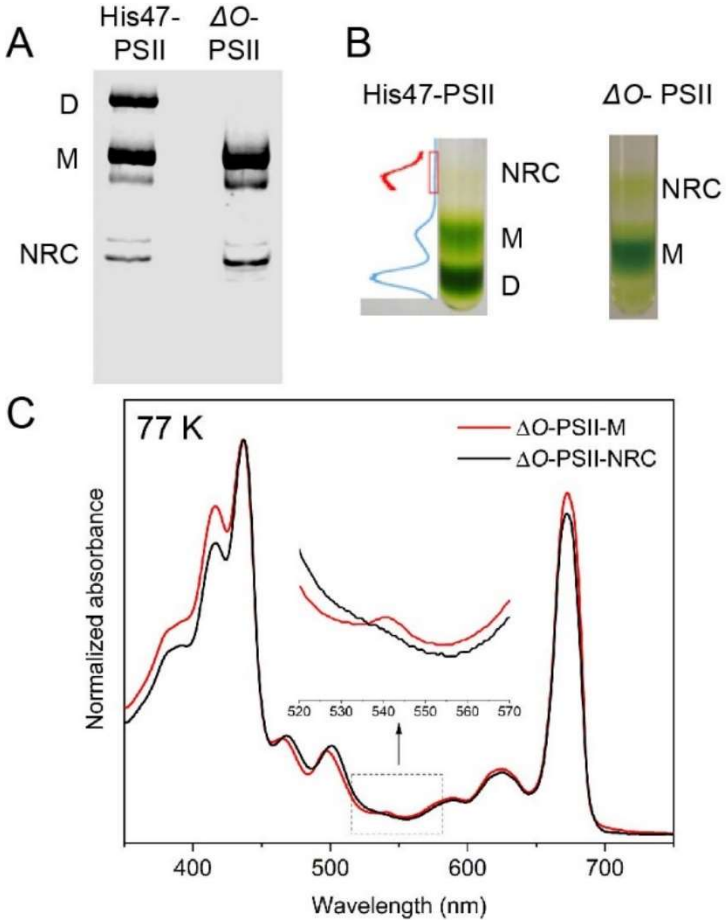

Figure 2.2 Isolation and characterization of a novel PSII subcomplex (NRC). (A) Clear Native PAGE of His-CP47-tagged PSII complexes from the His47 and Δ*psbO*-His47 strains. M, PSII monomer; D, PSII dimer. (B) Green bands corresponding to the NRC complex and PSII monomer (M) formed following ultracentrifugation of His-CP47-tagged PSII samples in a 5-30% linear glycerol gradient from the His47 and Δ*psbO*-His47 strains. Pixel intensity (plotted as inverse of gray value computed in ImageJ (45) is shown on the left of the His47 gradient. The red curve shows the zoomed-in view of the region corresponding to the NRC band. (C) Steady-state absorption spectra of PSII-M and PSII-NRC at 77 K. To enable comparison, spectra were normalized to unity at the maximum of the Soret band (417 nm). The arrow shows a small peak visible in the spectrum of PSII-M that corresponds to the Q_x band of pheophytin *a* present in the PSII reaction center, and which is missing in the NRC spectrum.

As expected, in the Δ*psb*O-His47 strain, a major band was seen that represents the PSII monomer (PSII-M), whereas no PSII dimer was found as it is not formed in this strain (10, 27). Additionally, a green band just below the monomer was observed that corresponds to the RC47 complex previously observed in the literature (14, 20). In the His47 strain, a major band was seen that represents the PSII dimer (PSII-D), while PSII-M and the RC47 bands were also present. Interestingly, an additional green band of unknown identity was present at a lower molecular weight than the monomer in each strain. In-gel digestion followed by tandem mass spectrometry (MS) indicated sharply decreased D1, D2, and PsbE content in the lower molecular weight band from both strains compared to PSII-M (Dataset S2.1), and presence of CP47 and CP43, though other assay methods were needed (see below) for more reliable quantitative information.

To obtain a sufficient quantity for further characterization of the unknown complex, PSII preparations were then subjected to glycerol gradient ultracentrifugation to separate distinct His-CP47-containing complexes (Fig. 2.2B). Again as expected, in the Δ*psb*O-His47 strain, a major band was seen that represents the PSII monomer (PSII-M), whereas no PSII dimer was found as it is not formed in this strain (10, 27), and in the His47 strain, a major band was seen that represents the PSII dimer (PSII-D) in addition to the monomer band. Consistent with the results in the clear native gel, a lower molecular weight chlorophyll-containing band was observed in each strain. This band was harvested and concentrated. When the purified lower molecular weight band from the *ΔpsbO* strain was run next to *ΔpsbO*-PSII by clear native gel electrophoresis, it co-migrated with the band observed initially (Fig. 2.3).

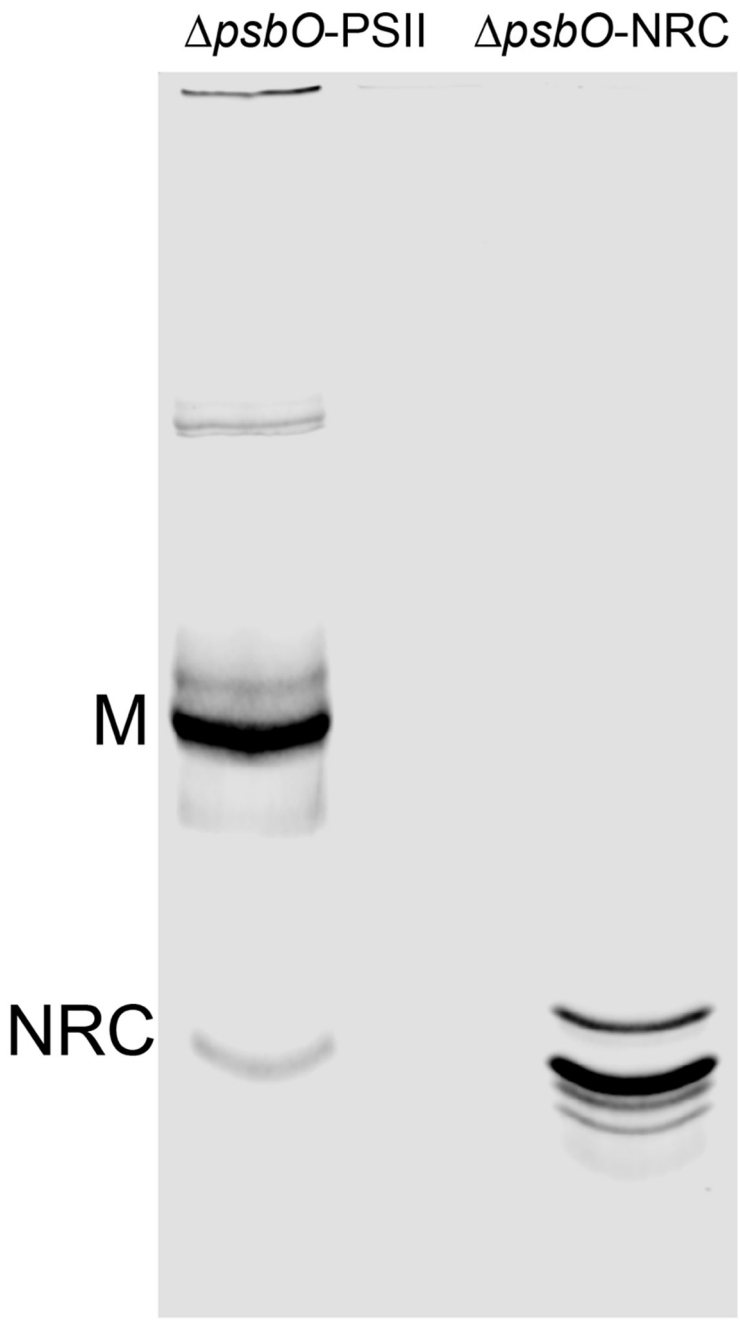

Figure 2.3. CN-PAGE of isolated PSII complexes. Clear Native polyacrylamide gel of *ΔpsbO*-PSII and purified NRC from glycerol gradient of *ΔpsbO*-PSII. The chlorophyll-containing NRC band co-migrates with the unknown band in the PSII sample.

Tandem MS was performed after in-solution digestion of the complex from Δ*psbO* cells. The dominant PSII proteins were CP47 and CP43. According to the semi-quantitative information

derived from such an experiment, levels of D1, D2, PsbE, and PsbF were markedly decreased compared to the corresponding PSII-M (Datasets S2.2-S2.3), consistent with the results from in-gel digestion on the lower molecular weight band described above.

The 77-K absorption spectra of *ΔpsbO*-PSII-M and the novel complex were nearly identical (Fig. 2.2C), with the exception that a small peak around 540 nm corresponding to pheophytin *a* (46) was absent in the spectrum of the new complex. Pheophytin *a* is a cofactor in the PSII electron-transfer chain and is coordinated by D1 and D2. SDS-PAGE analysis showed no band detectable for the core RC proteins D1 and D2 (Fig. 2.3A). It, however, contained the inner antenna subunits

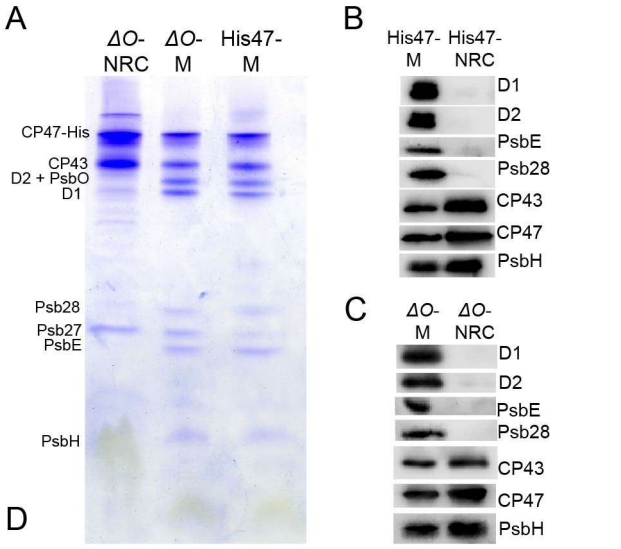

D

Protein	PSII Monomer	NRC	Observed mass (Da)	Calculated mass (Da)	Mass accu. (ppm)	Mod.	Example MS/MS ions observed (m/z)
PsbT	✓	✓	3565.93	3565.94	1	Form.	y_{24}^{2+}: 1373.29, y_{20}^{2+}: 1160.15
PsbM	✓	✓	3907.15	3907.15	<1	Form.	--
PsbK	✓	✓	4174.34	4174.33	2	-8 N Ter.	b_{18}^{+}: 1205.62, b_{24}^{+}: 1842.00
PsbX	✓	✓	4211.39	4211.37	4	Form.	y_{18}^{2+}: 987.57, y_{11}^{+}: 1322.74
PsbY	✓	✓	4227.35	4227.34	3	Form.	y_{21}^{2+}: 1075.60, y_{26}^{2+}: 1346.75
PsbI	✓	—	4331.35	4331.34	3	Form.	y_{22}^{2+}: 1265.64, y_{26}^{2+}: 1480.77
PsbL	✓	✓	4470.35	4470.35	<1	None	b_{27}^{3+}: 1022.55, b_{30}^{3+}: 1112.28
PsbF	✓	—	4798.56	4798.56	1	-M1	y_{11}^{+}: 1205.64, y_{14}^{+}: 1598.85
PsbH	✓	✓	6980.75	6980.75	<1	-M1	b_{33}^{3+}: 1150.62, b_{22}^{2+}: 1184.17
PsbE	✓	—	9311.65	9311.64	1	-M1	b_{26}^{3+}: 935.48, b_{34}^{3+}: 1278.34

Figure 2.4. Major protein components of NRC. (A) SDS-PAGE analysis of PSII-M and PSII-NRC samples from the Δ*psbO*-His47 strain, and of PSII-M purified identically from the His47 strain. (B) Immunoblot analysis of PSII-M and PSII-NRC samples from the His47 strain. (C) Immunoblot analysis of PSII-M and PSII-NRC samples from the Δ*psbO*-His47 strain. (D) Summary table of the low-molecular mass subunits in Δ*O*-NRC detected by intact mass spectrometry, including example fragment ions.

CP47 and CP43, as well as Psb27, which binds to CP43 transiently during PSII assembly and repair (23, 24, 47, 48). In functional PSII, Chls *a* bound to CP47 and CP43 harvest light and transfer excitation energy to Chls *a* on D1 and D2, where primary PSII photochemistry occurs. A subcomplex containing both antenna proteins but lacking the two RC subunits to which they transfer energy was a surprising finding, as such a complex has not been observed previously and does not appear in the current model of the PSII lifecycle (Fig. 2.1).

Consistent with SDS-PAGE, immunoblotting analysis (Figs. 2.4B, 2.4C) showed no detectable level of D1 and D2 in the novel complex isolated from both the *ΔpsbO* and His47 strains. Additionally, PsbE, another member of the PSII RC complex, was also absent (7). Presence of CP43 and CP47 in this complex, however, was confirmed, and the CP47-associated LMM subunit PsbH was detected as well. The MS results that showed severely decreased, but detectable, levels of D1 and D2 in the sample reflect the high sensitivity of the Q-Exactive mass spectrometry instrument and the inevitability of some impurities remaining in the sample following purification. The SDS-PAGE and immunoblot results show, however, that even if small amounts of D1 and D2 are present below their detection limits, they are not stoichiometric components of this complex.

For a more complete identification of the LMM subunits in this new complex, we employed MS to measure the mass of the intact protein components. We detected ten LMM subunits in the control *ΔpsbO*-PSII-M sample, whereas only seven of those ten were present in the new complex (Figs. 2.4D, 2.4, Datasets S2.4-S2.5). Remarkably, the three missing subunits are the three LMM components of the PSII RC: PsbE, PsbF, and PsbI. Taking our SDS-PAGE, immunoblot, and MS results together, we conclude that the novel subcomplex specifically lacks all five of the PSII RC components, D1, D2, PsbE, PsbF and PsbI, but contains the rest of the PSII subunits observed in

the control PSII-M sample. We therefore refer to it as the "no-reaction center" (NRC) complex.

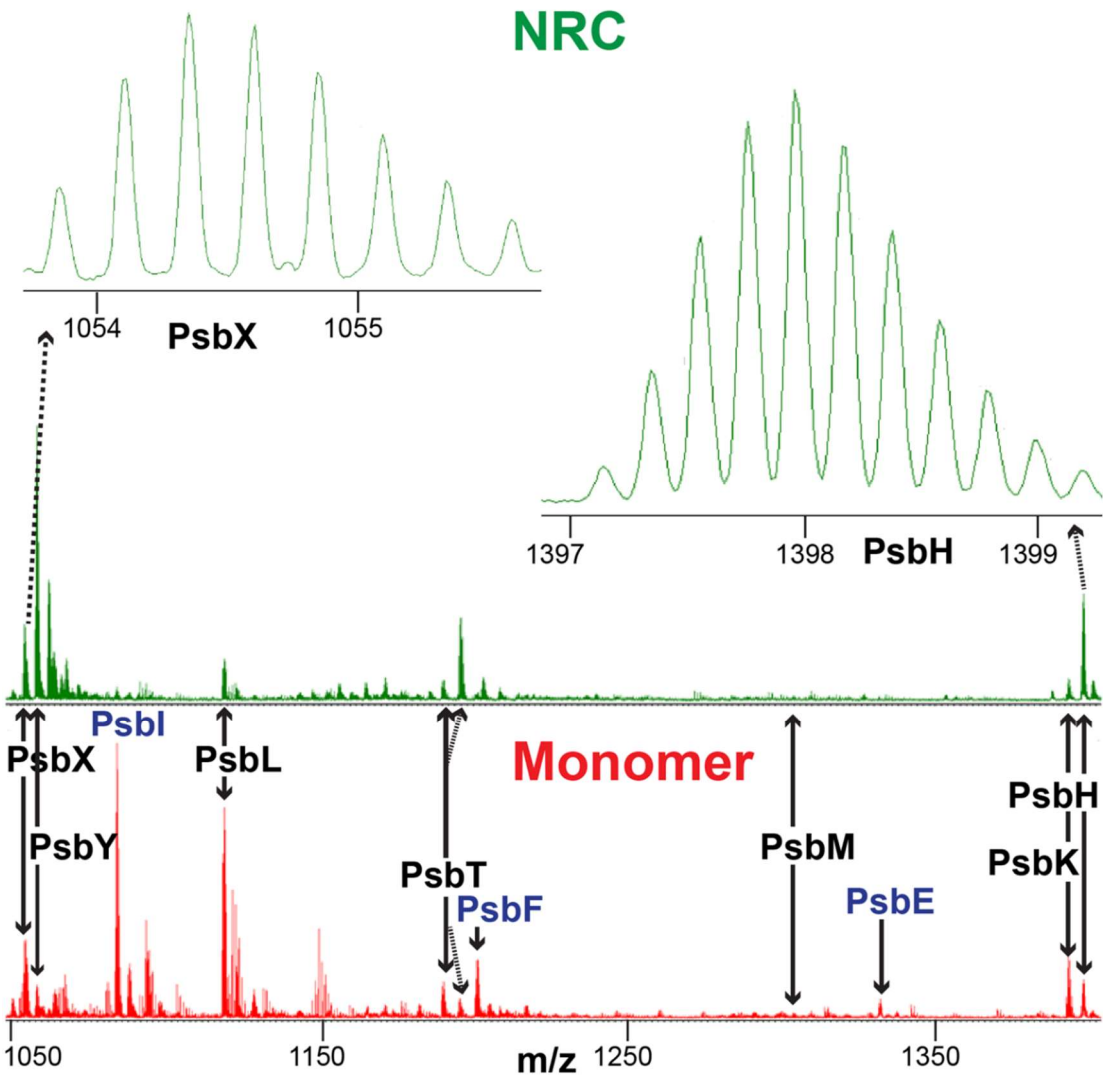

Figure 2.5 Mass spectra of the intact, low-molecular-mass subunits in Δ*O*-NRC (upper spectrum) and Δ*O*-PSII-M (lower spectrum). Most unlabeled peaks in the spectra correspond to additional charge states or oxidation products of labeled subunits. Subunits labeled in black afforded roughly comparable signal intensities in both samples; subunits labeled in blue (PsbE, PsbF, PsbI) were not observed in the NRC spectrum. Mod., modification; Form., formylation; -8 N-term., protein is cleaved after Alanine-8; -M1, loss of N-terminal methionine. MS/MS analysis was performed separately on each subunit (see Materials and Methods and Datasets S2.4-S2.5) to confirm the identification, and example fragment ions are shown in (B). Mass accuracy of all MS/MS ions shown was ≤0.01 Da.

The presence of NRC in the His47 strain, seen through native gel, glycerol gradient, mass spectrometry, and immunoblot characterization, demonstrates that this complex does not form as a result of the absence of PsbO in the Δ*psb*O-His47 strain. Unless otherwise mentioned, the

experiments described below were, therefore, performed using NRC from Δ*psb*O-His47 cells owing to the higher yield obtainable in this strain.

2.4.2 Determination of the size of the NRC complex

The SDS-PAGE, western blot, and MS results presented above identified the individual proteins in a denatured NRC sample. To determine the absolute molecular weight of the intact, native complex, we used analytical ultracentrifugation (AUC). Distributions of the Chl-containing species of the PSII-M and NRC samples were determined from sedimentation velocity.

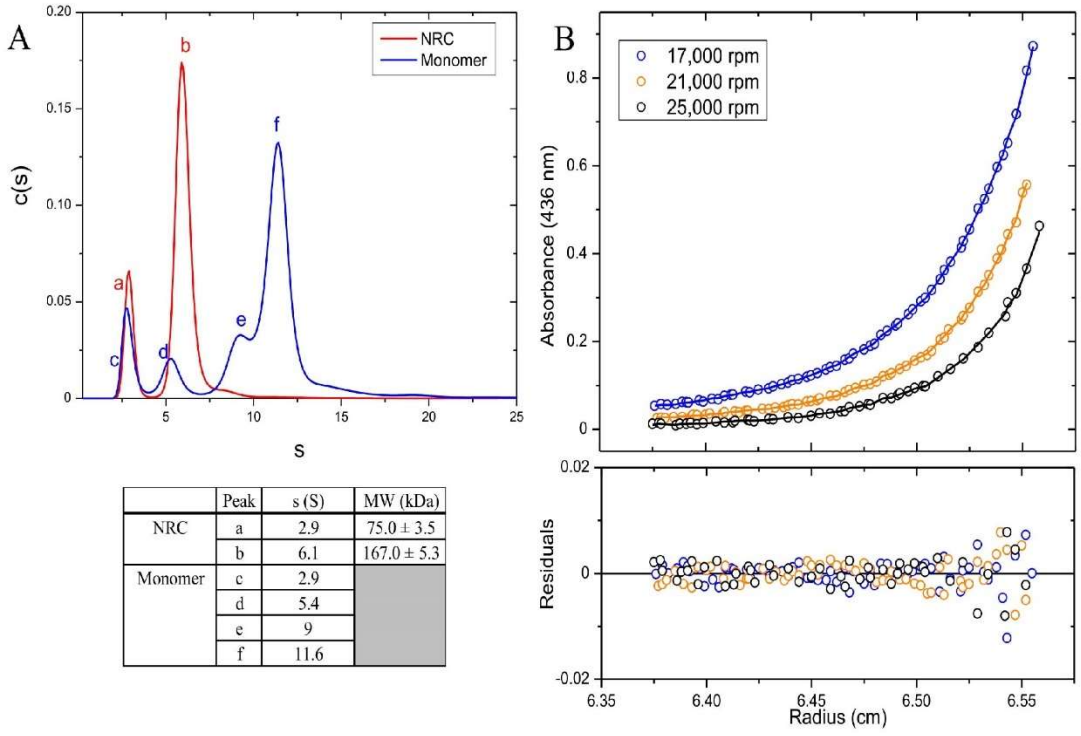

	Peak	s (S)	MW (kDa)
NRC	a	2.9	75.0 ± 3.5
	b	6.1	167.0 ± 5.3
Monomer	c	2.9	
	d	5.4	
	e	9	
	f	11.6	

Figure 2.6 AUC to determine size of NRC and PSII-M (A) Relative distribution of components in Δ*O*-PSII-NRC (red) and Δ*O*-PSII-M (blue) samples based on Svedberg coefficient (S), and (B) MW determination of the NRC complex from sedimentation equilibrium analysis. For experimental and calculation details, see "Materials and Methods."

experiments using AUC (Fig. 2.6A). The NRC sample showed a major species at 6.1 S (peak b), the molecular weight (MW) of which was determined as 167.0 ± 5.3 kDa in a subsequent sedimentation equilibrium experiment (Fig. 2.6B). A minor species at 2.9 S was also observed

(Fig. 2.5A), with MW 75.0 ± 3.5 kDa (Fig. 2.6B), which likely corresponds to dissociated CP47 (76 kDa) and/or CP43 (67 kDa) with their associated cofactors. For MW determination, the sedimentation equilibrium curves were analyzed using a two species fit based on the observation of two species from the sedimentation velocity experiments. The PSII-M sample showed a major species at 11.6 S (peak f), and three minor species at 2.9 S, 5.4 S, and 9.0 S. The MW of the major species was estimated as 436 kDa with a best-fit frictional coefficient ratio of 1.27, comparable to the MW of the PSII monomer determined in a previous study by Zouni and co-workers, using a similar method (42). The three minor species likely represent dissociation products.

2.4.3 The NRC complex lacks a functional reaction center

The absence of the RC proteins in NRC suggests that the complex cannot function as an RC. To test this hypothesis, we used ultrafast time-resolved fluorescence (TRF) measurements on the PSII-M and NRC samples. Both samples were excited at 625 nm, corresponding to a vibronic overtone of the Chl *a* Q_y band, and the Chl *a* fluorescence decay was monitored (Fig. 2.7A and 2.7B, shown as pseudo-color 2D profiles). The profiles revealed substantial differences between the two samples. The initial fluorescence profile of PSII-M, with a fluorescence maximum at ~680 nm, quickly evolved to a broader spectrum associated with another species with emission maximum at ~700 nm, consistent with energy transfer from antennae to a trap (the RC). Fluorescence spectra profiles of Chl *a* in NRC, however, remained relatively constant over time. The differences were further emphasized through kinetic analysis of the TRF data (Fig. 2.7C and 2.7D). Global analysis of the PSII-M and NRC spectra revealed two spectro-kinetic components (EAFS) for each sample (see Materials and Methods for more details). The faster PSII-M and NRC components, with lifetimes of 250 and 330 ps, respectively, resemble each other and correspond to excitation

equilibration within the protein. The slower PSII-M component, with a lifetime of 1.6 ns, was red-shifted and

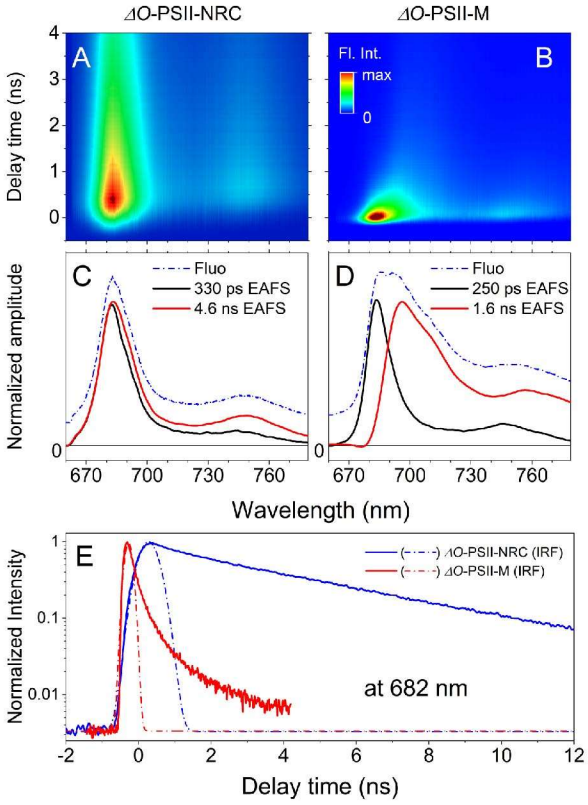

Figure 2.7 Time-resolved fluorescence of ΔO-PSII-NRC and ΔO-PSII-M samples. (A, B) 2D pseudo-color fluorescence decay profiles at 77 K upon excitation at 625 nm. (C, D) Global analysis results of TRF datasets. Dashed profiles (Fluo) correspond to time-integrated spectra and mimic steady-state fluorescence spectra. All profiles were normalized at their maxima for better comparability. (E) Exemplary kinetic traces at 682 nm (maximum of fluorescence emission from CP47/CP43) accompanied with instrument response functions (IRF). Substantial shortening of fluorescence decay of the ΔO-PSII-M sample is associated with rapid excitation energy transfer from antenna into the PSII core (excitation trapping by reaction center). The different signal rise observed in the two traces originates from different temporal resolutions of time windows in which data were collected as demonstrated by IRF. EAFS – evolution associated fluorescence spectra.

reflects excitation-energy transfer from CP47 and CP43 to deep energetic traps in the RC. These PSII-M results closely mimic those obtained for PSII core complexes from the cyanobacterium *Thermosynechococcus vulcanus* under similar conditions (49). The slower NRC component,

however, with a lifetime of 4.6 ns, was very similar to the fast NRC component, suggesting that both originate from the same species. The lifetime of 4.6 ns closely resembled that obtained for isolated CP47 and CP43 proteins (50), implying that no further excitation energy transfer occurs in the NRC complex, and this component corresponds to intrinsic decay of excited Chl *a*. Overall, these results demonstrated that excitation energy in PSII-M that was initially localized on Chl *a* bound to CP47 and CP43, was efficiently transferred to the RC. In contrast, no such RC energy trap exists in the NRC complex, and excitation energy remained localized on CP47 and CP43 until it decayed intrinsically.

2.4.4 NRC accumulates under high-light stress and in the absence of protein synthesis

As NRC is a previously unobserved subcomplex of PSII, we wished to determine whether NRC forms during *de novo* synthesis of PSII or during its repair cycle (Fig. 2.1). This can be accomplished by observing whether NRC accumulates or is depleted under PSII-damaging conditions and following the addition of a protein synthesis inhibitor. Accumulation under such conditions indicates NRC formation during the repair cycle, while depletion indicates formation during *de novo* synthesis. To this end, His47 cultures were treated with either high light (HL, 400 µM photons/m^2.s), low light (LL, 40 µM photons/m^2.s, normal growth conditions), or these conditions with the addition of 20 µg lincomycin (HL+, LL+) to halt protein synthesis. Cells were harvested when the HL+ culture declined to 50% of the initial photosynthetic efficiency following a move to high light and addition of lincomycin (F_v/F_m, SI Appendix, Table S1). PSII was isolated from cultures grown under each of these conditions and PSII samples containing 10 µg Chl *a* were run on a clear native PAGE gel (Figs. 2.7A, 2.8 for actual-color gel scan) to observe differences in NRC abundance. Intensities of each band were analyzed using the LiCOR analysis

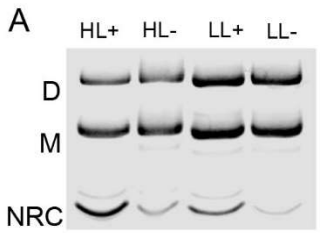

B

	NRC/M	NRC/D
HL+	0.81	1.20
HL-	0.22	0.30
LL+	0.28	0.32
LL-	0.10	0.11

Figure 2.8 Clear Native PAGE of high-light treated PSII samples. (A) Clear Native PAGE of His-CP47-tagged PSII complexes from cultures treated with high light (HL), low light (LL), and with or without (+/-) 20 µg/mL lincomycin. M, PSII monomer; D, PSII dimer. (B) Table of ratios of band intensities from (A) calculated using the LICOR analysis tool.

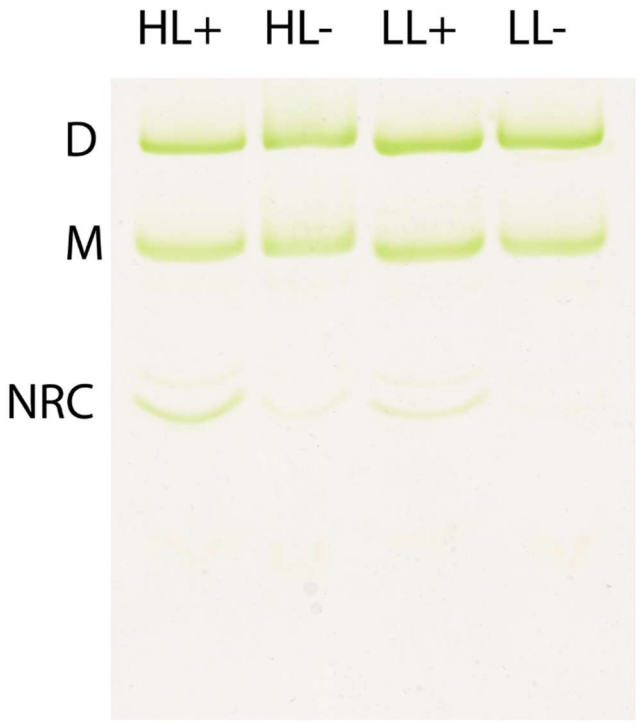

Figure 2.9. Scan of gel imaged in Figure 2.8A. Clear Native PAGE of His-CP47-tagged PSII complexes from cultures treated with high light (HL), low light (LL), and with or without (+/-) 20 µg/mL lincomycin. M, PSII monomer; D, PSII dimer.

tool, and the ratios of NRC/PSII monomer and NRC/PSII dimer were calculated for each condition (Fig. 2.8B). As seen in Fig. 2.8A, the HL+ treated cells have the highest quantity of NRC, and

ratios of NRC/PSII monomer and NRC/PSII dimer that are on average ten times higher than the LL condition. LL+ treated cells follow in highest NRC abundance, with NRC/monomer and dimer ratios close to three times higher than the control LL condition. The HL treated cells have a higher abundance of NRC (NRC/monomer and dimer ratios close to twice as high) than the LL control treatment, but the response is modest compared to those cells with impaired protein synthesis.

2.5 Discussion

In this study, we discovered and characterized the "no-reaction center" (NRC) complex, a PSII subcomplex that contains the inner antenna subunits CP43 and CP47, Psb27, and seven LMM subunits, but is missing the five subunits that comprise the PSII RC: D1, D2, PsbE, PsbF, and PsbI. An assembled complex without all five RC components has not been described before. Through analytical sedimentation experiments, we determined the MW of the NRC complex to be 167.0 ± 5.3 kDa. This value is in between the sum of the apo (153 kDa)- and holo (194 kDa)- masses of the NRC proteins, indicating that some NRC cofactors with D1 or D2 interfaces may be destabilized in their absence. The determined MW is also close to the sum of the apparent masses of the individual CP43 and CP47 pre-complexes (around 180 kDa) measured previously (35). These results are not consistent with the NRC sample comprising a mixture of separate CP43 and CP47 pre-complexes, as each of these pre-complexes have MWs roughly half of the determined MW. NRC is also not a mixture of homodimers of the CP43 and CP47 pre-complexes. Given the respective sizes of the two pre-complexes (35), such dimers would differ in mass by around 40 kDa, not consistent with the observed single, narrow, symmetrical major peak (Fig. 2.6, peak "b") indicating a single species. Homodimers were also not detected during previous characterization of the pre-complexes (35). Overall, the analytical sedimentation results indicate that the NRC

complex is a single species likely composed of a single copy of each of the PSII subunits identified within.

The LMM subunits identified in NRC are consistent with the PSII crystal structures (2, 4, 5) in that all share interfaces with either CP43 or CP47 (except PsbY, which interfaces with another NRC subunit, PsbX). PsbH, PsbL, and PsbT were previously identified in the CP47 pre-complex, and PsbK in the CP43 pre-complex (35), consistent with our results. The presence of Psb27 is reasonable because it binds to CP43 (24, 48, 51), and the absence of Psb28 (Figs. 2.4B, 2.4C) is also reasonable as Psb28 associates closely with PsbE and PsbF (27) and would not be expected to bind in their absence.

In the crystal structures of mature PSII, D1 and D2 bridge the gap in the transmembrane region between CP43 and CP47. In their absence, the NRC subunits do not form a continuous structure, except for a very small overlap between PsbL and PsbT at the cytosolic surface. A significant CP43-CP47 interface would likely be necessary to preserve the structural integrity of this complex and could occur with CP43 and CP47 approaching each other and at least partially closing the gap left by D1 and D2.

To test whether NRC occurs as an intermediate in the PSII repair cycle or as an intermediate in *de novo* PSII synthesis, we exposed His47 cells to high light to induce PSII damage and to lincomycin to stop protein synthesis, both separately and in combination with each other. If NRC were an intermediate in the PSII repair cycle, formed as a result of damage to intact PSII, we expect that it would accumulate in high light, which causes increased PSII damage, and in the absence of protein synthesis, which would otherwise deplete existing NRC as D1 and D2 are re-synthesized and inserted into the complex. Conversely, if NRC were an intermediate in *de novo* PSII synthesis, we expect that NRC levels would remain stagnant or decrease in the absence of protein synthesis,

as combination with newly synthesized D1 and D2 could not take place. Our results showed that NRC increased in abundance by 2.2- and 2.7-fold compared to PSII monomer and dimer, respectively, when His47 cultures were put into high-light conditions damaging to PSII. A similar increase of 2.8- and 2.9-fold compared to monomer and dimer, respectively, was observed upon addition of lincomycin to stop protein synthesis under control low-light conditions. The largest NRC increase, of 8.1- and 10.9-fold compared to monomer and dimer, respectively, occurred when cells were exposed to both high light and the presence of lincomycin (Fig. 2.8A, B). These results are consistent with a model of the PSII lifecycle in which NRC is an intermediate subcomplex in PSII repair and is not consistent with its formation during *de novo* synthesis. Furthermore, as more NRC accumulates in the absence of protein synthesis than in HL alone, we conclude that the NRC subunits are reincorporated into repaired PSII when newly synthesized D1 and D2 become available, depleting the level of NRC in the thylakoid and completing the PSII repair cycle (Fig. 2.10). Our observation that the NRC:dimer ratio increased slightly more than the NRC:monomer ratio in all three conditions is consistent with this model, as photodamaged PSII dimers dissociate into monomers early in the PSII repair cycle.

Assignment of NRC to the repair cycle also helps explain why this complex has not previously been detected. Most studies of PSII subcomplexes have focused on the assembly of PSII, not the intermediates that form following photodamage. Many of these studies used mutants that block assembly before formation of active PSII, e.g. ΔCtpA, ΔD2, ΔCP43, or ΔCP47 strains. This valuable strategy has enabled isolation of numerous *de novo* assembly intermediates, but as active PSII is never formed in these strains, it has precluded the possibility of observing NRC. (48, 52, 53) The currently known steps in the PSII repair process are: 1) dissociation of the extrinsic proteins PsbO, PsbU, PsbV, and PsbQ (22), 2) rebinding of Psb27 (23), 3) monomerization of the

complex (22), 4) an undefined further dissociation step (20), 5) D1 degradation (54-56), 6) insertion of a new D1 copy (14), and 7) PSII reassembly (14). Within this known framework, NRC formation would most logically occupy step 4, the undefined dissociation step, with the damaged Psb27-PSII monomer splitting into RC and NRC components (Fig. 2.10. Note that steps 1-3 are omitted in Figs. 2.10 and 2.1 for clarity). An implication is that D1 (and D2) replacement would occur at the level of the RC complex (Fig. 2.10), not at RC47 as has been previously

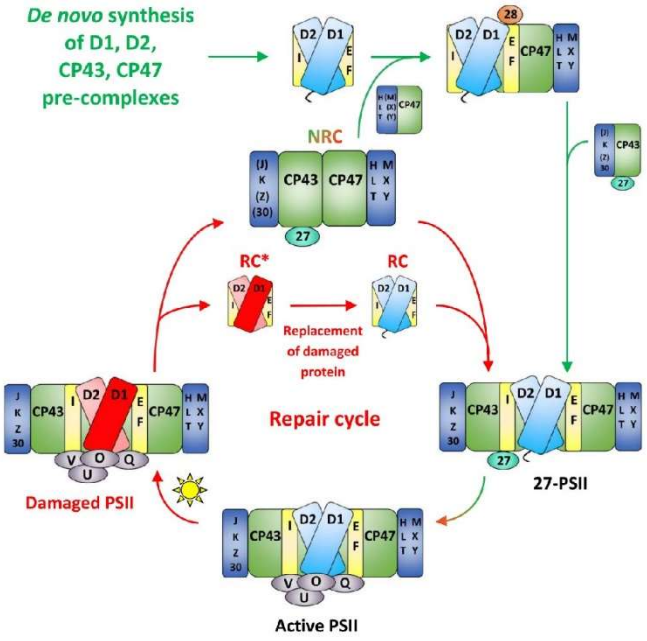

Figure 2.10 Schematic of the PSII life cycle based on previous findings (reviewed in (14, 19, 21, 22) and current results, focusing on the proposed positioning of NRC in the repair cycle. Red arrows, repair cycle steps; red D1, damaged version of D1; light red D2, slightly less frequently damaged version of D2. n a given RC* complex, either D1, D2, or both may be damaged. Several intermediary stages (steps 1-3 in the Discussion section) in the life cycle are omitted for clarity: after damage, PsbO, PsbU, PsbV, and PsbQ dissociate (22), Psb27 rebinds (23), and the complex monomerizes (22) before the proposed NRC formation step. Black text and red-green coloring represent steps common to both *de novo* synthesis and repair.

proposed (Fig. 2.1) (14, 20, 57). Meanwhile, the longer-lived (15) CP43 and CP47 would be sequestered efficiently in one location, ready to be recycled back into PSII after synthesis of a new D1 and/or D2 (15). Dissociation of PSII into RC and NRC complexes following photodamage would allow maximal access for proteases to both D1 and D2, whereas, by interacting closely, CP43 and CP47 would shield each other from such protease attack (58). The recent interesting

finding that PSII can remain stable and fully intact following Mn cluster removal (59) supports the notion that there may be an important efficiency benefit to maintaining a PSII subcomplex, once assembled, in as intact a state as possible, while still allowing for necessary repair to occur.

Damaged PSII is a liability because aberrant PSII photochemistry could result in further oxidative damage to the complex. During PSII assembly, D1 processing is a checkpoint that prevents premature formation of the highly oxidizing Mn cluster, which could result in damage to nearby subunits (47). The dissociation of the extrinsic proteins and the rebinding of Psb27 following photodamage likely achieves the same goal: inactivation of the Mn cluster at a time when it could only cause further damage. The formation of the NRC complex can be understood in a similar manner. In addition to being an efficient disassembly/reassembly mechanism, separating into RC and NRC complexes following initial damage to D1 or D2 could serve a twofold protective purpose: 1) it lowers the total excitation energy reaching the RC by "unplugging" it from the CP47 and CP43 antenna subunits, and 2) it prevents aberrant PSII photochemistry from causing collateral damage to the NRC components, which are unlikely to have been harmed in the initial photodamage event. Future structural studies of the NRC Chl-protein complex are expected to shed light on the dynamic process during the PSII repair cycle.

2.6 Supplementary Dataset Legends

Table S2.1 (separate file). Proteins identified in the bands corresponding to Δ*O*-PSII-M, Δ*O*-NRC, and His47-NRC by LC-MS/MS following in-gel digestion of Δ*O*-PSII and His47-PSII samples.

Table S2.2 (separate file). Proteins identified by LC-MS/MS following in-solution digestion of Δ*O*-PSII-M.

Table S2.3 (separate file). Proteins identified by LC-MS/MS following in-solution digestion of Δ*O*-NRC.

Table S2.4 (separate file). Inclusion list used to fragment intact LMM proteins in Δ*O*-PSII-M and Δ*O*-NRC during MS analysis.

Table S2.5 (separate file). MS/MS fragment ions observed for intact LMM proteins in Δ*O*-PSII-M.

2.7 References

1. Suga M*, et al.* (2015) Native structure of photosystem II at 1.95 A resolution viewed by femtosecond X-ray pulses. *Nature* 517(7532):99-103.
2. Suga M*, et al.* (2017) Light-induced structural changes and the site of O=O bond formation in PSII caught by XFEL. *Nature* 543(7643):131-135.
3. Kupitz C*, et al.* (2014) Serial time-resolved crystallography of photosystem II using a femtosecond X-ray laser. *Nature* 513(7517):261-265.
4. Umena Y, Kawakami K, Shen JR, & Kamiya N (2011) Crystal structure of oxygen-evolving photosystem II at a resolution of 1.9 A. *Nature* 473(7345):55-60.
5. Zouni A*, et al.* (2001) Crystal structure of photosystem II from Synechococcus elongatus at 3.8 A resolution. *Nature* 409(6821):739-743.
6. Young ID*, et al.* (2016) Structure of photosystem II and substrate binding at room temperature. *Nature* 540(7633):453-457.
7. Nanba O & Satoh K (1987) Isolation of a photosystem II reaction center consisting of D-1 and D-2 polypeptides and cytochrome *b*-559. *Proc Natl Acad Sci U S A* 84:109-112.
8. Shi LX, Hall M, Funk C, & Schroder WP (2012) Photosystem II, a growing complex: updates on newly discovered components and low molecular mass proteins. *Biochim Biophys Acta* 1817(1):13-25.
9. Roose JL, Frankel LK, Mummadisetti MP, & Bricker TM (2016) The extrinsic proteins of photosystem II: update. *Planta* 243(4):889-908.
10. Liu H*, et al.* (2014) MS-based cross-linking analysis reveals the location of the PsbQ protein in cyanobacterial photosystem II. *Proc Natl Acad Sci U S A* 111(12):4638-4643.
11. Weisz DA, Gross ML, & Pakrasi HB (2017) Reactive oxygen species leave a damage trail that reveals water channels in Photosystem II. *Sci Adv* 3(11):eaao3013.
12. Kale R*, et al.* (2017) Amino acid oxidation of the D1 and D2 proteins by oxygen radicals during photoinhibition of Photosystem II. *Proc Natl Acad Sci U S A* 114(11):2988-2993.

13. Pospisil P (2016) Production of Reactive Oxygen Species by Photosystem II as a Response to Light and Temperature Stress. *Front Plant Sci* 7:1950.

14. Nickelsen J & Rengstl B (2013) Photosystem II assembly: from cyanobacteria to plants. *Annu Rev Plant Biol* 64:609-635.

15. Yao DC, Brune DC, & Vermaas WF (2012) Lifetimes of photosystem I and II proteins in the cyanobacterium Synechocystis sp. PCC 6803. *FEBS Lett* 586(2):169-173.

16. Komenda J & Masojidek J (1995) Functional and structural changes of the photosystem II complex induced by high irradiance in cyanobacterial cells. *European Journal of Biochemistry* 233:677-682.

17. Christopher DA & Mullet JE (1994) Separate photosensory pathways co-regulate blue light/ultraviolet-A-activated *psb*D-*psb*C transcription and light-induced D2 and CP43 degradation in barley (*Hordeum vulgare*) chloroplasts. *Plant Physiol* 104:1119-1129.

18. Bonisteel EM*, et al.* (2018) Strain specific differences in rates of Photosystem II repair in picocyanobacteria correlate to differences in FtsH protein levels and isoform expression patterns. *PLOS ONE* 13(12):e0209115.

19. Weisz DA, Gross ML, & Pakrasi HB (2016) The Use of Advanced Mass Spectrometry to Dissect the Life-Cycle of Photosystem II. *Front Plant Sci* 7:617.

20. Komenda J, Sobotka R, & Nixon PJ (2012) Assembling and maintaining the Photosystem II complex in chloroplasts and cyanobacteria. *Curr Opin Plant Biol* 15(3):245-251.

21. Heinz S, Liauw P, Nickelsen J, & Nowaczyk M (2016) Analysis of photosystem II biogenesis in cyanobacteria. *Biochim Biophys Acta* 1857(3):274-287.

22. Mabbitt PD, Wilbanks SM, & Eaton-Rye JJ (2014) Structure and function of the hydrophilic Photosystem II assembly proteins: Psb27, Psb28 and Ycf48. *Plant Physiol Biochem* 81:96-107.

23. Grasse N*, et al.* (2011) Role of novel dimeric Photosystem II (PSII)-Psb27 protein complex in PSII repair. *J Biol Chem* 286(34):29548-29555.

24. Liu H, Huang RY, Chen J, Gross ML, & Pakrasi HB (2011) Psb27, a transiently associated protein, binds to the chlorophyll binding protein CP43 in photosystem II assembly intermediates. *Proc Natl Acad Sci U S A* 108(45):18536-18541.

25. Roose JL & Pakrasi HB (2008) The Psb27 protein facilitates manganese cluster assembly in photosystem II. *J Biol Chem* 283(7):4044-4050.

26. Dobakova M, Sobotka R, Tichy M, & Komenda J (2009) Psb28 protein is involved in the biogenesis of the photosystem II inner antenna CP47 (PsbB) in the cyanobacterium Synechocystis sp. PCC 6803. *Plant Physiol* 149(2):1076-1086.

27. Weisz DA*, et al.* (2017) Mass spectrometry-based cross-linking study shows that the Psb28 protein binds to cytochrome b559 in Photosystem II. *Proc Natl Acad Sci U S A* 114(9):2224-2229.

28. Bricker TM, Morvant J, Masri N, Sutton HM, & Frankel LK (1998) Isolation of a highly active Photosystem II preparation from *Synechocystis* 6803 using a histidine-tagged mutant of CP 47. *Biochim Biophys Acta* 1409:50-57.

29. Kashino Y*, et al.* (2002) Proteomic analysis of a highly active Photosystem II preparation from the cyanobacterium *Synechocystis* sp. PCC 6803 reveals the presence of novel polypeptides. *Biochemistry* 41:8004-8012.

30. Kashino Y, Koike H, & Satoh K (2001) An improved sodium dodecyl sulfate-polyacrylamide gel electrophoresis system for the analysis of membrane protein complexes. *Electrophoresis* 22:1004-1007.

31. Kashino Y*, et al.* (2002) Low-molecular-mass polypeptide components of a Photosystem II preparation from the thermophilic cyanobacterium *Thermosynechococcus vulcanus*. *Plant Cell Physiol* 43:1366-1373.

32. Wittig I, Karas M, & Schagger H (2007) High resolution clear native electrophoresis for in-gel functional assays and fluorescence studies of membrane protein complexes. *Mol Cell Proteomics* 6(7):1215-1225.

33. Bern M, Kil YJ, & Becker C (2012) Byonic: Advanced peptide and protein identification software. *Curr Protoc Bioinformatics* CHAPTER: Unit13.20.

34. Zhang J*, et al.* (2012) PEAKS DB: de novo sequencing assisted database search for sensitive and accurate peptide identification. *Mol Cell Proteomics* 11(4).

35. Boehm M*, et al.* (2011) Investigating the early stages of photosystem II assembly in Synechocystis sp. PCC 6803: isolation of CP47 and CP43 complexes. *J Biol Chem* 286(17):14812-14819.

36. Zhang Z & Marshall AG (1998) A Universal Algorithm for Fast and Automated Charge State Deconvolution of Electrospray Mass-to-Charge Ratio Spectra. *Journal of the American Society for Mass Spectrometry* 9:225-233.

37. Niedzwiedzki DM, Jiang J, Lo CS, & Blankenship RE (2013) Low-temperature spectroscopic properties of the peridinin-chlorophyll *a*-protein (PCP) complex from the coral symbiotic dinoflagellate *Symbiodinium*. *Journal of Physical Chemistry B* 117:11091-11099.

38. Hofrichter J & Henry ER (1992) Singular value decomposition: Application to analysis of experimental data. *Methods in Enzymology* 210:129-192.

39. van Stokkum IH, Larsen DS, & van Grondelle R (2004) Global and target analysis of time-resolved spectra. *Biochim Biophys Acta* 1657(2-3):82-104.

40. Kozlov AG, Shinn MK, Weiland EA, & Lohman TM (2017) Glutamate promotes SSB protein-protein interactions via intrinsically disordered regions. *Journal of Molecular Biology* 429:2790-2801.

41. Schuck P & Dam J (2004) Calculating sedimentation coefficient distributions by direct modeling of sedimentation velocity concentration profiles. *Methods in Enzymology* 384:185-212.

42. Zouni A*, et al.* (2005) Size determination of cyanobacterial and higher plant Photosystem II by gel permeation chromatography, light scattering, and ultracentrifugation. *Biochemistry* 44:4572-4581.

43. Niedziela-Majka A, Maluf NK, Antony E, & Lohman TM (2011) Self-Assembly of *Escherichia coli* MutL and its complexes with DNA. *Biochemistry* 50:7868-7880.

44. Vistica J*, et al.* (2004) Sedimentation equilibrium analysis of protein interactions with global implicit mass conservation constraints and systematic noise decomposition. *Anal Biochem* 326:234-256.

45. Schneider CA, Rasband WS, & Eliceiri KW (2012) NIH Image to ImageJ: 25 years of image analysis. *Nat Methods* 9:671-675.

46. Rögner M, Chishold DA, & Diner BA (1991) Site-directed mutagenesis of the *psb*C gene of Photosystem II: Isolation and functional characterization of CP43-less Photosystem II core complexes. *Biochemistry* 30:5387-5395.

47. Liu H, Roose JL, Cameron JC, & Pakrasi HB (2011) A genetically tagged Psb27 protein allows purification of two consecutive photosystem II (PSII) assembly intermediates in Synechocystis 6803, a cyanobacterium. *J Biol Chem* 286(28):24865-24871.

48. Komenda J*, et al.* (2012) The Psb27 assembly factor binds to the CP43 complex of photosystem II in the cyanobacterium Synechocystis sp. PCC 6803. *Plant Physiol* 158(1):476-486.

49. Shibata Y, Nishi S, Kawakami K, Shen JR, & Renger T (2013) Photosystem II does not possess a simple excitation energy funnel: time-resolved fluorescence spectroscopy meets theory. *J Am Chem Soc* 135(18):6903-6914.

50. Casazza AP, Szczepaniak M, Muller MG, Zucchelli G, & Holzwarth AR (2010) Energy transfer processes in the isolated core antenna complexes CP43 and CP47 of photosystem II. *Biochim Biophys Acta* 1797(9):1606-1616.

51. Cormann KU, Moller M, & Nowaczyk MM (2016) Critical Assessment of Protein Cross-Linking and Molecular Docking: An Updated Model for the Interaction Between Photosystem II and Psb27. *Front Plant Sci* 7:157.

52. Boehm M*, et al.* (2012) Subunit composition of CP43-less photosystem II complexes of Synechocystis sp. PCC 6803: implications for the assembly and repair of photosystem II. *Philos Trans R Soc Lond B Biol Sci* 367(1608):3444-3454.

53. Komenda J*, et al.* (2004) Accumulation of the D2 protein is a key regulatory step for assembly of the photosystem II reaction center complex in Synechocystis PCC 6803. *J Biol Chem* 279(47):48620-48629.

54. Komenda J*, et al.* (2006) The FtsH protease slr0228 is important for quality control of Photosystem II in the thylakoid membrane of *Synechocystis* sp. PCC 6803. *Journal of Biological Chemistry* 281:1145-1151.

55. Sacharz J*, et al.* (2015) Sub-cellular location of FtsH proteases in the cyanobacterium *Synechocystis* sp. PCC 6803 suggests localised PSII repair zones in the thylakoid membranes. *Molecular Microbiology* 96:448-462.

56. Boehm M*, et al.* (2012) Subunit organization of a *Synechocystis* hetero-oligomeric thylakoid FtsH complex involved in Photosystem II repair. *Plant Cell* 24:3669-3683.

57. Nixon PJ, Barker M, Boehm M, de Vries R, & Komenda J (2005) FtsH-mediated repair of the photosystem II complex in response to light stress. *J Exp Bot* 56(411):357-363.

58. Krynicka V, Shao S, Nixon PJ, & Komenda J (2015) Accessibility controls selective degradation of photosystem II subunits by FtsH protease. *Nat Plants* 1:e15168.

59. Zhang M*, et al.* (2017) Structural insights into the light-driven auto-assembly process of the water-oxidizing Mn_4CaO_5-cluster in photosystem II. *eLIFE* 6:1-20.

Chapter 3

A reversibly induced CRISPRi system targeting Photosystem II in the cyanobacterium *Synechocystis* sp. PCC 6803

This chapter is adapted, with permission, from:

Deng Liu*, Virginia M. Johnson*, and Himadri B. Pakrasi (2020) A Reversibly Induced CRISPRi System Targeting Photosystem II in the Cyanobacterium Synechocystis sp. PCC 6803. *ACS Synth. Bio.* 9 (6), 1441-1449. DOI: 10.1021/acssynbio.0c00106

*co-first authors

Chapter Contributions: Data presented in Figures 3.1C, 3.3 C,E, and 3.4 B,C were generated by VMJ.

3.1 Summary

The cyanobacterium *Synechocystis* sp. PCC 6803 (S6803) is used as a model organism to study photosynthesis, as it can utilize glucose as the sole carbon source to support its growth under heterotrophic conditions. CRISPR interference (CRISPRi) has been widely applied to repress the transcription of genes in a targeted manner in cyanobacteria. However, a robust and reversible induced CRISPRi system has not been explored in S6803 to knock down and recover the expression of a targeted gene. In this study, we built a tightly controlled chimeric promoter, $P_{rhaBAD\text{-}RSW}$, in which a theophylline responsive riboswitch was integrated into a rhamnose-inducible promoter system. We applied this promoter to drive the expression of ddCpf1 (DNase-dead Cpf1 nuclease) in a CRISPRi system and chose the PSII reaction center gene *psbD* (D2 protein) to target for repression. *psbD* was specifically knocked down by over 95% of its native expression, leading to severely inhibited Photosystem II activity and growth of S6803 under photoautotrophic conditions. Significantly, removal of the inducers rhamnose and theophylline reversed repression by CRISPRi. Expression of PsbD recovered following release of repression, coupled with increased Photosystem II content and activity. This reversibly induced CRISPRi system in S6803 represents a new strategy for study of the biogenesis of photosynthetic complexes in cyanobacteria.

3.2 Introduction

Cyanobacteria are oxygenic photosynthetic prokaryotes that can use light energy to fuel all intracellular biological processes. Cyanobacteria have been used as hosts to study photosynthetic processes due to their relative ease of genetic manipulation as compared to eukaryotic phototrophs. *Synechocystis* sp. PCC 6803 (S6803) has been used as a model cyanobacterial organism for decades (1), and many genetic tools and elements have been adapted and developed for this strain, which facilitate its genetic modification (2). Importantly, S6803 can use glucose as a carbon source to support heterotrophic growth, a desirable trait for the study of genes essential for photosynthesis.

Photosystem II (PSII) is a unique light-driven enzyme that oxidizes water into molecular oxygen, providing oxygen and the reducing equivalents to fix carbon, powering much of life on earth.(3, 4) PSII is an approximately 20 subunit membrane-protein complex. It binds numerous pigments and metal cofactors, as well as additional proteins that aid in assembly of the complex.(5) PSII has a modular architecture, consisting of a reaction-center "core" module where primary charge separation occurs and two chlorophyll-binding "antenna" modules. The reaction center consists of the D1 and D2 protein subunits that bind the primary electron-transfer cofactors, along with several lower-molecular weight structural proteins. The antenna modules are based around the chlorophyll-binding protein subunits CP43 and CP47 and associated lower molecular weight structural proteins. A catalytic tetra-manganese cofactor is liganded primarily by the D1 protein, with one ligand supplied by the CP43 protein.

PSII, due to its demanding photochemistry, undergoes frequent photo-oxidative damage and must be assembled and repaired in an efficient and tightly regulated manner to maintain high photosynthetic activity.(6-12) The D1 and D2 reaction center proteins are the most frequently

damaged, as they are closest in proximity to the high-energy electron-transfer reactions taking place.(12-14) To repair the damaged complex while maintaining the undamaged and expensive-to-synthesize chlorophyll-protein antenna modules, D1 and D2 are selectively removed and replaced by newly synthesized protein copies. This process of continual assembly and repair is called the PSII lifecycle, and has been extensively studied in mutants lacking key proteins in photosynthetic processes that are halted at various stages in PSII assembly (15-18). However, the lifecycle has been difficult to study as a complete cycle in the same organism due to the low abundance of intermediate complexes in photosynthetic cells, and the simultaneous presence of various PSII intermediate complexes at different stages of the lifecycle

CRISPR/Cas (clustered regularly interspersed palindromic repeats/CRISPR-associated protein) technology has revolutionized the biotechnology field as a technique to precisely edit both eukaryotic and prokaryotic genomes, including cyanobacteria (19-22). As a complement to CRISPR/Cas technology, CRISPR interference (CRISPRi) utilizes a nuclease-deficient Cas protein (dCas protein) to bind to a target sequence but not introduce a double-stranded break. A CRISPRi system contains a dCas protein and a guide RNA (gRNA), which together form a dCas-gRNA ribonucleoprotein complex that binds to a genomic site complementary to the gRNA sequence. By binding to its target site, the dCas-gRNA complex blocks transcription and inhibits the expression of specific genes (23). CRISPRi, utilizing either dCas9 or ddCpf1 (DNase-dead Cpf1, also known as dCas12a), has been applied to several species of cyanobacteria (19, 24-28). However, only dCas9-CRISPRi systems have been tested for regulation of genes in *Synechocystis* 6803 (24, 29).

To dynamically and precisely regulate the expression of target genes, a CRISPRi system driven by a tightly controlled inducible promoter is of great interest. For *Synechocystis* 6803, many

inducible promoters have been characterized (30-32), but only the anhydrotetracycline (aTc)-inducible promoter has been applied to CRISPRi in S6803 (33). This TetR-regulated inducible system is challenging because aTc is light degradable, which leads to unreliable performance under phototrophic conditions. The rhamnose responsive promoter P_{rhaBAD} has been shown to be a robust and inducible system in S6803. This promoter uses the *E. Coli* transcription factor RhaS as the regulator (32, 34). In this study, we used and modified the P_{rhaBAD} promoter to drive expression of the ddCpf1 protein for CRISPRi, as the ddCpf1 protein has been shown to have lower toxicity in cyanobacteria than dCas9 (21, 22). We added a riboswitch to construct a tightly controlled promoter cassette that showed titratable behavior over a broad range of expression. When this inducible promoter is applied to our CRISPRi system, expression of the targeted gene *psbD* (encoding for D2 protein of Photosystem II) is reduced by over 95% with inducers added, while no repression was observed without inducers. Importantly, recovery of D2 expression was detected after release of CRISPRi repression by washing out inducers. We knocked down key PSII proteins through CRISPRi to almost eliminate formation of Photosystem II and then recovered the formation of the photosystem in its native milieu. Our system is an invaluable resource to study the PSII life cycle in a targeted manner and represents a new framework for studying *de novo* assembly of photosystems.

3.3 Results

3.3.1 Repression of *psbD* genes in *Synechocystis* 6803 by CRISPRi.

The plasmid pCRISPR i-D2 was constructed, using P_{rhaBAD} to drive transcription of both *ddcpf1* and a gRNA targeted to the *psbD* genes (Figure 3.1A and Table S3.1). PsbD (D2) is a structural part of the core PSII reaction center (18), and essential for photoautotrophy. In *Synechocystis* 6803, there are two *psbD* genes, *psbD1* and *psbD2*, which encode identical proteins but have slightly different nucleotide sequences. The site targeted on both *psbD* genes has the same sequence in both (the PAM sequence TTG is 7 nucleotides behind the start codon), so both *psbD* genes will be targeted by the same gRNA. Furthermore, *psbD* shares an operon with and is directly upstream of the *psbC* gene, which codes for the CP43 protein (Figure 3.1A), so with one gRNA, we expect to observe repression of both *psbD* genes and *psbC*.

After transfer of pCRISPR i-D2 (Figure S1) into wild type (WT) of *Synechocystis* 6803, we observed growth under autotrophic conditions (Figure 3.1B). WT and the CK01 control strain (CRISPRi plasmid with gRNA targeted to *eyfp*) grew similarly. However, growth of CRISPRi-D2 was impaired compared to WT, indicating that PSII is impaired in this strain even under un-induced conditions, and that P_{rhaBAD} drives expression of ddCpf1 even without the addition of rhamnose. Conversely, in the cells induced with 2 g/L rhamnose, growth was not completely abolished, indicating that there is not full repression of PSII genes by CRISPRi in the induced strain, even though the growth rate is slower than the culture without rhamnose (Figure 3.1B). Intracellular protein levels of D2 and CP43 as measured by western blot were consistent with growth phenotypes. About 50% of WT D2 and CP43 protein levels were detected in the uninduced CRISPR i-D2 strain (Figure 3.1C) and about 20% of D2 and CP43 protein levels were observed

in the CRISPR i-D2 strain with added rhamnose. These results show that the P_{rhaBAD} promoter is not tightly regulated nor is it strong enough to support full repression.

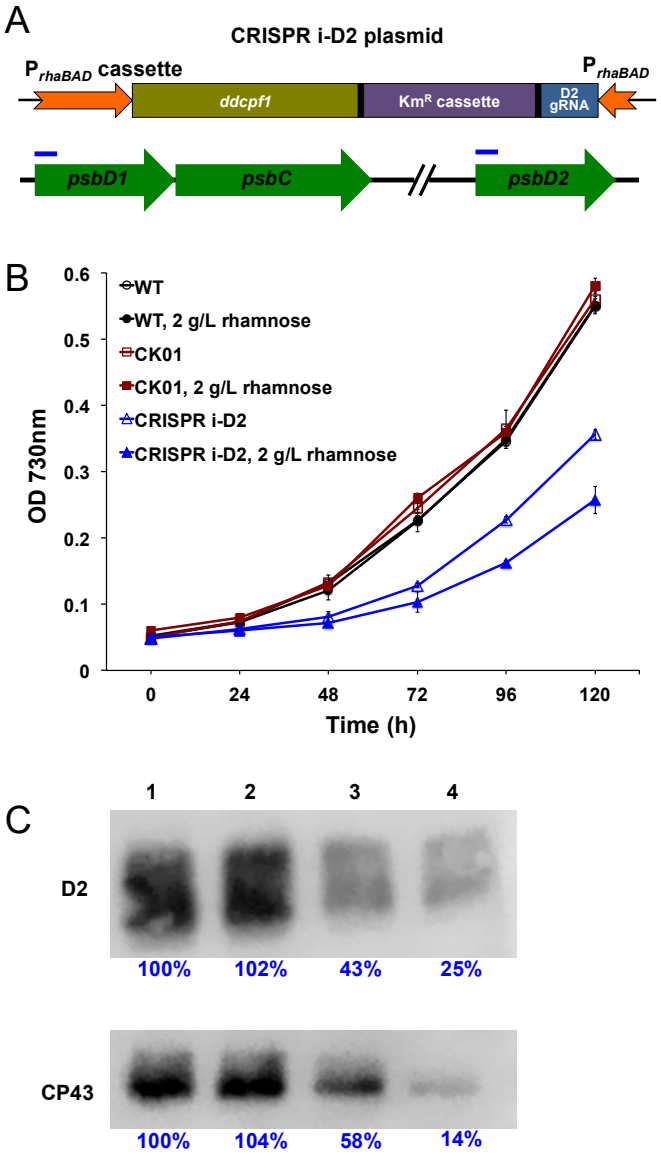

Figure 3.1 Repressing the expression of the *psbD* gene in *Synechocystis* 6803 through CRISPRi. (A) Diagram of CRISPRi system on the replicating plasmid pRSF1010. Promoters are shown as orange arrows, while *ddcpf1* gene and gRNA part are yellow and blue rectangles, respectively. Terminators are shown as short black rectangles surrounding the antibiotics resistance gene cassette. The targeting sites of gRNA to the *psbD* genes are indicated by blue bars. (B) Growth curves of *Synechocystis* 6803 strains cultured in BG11 medium, shaking in flask under 30°C with light intensity 30 μmol photons m^{-2} s^{-1}. CRISPR i-D2 is the strain containing the CRISPRi plasmid with gRNA targeting to *psbD* genes. CK01 is the control strain containing the CRISPRi plasmid but with the gRNA targeting to the *eyfp* gene. 2 g/L rhamnose was added to the culture as the inducer to promote the transcription of *ddcpf1* and gRNA. Error bars represent the standard deviations observed from at least three independent experiments. (C) Expression levels of D2 and CP43 detected by western blot. Lane 1 to 4 represent loading 20 μg of total membrane

proteins extracted from WT, CK01, CRISPR i-D2, and CRISPR i-D2 with 2 g/L rhamnose, respectively. Blue percentages are the relative blot intensities for each protein band.

To confirm that the P_{rhaBAD} promoter has leaky expression, we placed the P_{rhaBAD} cassette in front of the EYFP coding gene in *Synechocystis* 6803 to make the plasmid pRhaBAD-eyfp (Figure S2). EYFP fluorescence was compared to a control strain CK3068 (35), in which the promoter in front of *eyfp* is removed. We observed a 2 to 2.5-fold higher level of fluorescence over the CK3068 strain in the uninduced culture (Figure S2). This directly confirmed that the P_{rhaBAD} cassette as utilized here does not have tight control over expression of downstream genes. A reason might be the promoter P_{lacOI} we use to drive the regulator protein RhaS in the cassette (Figure S2). RhaS is the regulator for the rhamnose responsive system, and its expression level is a key factor for the RhaBAD promoter to control downstream gene(s) (36). The promoter used here might lead to an unbalanced intracellular level of the RhaS protein as compared with that used by Kelly et. al (34).

Ideally, the CRISPRi system would maintain full photosynthetic activity under un-induced conditions, while being repressed nearly 100% in an induced condition, to become photoautotrophic and non-photoautotrophic in each state, respectively. This would allow us to observe complete *de novo* assembly of Photosystem II.

3.3.2 Construction of a chimeric promoter optimized the performance of the P_{rhaBAD} promoter.

To tighten the control and improve the strength of the promoter P_{rhaBAD}, we switched out its ribosome binding sequence (RBS) for an RBS containing the theophylline responsive riboswitch (RSW), which has been effective in controlling the translation of downstream genes in cyanobacteria (37, 38). We used the riboswitch sequence ‘E’ from Ma et. al (37) (Table S3.1). We

call this new promoter $P_{rhaBAD\text{-}RSW}$ and placed the EYFP coding gene under its control to make the $P_{rhaBAD\text{-}RSW}$-EYFP strain (Figure 3.2A).

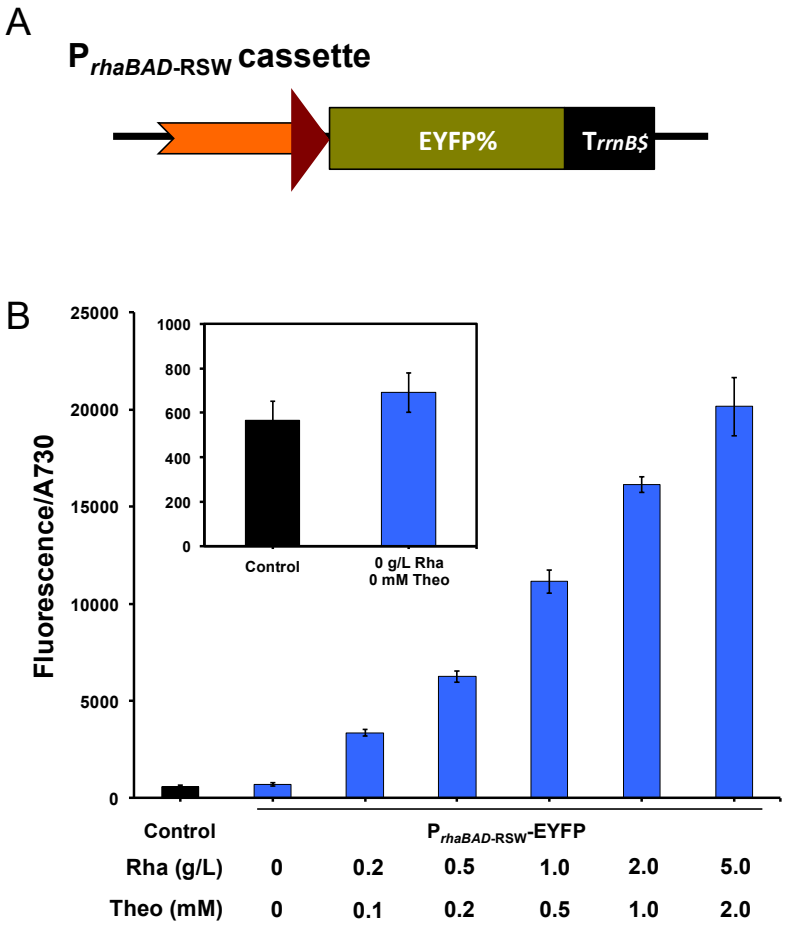

Figure 3.2 Adding a theophylline responsive riboswitch (RSW) optimizes the inducible promoter system. (A) Diagram of the $P_{rhaBAD\text{-}RSW}$ cassette driving the expression of EYFP on the replicating plasmid pRSF1010. The riboswitch is shown in red triangle, switching the RBS of promoter P_{rhaBAD}, which is shown in orange arrow. (B) Expression of reporter gene coding for EYFP driven by $P_{rhaBAD\text{-}RSW}$. Fluorescence data were normalized to optical density at 730 nm. Control is the CK3068 strain containing the plasmid with EYFP encoding gene but without any promoters to drive it. Rhamnose (Rha) and theophylline (Theo) were added to the culture with the concentrations as indicated. The inset panel magnifies the control and un-induced strains. Strains were cultured in BG11 medium, shaking in flask under 30°C with light intensity 30 µmol photons m^{-2} s^{-1}. Samples were collected after 96 hours culture for EYFP assay. Error bars represent the standard deviations observed from at least three independent experiments.

Cell samples of $P_{rhaBAD\text{-}RSW}$-EYFP strain were collected for fluorescence assay after 96 hours of growth in BG11 medium under various inducer concentrations. Fluorescence of the culture without inducers was not significantly different from that of the control strain CK3068

(Figure 2B), which indicated that there is not leaky expression from $P_{rhaBAD\text{-RSW}}$. Fluorescence intensity increased with the concentration of inducers up to 5 g/L rhamnose and 2 mM theophylline, with a 120-fold difference between the uninduced culture and the culture with the highest concentrations of inducers (Figure 2B). Additionally, we tested the effect of adding either inducer at a time on the expression of the *eyfp* gene. We observed that adding only rhamnose achieved 90% of the fluorescence level as adding both inducers (Figure S3), indicating that activation by the chimeric promoter occurs mainly on the transcriptional level, and the riboswitch primarily prevents un-induced expression. All above results suggested that $P_{rhaBAD\text{-RSW}}$ is a tightly controllable and titratable promoter cassette with a wide induction range. We applied $P_{rhaBAD\text{-RSW}}$ to drive the expression of *ddcpf1* in our CRISPRi system in subsequent experiments.

3.3.3 Tightly controlled expression of D2 and CP43 by the CRISPRi$_{RSW}$ system

We constructed a new plasmid applying the $P_{rhaBAD\text{-RSW}}$ promoter to control the expression of *ddcpf1* and containing the same gRNA sequence targeting to *psbD* genes, named as the pCRISPR i$_{RSW}$-D2 plasmid (Figure 3A). After transfer into WT *Synechocystis* 6803, the CRISPR i$_{RSW}$-D2 strain grew similarly to WT under photoautotrophic conditions without inducers. When 5 g/L rhamnose and 2 mM theophylline were added, growth of the CRISPR i$_{RSW}$-D2 strain was severely inhibited under autotrophic conditions (Figure 3B). This growth phenotype indicates that PSII is fully active in the un-induced strain, while has low to no activity when the strain is induced. To further analyze CRISPR i$_{RSW}$-D2, subsequent experiments are performed with the addition of 10g/L glucose to the growth medium.

If PSII content is reduced by the CRISPRi$_{RSW}$ system, then we expect PSII activity to be lower in cells cultured with inducers than without inducers. We used a PAM fluorometer to assay the Fv/Fm, or PSII quantum yield, of cultures. The ratio Fv/Fm is a relative measure of PSII

activity in cells, and the higher the value, the more functional PSII is present. F_V (variable fluorescence) represents the difference between F_m (maximal fluorescence) and F_0 (background fluorescence) and can be attributed to fluorescence arising directly from active PSII reaction centers.(39) The Fv/Fm of the CRISPR i_{RSW}-D2 strain decreased with increased concentrations of inducers (Figure 3C). At the highest concentration of inducers, 5 g/L rhamnose and 2 mM theophylline, the Fv/Fm is 18% of that of the un-induced culture. The above results indicate that, consistent with control of EYFP by CRISPRi$_{RSW}$, control of PSII content is titratable by our CRISPRi$_{RSW}$ system.

To check the specificity of CRISPR i_{RSW}-D2 and quantify the level of repression, both semi-quantitative RT-PCR and quantitative PCR (q-PCR) were performed on WT, the CK02 control strain (containing the CRISPRi$_{RSW}$ plasmid with gRNA targeted to *eyfp*), and the CRISPR i_{RSW}-D2 strain. In addition to the targeted genes *psbD* (D2) and *psbC* (CP43), the Photosystem I structural gene *psaA* and PSII reaction center genes *psbA* (D1) and *psbB* (CP47) were assayed as transcriptional controls. Both RT-PCR and q-PCR showed that no difference was observed between the three strains under photoautotrophic, uninduced conditions for all 5 genes (Figure S4 and S5). Because the CRISPR i_{RSW}-D2 strain does not grow when induced under photoautotrophic conditions in BG11, samples were collected only from WT, CK02, and the un-induced CRISPR i_{RSW}-D2 strain after 7 days growth under this condition.

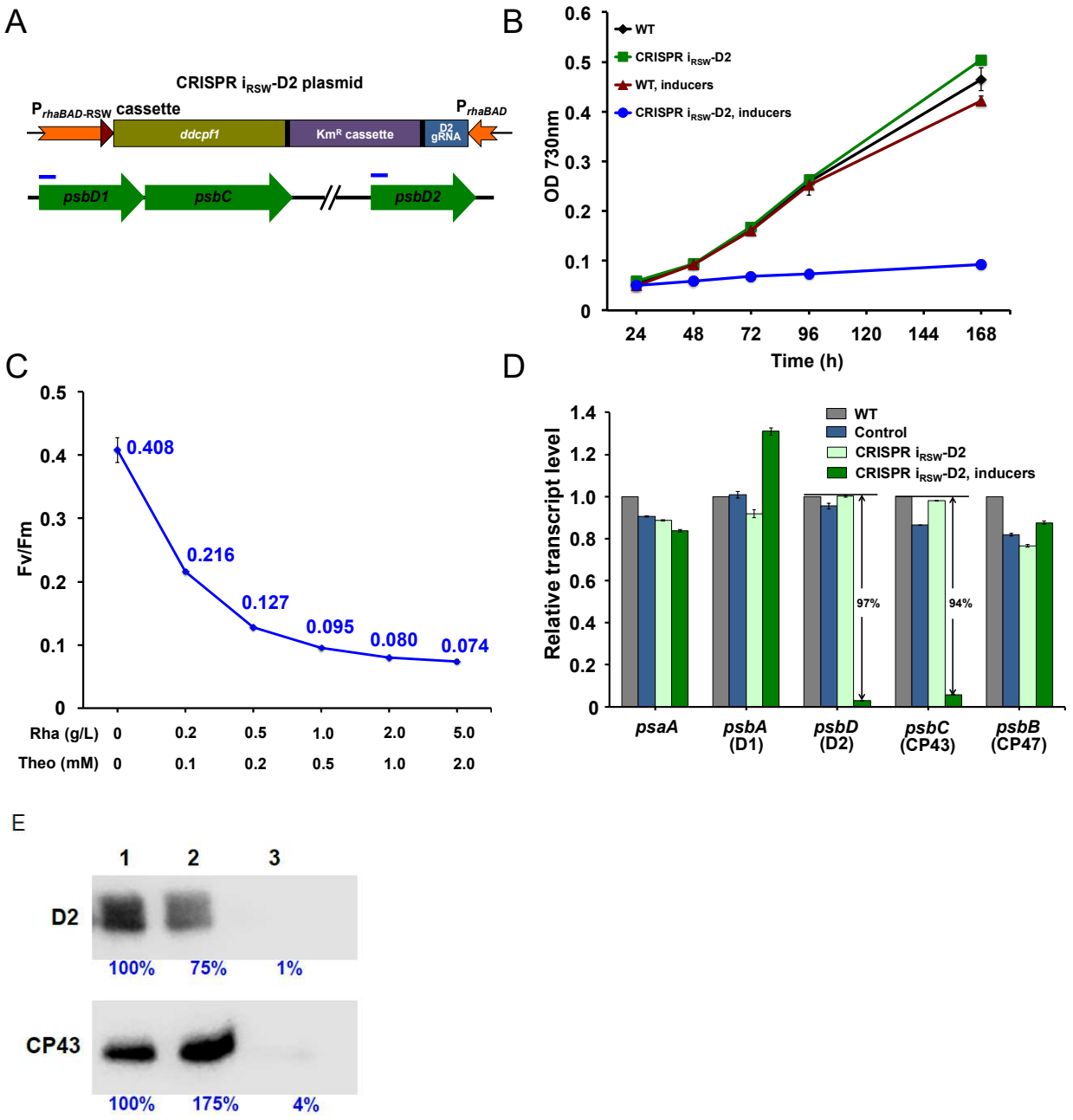

Figure 3.3. Repressing the expression of D2 and CP43 encoding genes by the inducible CRISPR i$_{RSW}$ system. (A) Diagram of CRISPR i$_{RSW}$ system on the replicating plasmid pRSF1010. Promoters are shown in orange, the riboswitch in red triangle, and *ddcpf1* gene and gRNA are in yellow and blue, respectively. The targeting sites of gRNA to the *psbD* genes are indicated by blue bars. Terminators are shown as short black rectangles surrounding the antibiotics resistance gene cassette. (B) Growth curves of *Synechocystis* 6803 strains cultured in BG11 medium. The strain containing the CRISPR i$_{RSW}$ system with the gRNA targeting to *psbD* genes was labeled as CRISPR i$_{RSW}$-D2. (C) The Fv/Fm values correspond to inducer concentrations. Rhamnose (Rha) and theophylline (Theo) were added to the culture with the concentrations indicated. All strains were cultured in BG11 medium with 10 g/L glucose and sampled for Fv/Fm assay when OD 730nm reached 1.0-1.5. (D) Transcriptional levels of photosystem genes quantified by q-PCR. Cell samples were collected from the culture in BG11 medium with 10 g/L glucose when OD 730nm reached 1.0-1.5, and total RNA was extracted for analysis. (E) Protein levels of D2 and CP43 detected by western blot. Lane 1 to 3 represent loading 20 μg of total membrane proteins extracted from cell samples of control, CRISPR i$_{RSW}$-D2,

and CRISPR i_{RSW}-D2 with inducers, respectively. Blue numbers are the relative blot intensities of corresponding proteins. Cell samples were collected when OD 730nm reached 1.0-1.5 from the culture in BG11 medium with 10 g/L glucose. Error bars in the figure represent the standard deviations observed from at least three independent experiments. Except where notified, 5 g/L rhamnose and 2 mM theophylline were added as inducers to the culture. Control is the CK02 strain containing the CRISPR i_{RSW} plasmid but with the gRNA targeting to the *eyfp* gene. Cells are cultured in flask shaking under 30°C with light intensity 30 μmol photons m^{-2} s^{-1}.

However, when the strains were grown in BG11 medium with glucose, the *psbD* and *psbC* genes in the induced CRISPR i_{RSW}-D2 strain showed 97% and 94% decrease in transcription, respectively (Figure 3D and Figure S4). Transcription of the *psaA* gene and the *psbB* gene (CP47) of PSII were unchanged, indicating a specific transcriptional response to induction of CRISPRi. Interestingly, *psbA*, which codes for the PSII protein D1, was up-regulated around 30% under induced conditions, indicating that its transcription is up-regulated in response to severely inhibited photosynthesis as a compensation mechanism, as the D1 protein is the most frequently damaged and replaced under normal and photo-inhibitory conditions.(12) Intracellular protein levels of D2 and CP43 as measured by western blot are consistent with the mRNA levels. D2 and CP43 are reduced to 1% and 4% of un-induced levels, respectively, in the induced samples (Figure 3E).

The above results show that our $CRISPRi_{RSW}$ system is a powerful tool to tightly and specifically control the expression of target genes over a broad range and in a titratable way in *Synechocystis* 6803. Because there is no expression of ddCpf1 without inducers, and expression of target genes is reduced by over 90% with inducers added, it is an ideal system to study the recovery process after release of repression.

3.3.4 Release of CRISPRi repression allows recovery of the expression of D2 and CP43 proteins.

The $CRISPRi_{RSW}$ system effectively knocks down D2 and PSII activity and is tightly regulated. However, to study Photosystem II assembly we require relief of this inhibition, to allow PSII to rebuild following repression. We did further experiments to observe the recovery of targeted genes

after release of the CRISPRi induction. To test whether PSII can fully recover in the CRISPR i_{RSW}-D2 strain, the CRISPR i_{RSW}-D2 strain was cultured in BG11 medium with glucose and inducers. When the OD730 nm reached 2.0, cells were washed twice and re-suspended in fresh BG11 medium at a 20-fold dilution to OD730 nm of 0.1 (time point 0). During the recovery process, cells were collected to verify the *de novo* synthesis of D2 and CP43 proteins, as well as PSII.

After release of repression, we first checked the transcription of *psbD* and *psbC* through q-PCR. Samples were collected over a time course, and we observed the gradual increase of transcript levels with time, reaching around 40% of the WT mRNA level after 8 hours and 100% after 96 hours (Figure 4A). Two phases of recovery were observed. In the first phase, the initial 24 hours, transcript level increases from 5% to 50% of WT level. This is followed by a second, slower phase over the next 72 hours when transcript levels increase back to 100%. We also monitored the Fv/Fm increase over time (Figure 4B) following release of inhibition, which showed accumulation of active PSII in cells. Two phases of recovery were also observed for Fv/Fm. The first phase occurs over day 0 to day 3, during which the Fv/Fm value increased from 0.07 to 0.18, which was 1.5-fold increase in 3 days, while in the second phase Fv/Fm increased slowly and linearly up to 0.35 over the following 13 days, which increased another fold to finally reach the level in WT (Figure 4B).

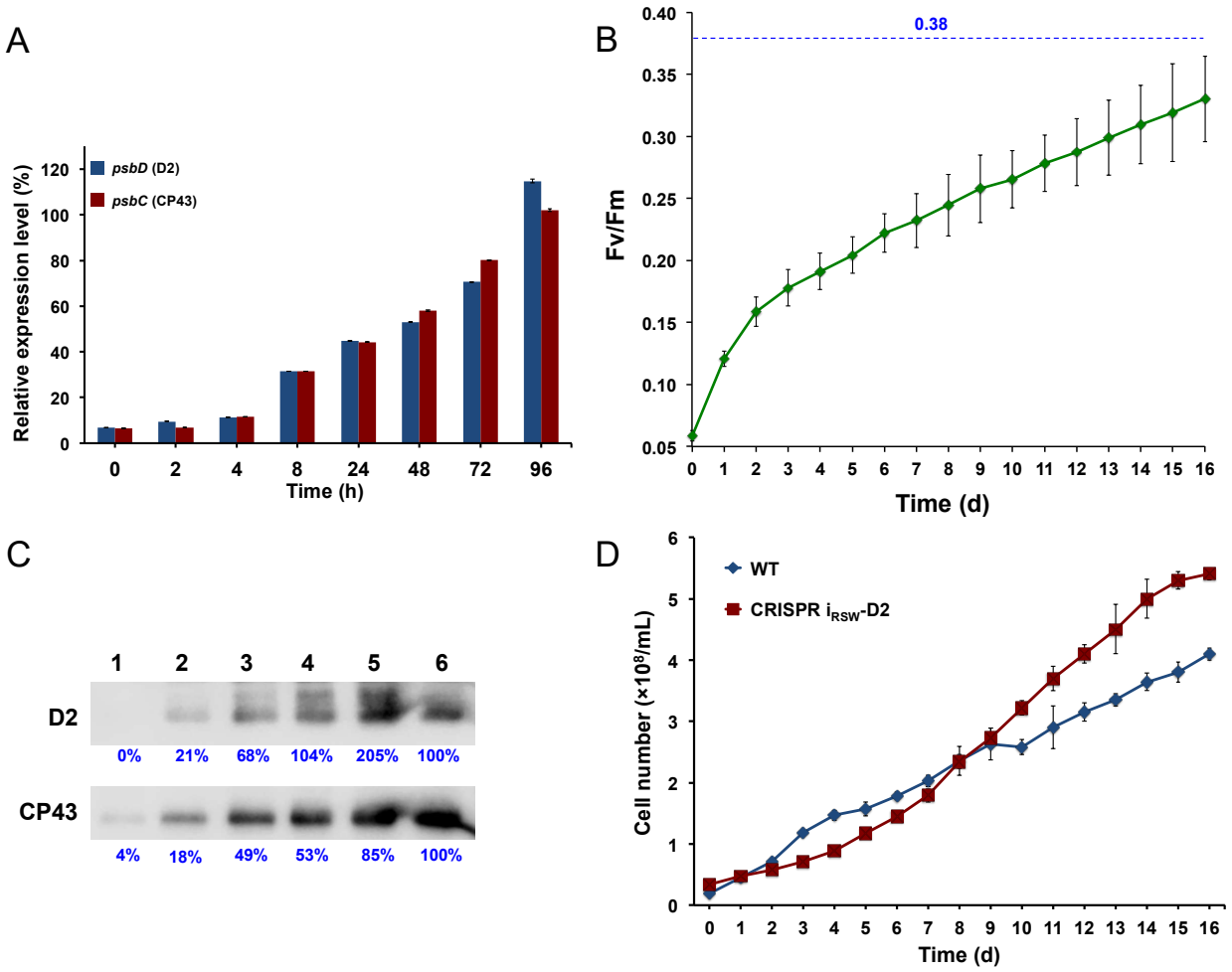

Figure 3.4. Recovery of the expression of D2 and CP43 after release of repression by the CRISPR i_{RSW} system. Both WT and CRISPR i_{RSW}-D2 strains were initially cultured in BG11 with glucose and inducers. After 4 days growth, cells were collected, washed twice, and re-suspended in fresh BG11 medium for monitoring. (A) Recovery of *psbD* and *psbC* transcript levels in the CRISPR i_{RSW}-D2 strain determined by q-PCR. Transcript levels of both genes in WT were set as 100%. (B) The Fv/Fm values of the CRISPR i_{RSW}-D2 strain increased along with time. The dotted blue line is the Fv/Fm value of WT after 16 days culture in BG11. (C) Recovery of D2 and CP43 protein levels in the CRISPR i_{RSW}-D2 strain determined by western blot. Lane 1 to 5 represent 20 µg of total membrane proteins extracted from CRISPR i_{RSW}-D2 when the Fv/Fm value is 0.07, 0.16, 0.25, 0.35, and 0.39, respectively. Lane 6 represents 20 µg of total membrane proteins extracted from WT. Blue numbers are the corresponding blot intensities of each band. (D) Cell numbers of both strains along with time during the recovery process. Error bars in the figure represent the standard deviations observed from at least three independent experiments. Cells are cultured in flask shaking under 30°C with light intensity 30 µmol photons m^{-2} s^{-1}.

Western blots (Figure 4C) showing protein recovery with increasing Fv/Fm levels demonstrate a slow increase in CP43 and D2 protein levels over time. At time point 0, corresponding to Fv/Fm of 0.07, D2 and C43 are less than 5% of the WT level. Interestingly, D2

protein level increases above wild type level as recovering cells approach the PSII activity of WT, while CP43 increases to slightly less of its wild type protein level. While a direct comparison between the WT and recovering samples is impossible, as they are at different growth phases and metabolic states, and there was some variation among biological replicates, this pattern held true. This creates a situation in which there are "extra" D2 copies. These copies of D2 could be in PSII assembly intermediate complexes, as *de novo* PSII assembly is thought to occur step-wise, first incorporating the D1 and D2 proteins, and then later the CP43 and CP47 proteins.(40)

Under photoautotrophic conditions, photosynthesis is the sole energy source for intracellular biological processes in *Synechocystis* 6803, including cell division. We expect cell division rate to be affected for the CRISPR i_{RSW}-D2 strain over the recovery process. Cell numbers were counted every 24 hours during recovery for both WT and the CRISPR i_{RSW}-D2 strain. As shown in Figure 4D, the two strains showed divergent cell division rate phenotypes. Compared to the WT strain, which showed more rapid division over the first 4 days before slowing, the CRISPR i_{RSW}-D2 strain showed a lag phase before day 4, at which time point cells began to divide at a faster rate. The averaged doubling time for WT (around 18 hours) is a fold lower than the CRISPR i_{RSW}-D2 strain (around 35 hours) in the first 4 days. This 4-day lag before division begins suggests that cell division was inhibited because of the insufficient energy generated from the low level of intracellular PSII, and correlates to the phases of the Fv/Fm curve (Figure 4B). The initial rapid increase in Fv/Fm can be explained by the fact that the F_V (or the difference in fluorescence due to PSII activity compared to background chlorophyll fluorescence) increases due to the small new amount of active PSII, while the total background chlorophyll fluorescence (F_0) does not start to increase until the cells begin to divide. Once cells begin to grow and divide, photosystem I-

associated chlorophyll increases, as does synthesis of unassembled PSII subunits containing chlorophyll, which contribute to F_0, making the subsequent increase in Fv/Fm slower.

D2 and CP43 are essential proteins in the core reaction center of PSII, and inhibiting their biosynthesis eliminates the formation of PSII.(18) As shown in Figure 4, a two-phase recovery was observed for all parameters measured, including transcription of *psbD* and *psbC* genes, Fv/Fm values, and cell numbers. This two-phase phenomenon is correlated with the PSII content, which affects the energy supply for biological processes, such as transcription, translation, and cell division. Because the CRISPRi$_{RSW}$ system constructed here knocks down the expression of targeted genes by over 90%, the intracellular PSII activity is very low, around 15% of WT based on Fv/Fm (Figure 3C and 4B), and less than 5% based on D2 and CP43 protein levels (Figure 3E and 4C). The CRISPR i$_{RSW}$-D2 strain grew under near photoheterotrophic conditions when glucose and inducers were added to the medium. After resuspension in BG11 medium, cells must convert to autotrophic growth but with a very low initial PSII content. So, there is a rapid initial increase in mRNA and Fv/Fm, but energy stores are quickly used up, inhibiting cell division until sufficient energy derived from the small amount of initial PSII has allowed cells to divide and synthesize more PSII to make more energy. Therefore, there is a subsequent slow recovery of PSII activity, mRNA, and protein levels.

To study the process of PSII biogenesis, deletion of target genes is the classical genetic strategy. Using a deletion strategy, intermediate PSII assembly complexes form in the specific gene knockout mutant, and these complexes are analyzed to infer the PSII biogenesis process.(41) The function of numerous proteins in PSII biogenesis has been identified through this strategy. However, deletion mutants cannot recover the expression of the deleted gene, so the biogenesis process cannot be systematically studied. The CRISPRi technology supplies an alternative and

valuable way to uncover the biogenesis process. With this tightly controlled CRISPRi$_{RSW}$ system in *Synechocystis* 6803, we have developed a new platform to study not only PSII biogenesis, but also assembly of other protein complexes such as Photosystem I.

3.4 Discussion

We built a chimeric promoter system, P$_{rhaBAD\text{-}RSW}$, which exhibits tight control and a broad, titratable inducible range in *Synechocystis* 6803. Expression of ddCpf1 driven by this chimeric promoter in a CRISPRi system effectively and reversibly represses the expression of the targeted genes, *psbD* and *psbC*, and nearly inhibits the formation of PSII protein complex. Following release of the repression by removing inducers, PSII is re-built in the same cells. In contrast to a strategy of knocking-out to study gene function, our CRISPRi$_{RSW}$ system does not modify or edit the genome. Furthermore, we supply a new platform to study the biogenesis processes, during which protein complex intermediates can be tracked dynamically following release of inhibition.

3.5 Materials and Methods

3.5.1 Strains and culture conditions

All cloning work was performed in *E. coli* strain XL1-Blue grown in LB medium in culture tubes or on agar plates at 37 °C, supplemented with 50 µg/ml kanamycin, 20 µg/ml chloramphenicol, or 100 µg/ml ampicillin, as needed. *Synechocystis* 6803 cells were cultured in BG11 medium supplemented with 30 µg/ml kanamycin as needed, under continuous white light at 30 µmol photons m^{-2} s^{-1} at 30 °C. Cultures were grown in 125-ml glass flasks or on agar plates. To monitor

growth, 150 µL of cells suspension was loaded onto a 96-well plate and OD at 730 nm was measured on a plate reader (BioTek, VT).

3.5.2 Construction of recombinant plasmids and engineered strains.

Plasmids and strains used in this study are listed in Table S3.2, and all primers used in this study are listed in Table S3.3. All plasmids were constructed by Gibson Assembly strategy (42), using linear fragments purified from PCR products. All plasmids used in this study are based on the broad host replicating plasmid pRSF1010 (43). The DNA fragments used to assemble the CRISPRi plasmid were amplified from other plasmids in the Pakrasi lab.

A tri-parental conjugation method was used to transfer all pRSF1010 derivative plasmids to *Synechocystis* 6803 wild-type cells (44), using a helper strain of *E. coli* containing the pRL443 and pRL623 plasmids (45, 46). Transformants were isolated on BG11 agar plates containing 20 µg/mL kanamycin, as needed. Isolated *Synechocystis* 6803 transformants were checked by PCR to confirm presence of the desired constructs.

All PCR amplifications were performed using Phusion High-fidelity DNA polymerase (Thermo Scientific). Plasmids and PCR products were purified using the GeneJET (Thermo Scientific) plasmid miniprep kit and gel extraction kit, respectively. Oligonucleotides were designed using the SnapGene software (GSL Biotech LLC) and synthesized by IDT (Coralville, IA). The sequences of all the plasmids constructed in this study were verified (Genewiz, NJ).

3.5.3 Measurement of EYFP fluorescence

EYFP fluorescence was measured directly from cells suspension in culture. The fluorescence intensity and the optical density of each culture were determined in 96-well black-walled clear-

bottom plates on a BioTek Synergy Mx plate reader (BioTek, Winooski, VT). The excitation and emission wavelengths were set to 485 nm and 528 nm for EYFP. All measured fluorescence data were normalized by culture density.

3.5.4 Reverse transcription-PCR (RT-PCR) and quantitative PCR (q-PCR).

Total RNA samples for RT-PCR and q-PCR were extracted using the reagent RNAwiz (Ambion). After quantification of RNA, 200 ng of DNase-treated RNA samples, Superscript II reverse transcriptase, and random primers (Invitrogen) were used for reverse transcription according to the manufacturer's instructions. cDNA generated after reverse transcription was used as the template for PCR to validate the transcription of genes.

qRT-PCR SYBR green dUTP mix (ABgene) was used for the q-PCR assay on an ABI 7500 system (Applied Biosystems). Each reaction was performed in triplicate, and the average threshold cycle (CT) value was used to calculate the relative transcriptional levels for the amounts of RNA. All primers used for RT-PCR and q-PCR are listed in Table S3.3.

3.5.5 Western blot analysis

Cyanobacterial cells were harvested and broken by bead beating as described previously (47) with minor modifications. Cells were re-suspended in RB buffer (25% glycerol (wt/vol), 10mM $MgCl_2$, 5mM $CaCl_2$, 50 mM MES buffer pH 6.0) and broken by vortexing with 0.17 mm glass beads. Membrane fraction was isolated by centrifugation, re-suspended in RB, and solubilized by addition of β-D-dodecyl maltoside (DDM) to a final concentration of 0.8%. After incubation on ice in dark for 30 min, the solubilized membranes were separated from the insoluble material by centrifugation at gradually increasing speed from 120×g to 27,000×g at 4 °C for 20 min. The

solubilized membranes were then stored at −80 °C for future use. The protein content was determined using bicinchoninic acid (BCA) protein assay reagent (Thermo Scientific).

SDS-PAGE was performed by loading the same amount of isolated membrane proteins on a 12.5% acrylamide resolving gel. After electrophoresis, proteins were transferred to a polyvinylidene difluoride (PVDF) membrane (Millipore), blocked using 5% bovine serum albumin (BSA) for 2 h at room temperature, and then separately incubated with the primary rabbit antibodies raised against D2 and CP43 proteins overnight at 4°C. The D2 primary antibody was a generous gift from Dr. Louis Sherman and was diluted 1:1500. The CP43 primary antibody was a generous gift from Dr. Masahiko Ikeuchi and was diluted 1:2000. The horseradish peroxidase (HRP)-conjugated secondary antibody goat anti-rabbit IgG (H+L)-HRP conjugate (Bio-Rad) was diluted at 1:5,000 in 1.5% BSA. Bands were visualized using chemiluminescence reagents (EMD Millipore, Billerica, MA, USA) with an ImageQuant LAS-4000 imager (GE Healthcare).

3.5.6 Measurement of photosynthetic activity

PSII efficiency was analyzed *in vivo* using a double-modulation fluorometer, FL-200 (Photon System Instruments, Brno, Czech Republic). 1 mL sample was dark-adapted for 2 min before measurement. The instrument contains red LEDs for both actinic (20-s) and measuring (2.5-s) flashes and was used in the time range of 100 μs to 100 s. The maximal PSII quantum yield (Fv/Fm) was determined with the saturation pulse method (48).

3.5.7 Cell number counting

20 μL of culture was sampled, and cells were counted with an automated cell counter (Cellometer Vision; Nexcelom). The counted images were manually curated to improve accuracy of the counts. The accompanying Cellometer software reported cell counts in cells per milliliter.

3.6 Supporting Information

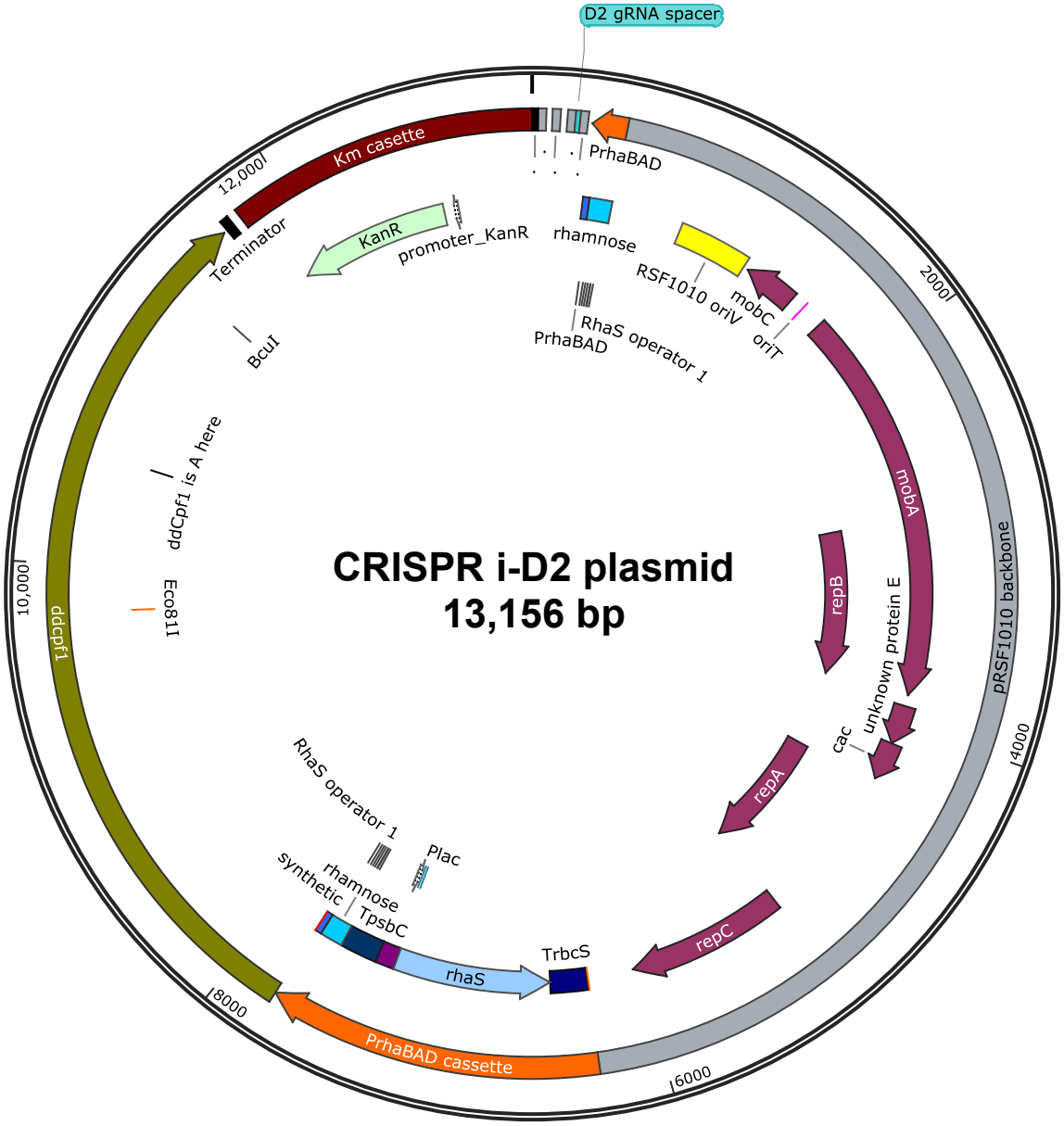

Figure S3.1 Schematic map of the plasmid containing the CRISPRi system. The coding gene of regulator protein RhaS is driven by the promoter P_{lacOI}. The sequence of the promoter P_{rhaBAD} is identical with the published paper (34). This replicating plasmid was constructed with the Gibson Assembly strategy (42) and introduced into WT of *Synechocystis* 6803 by conjugation.

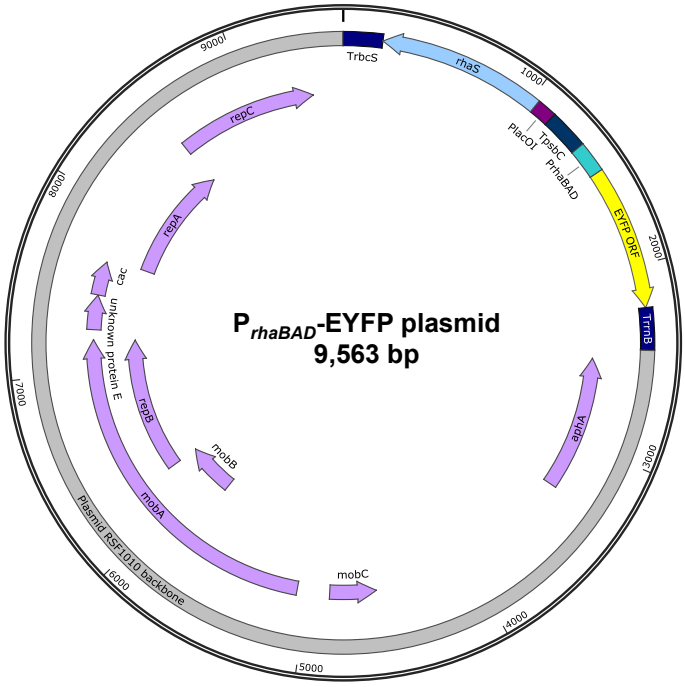

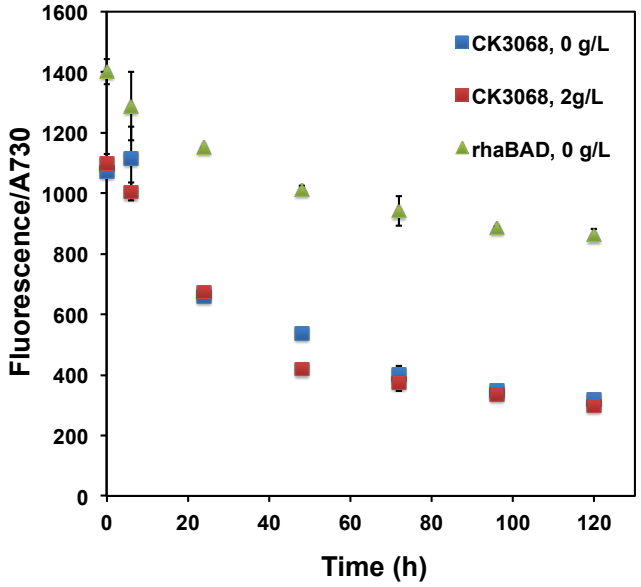

Figure S3.2. EYFP is expressed by the P_{rhaBAD} promoter even without rhamnose. CK3068 is the control strain in Figure 3.2, which contains the plasmid with EYFP encoding gene but without any promoters to drive it. Fluorescence data were normalized to optical density at 730 nm. Concentration of rhamnose added to the culture is labeled following the strain name. All strains were cultured in BG11 medium, shaking in flask under 30°C with light intensity 30 μmol photons m^{-2} s^{-1}. Each dot represents the averaged data observed from at least three independent experiments.

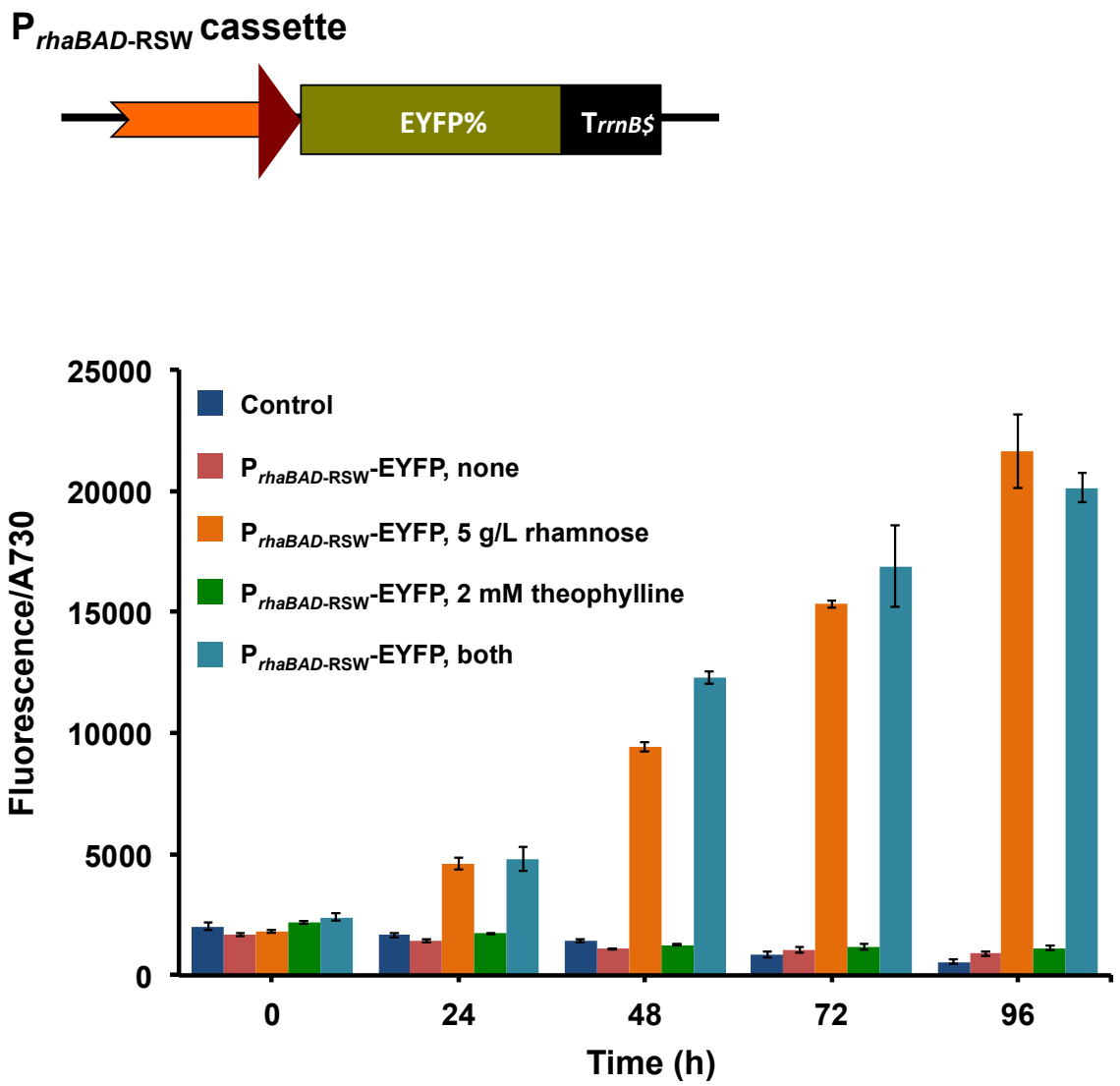

Figure S3.3 Expression levels of EYFP driven by $P_{rhaBAD\text{-RSW}}$. Control is the strain containing the plasmid with EYFP coding gene but without any promoters to drive it. Rhamnose and theophylline was added at the concentrations labeled in the figure. "None" in the panel means no of inducers were added in the culture. Fluorescence data were normalized to optical density at 730 nm. All strains were cultured in BG11 medium, shaking in flask under 30°C with light intensity 30 μmol photons m^{-2} s^{-1}. Error bars represent the standard deviations observed from at least three independent experiments.

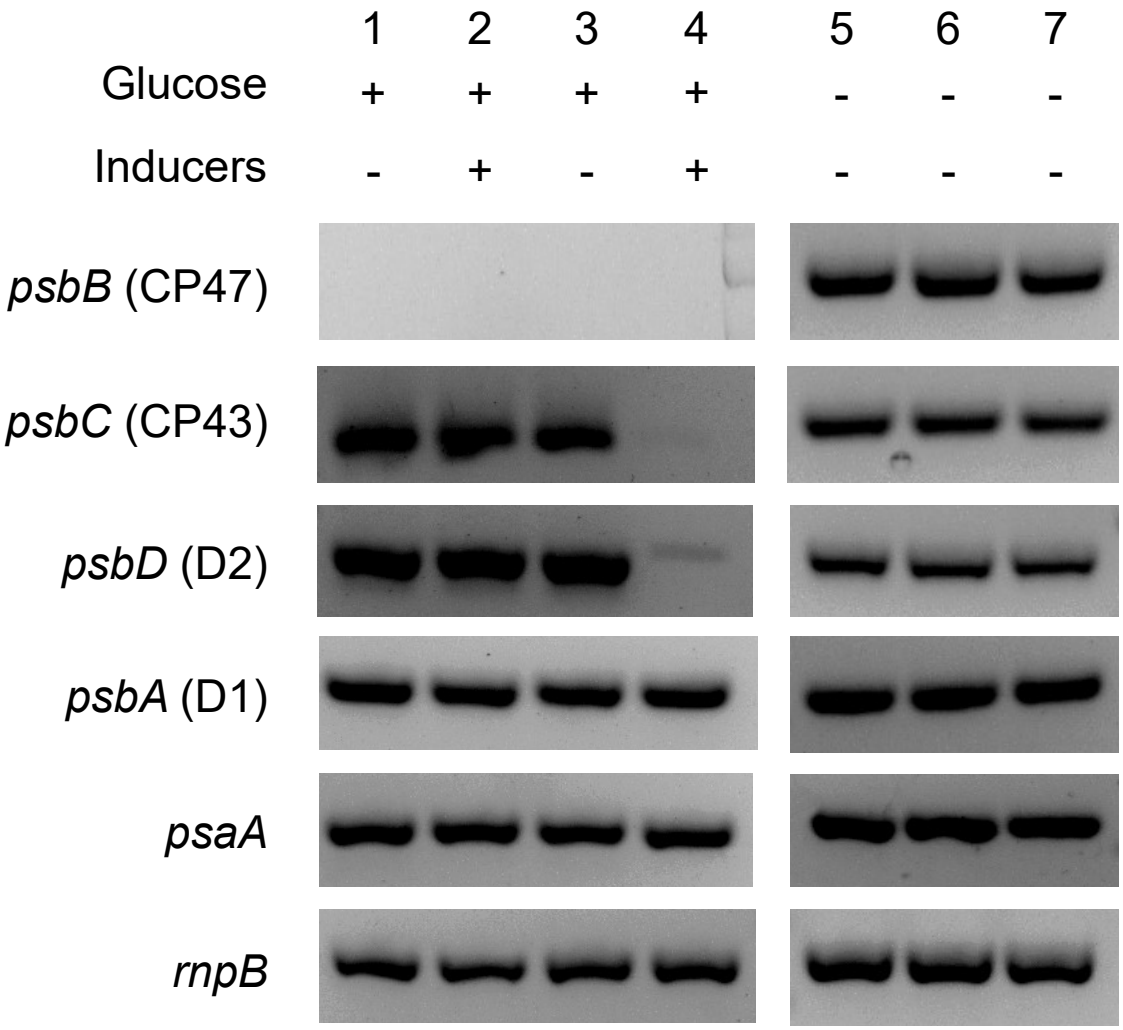

Figure S3.4 Semiquantitative RT-PCR of photosystem genes. Total RNA was extracted from cell samples cultured in BG11 medium, shaking in flask under 30°C with light intensity 30 μmol photons m^{-2} s^{-1}. Cells were grown with 10 g/L of glucose and 5 g/L rhamnose and 2 mM theophylline as inducers as indicated. Lane 1&5 are WT of *Synechocystis* 6803. Lane 2&6 are the control strain containing the CRISPR i_{RSW} plasmid with the gRNA targeted to the *eyfp* gene. Lane 3, 4 &7 are the CRISPR i_{RSW}-D2 strain.

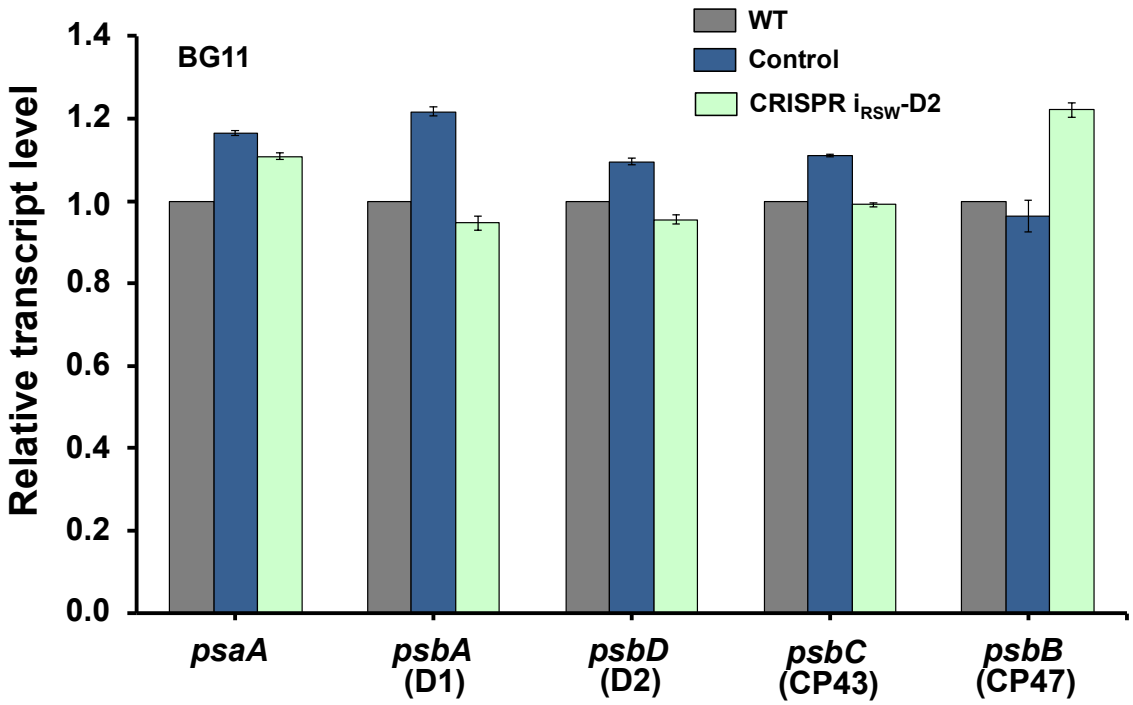

Figure S3.5 Transcriptional levels of photosystem genes quantified by q-PCR. Cell samples were collected from the culture in BG11 medium shaking at 30°C with light intensity 30 μmol photons m^{-2} s^{-1}, and total RNA were extracted for the analysis. Control is the strain containing the CRISPR i_{RSW} plasmid but with the gRNA targeting to the *eyfp* gene. Error bars represent the standard deviations observed from at least three independent experiments.

Table S3.1. Nucleotide sequences of promoters and genes in Chapter 3.

Promoter and gene	**Sequence**	**Note**
P_{rhaBAD} promoter cassette	taattgacaattgacaattccccacttagataaaaaatccggtcaggatgcggtcaacattataca aaaactgtccaaagaacagggccgtattgtgttgctgattacctatagtcactgtgaaaaagcaa caaaaaacccgcgggagcgggctaacattgaattgaagtcagttttttagtaattgccaaaactg taattattgcagaaagccatcccgtccctggcgaatatcacgcggtgaccagttaaactctcggc gaaaaagcgtcgaaaagtggttactgtcgctgaatccacagcgataggcgatgtcagtaacgc tggcctcgctgtggcgtagcagatgtcgggctttcatcagtcgcaggcggttcaggtatcgctg aggcgtcagtcccgtttgctgcttaagctgccgatgtagcgtacgcagtgaaagagaaaattga tccgccacggcatcccaattcacctcatcggcaaaatggtcctccagccaggccagaagcaag ttgagacgtgatgcgctgttttccaggttctcctgcaaactgcttttacgcagcaagagcagtaatt gcataaacaagatctcgcgactggcggtcgagggtaaatcattttccccttcctgctgttccatct gtgcaaccagctgtcgcacctgctgcaatacgctgtggttaacgcgccagtgagacggatact gcccatccagctcttgtggcagcaactgattcagcccggcgagaaactgaaatcgatccggcg agcgatacagcacattggtcagacacagattatcggtatgttcatacagatgccgatcatgatcg cgtacgaaacagaccgtgccaccggtgatggtatagggctgcccattaaacacatgaataccc gtgccatgttcgacaatcacaatttcatgaaaatcatgatgatgttcaggaaaatccgcctgcgg gagccggggttctatcgccacggacgcgttaccagacggaaaaaaatccacactatgtaatac ggtcatagctgtttcctgtgtgaaattgttatccgctcacaattccacacaacatacgagccggaa gcataaagtgtaaagcctggggtgcctaatgagtgagctaattgagacttttctgattttgcaaag gttttgctttagttaaacccaattgattagtgtcccctgcccatttggtgggggattattatttttaaga taatcctatttttttggagtgaggccagttacctattagacgcgcgactcgaaagtcgttcagggga gttggaacggcttccaaaaaccttttccccgctggtgttccacaattcagcaaattgtgaacatcat cacgttcatctttccctggttgccaatggcccattttcctgtcagtaacgagaaggtcgcgaattca ggcgctttttagactggtcgtaatgaatcgggtaagtttataatatacaaaggaggtagaaATG	Green is the RhaS coding sequence. Blue is the P_{lacOI} promoter. Orange is the P_{rhaBAD} promoter. Black is the terminators. The start codon of *ddcpf1* gene is highlighted with yellow color.

$P_{rhaBAD\text{-RSW}}$ promoter cassette	aattgacaattgacaattccccacttagataaaaaatccggtcaggatgcggtcaacattatacaa aaactgtccaaagaacagggccgtattgtgttgctgattacctatagtcactgtgaaaaagcaac aaaaaacccgcgggagcgggctaacattgaattgaagtcagtttttagtaattgccaaaactgt aattattgcagaaagccatcccgtccctgacgaatatcacgcggtgaccagttaaactctcggc gaaaaagcgtcgaaaagtggttactgtcgctgaatccacagcgataggcgatgtcagtaacgc tggcctcactgtggcgtagcagatgtcgggctttcatcagtcgcaggcggttcaggtatcgctg aggcgtcagtcccgtttgctgcttaagctgccgatgtagcgtacgcagtgaaagagaaaattga tccgccacggcatcccaattcacctcatcggcaaaatggtcctccagccaggccagaagcaag ttgagacgtgatgcgctgttttccaggttctcctgcaaactgcttttacgcagcaagagcagtaatt gcataaacaagatctcgcgactggcggtcgagggtaaatcattttcccctcctgctgttccatct gtgcaaccagctgtcgcacctgctgcaatacgctgtggttaacgcgccagtgagacggatact gcccatccagctcttgtggcagcaactgattcagcccggcgagaaactgaaatcgatccggcg agcgatacagcacattggtcagacacagattatcggtatgttcatacagatgccgatcatgatcg cgtacgaaacagaccgtgccaccggtgatggtatagggctgcccattaaacacatgaataccc gtgccatgttcgacaatcacaatttcatgaaaatcatgatgatgttcaggaaaatccgcctgcgg gagccggggttctatcgccacggacacgttaccagacggaaaaaaatccacactatgtaatac ggtcatagctgtttcctgtgtgaaattgttatccgctcacaattccacacaacatacgagccggaa gcataaagtgtaaagcctggggtgcctaatgagtgagctaattgagacttttctgattttgcaaag gttttgctttagttaaacccaattgattagtgtcccctgcccatttggtgggggattattatttttaaga taatcctatttttttggagtgaggccagttacctattagacgcgcgactcgaaagtcgttcagggga gttggaacggcttccaaaaacctttccccgctggtgttccacaattcagcaaattgtgaacatcat cacgttcatctttccctggttgccaatggcccattttcctgtcagtaacgagaaggtcgcgaattca ggcgctttttagactggtcgtaatgaataccggtgataccagcatcgtcttgatgcccttggcagc accctgctaaggaggtaacaacaagATG	Green is the RhaS coding sequence. Blue is the P_{lacOI} promoter. Orange is the $P_{rhaBAD\text{-RSW}}$ promoter. The riboswitch sequence is underlined. Black is the terminators. The start codon of *ddcpf1* gene is highlighted with yellow color.
psbD1 gene in *Synechocystis* 6803	ATGACTATTGCAGTCGGACGCGCCCCAGTCGAAAGAGGA TGGTTTGATGTCCTCGACGATTGGCTAAAGCGTGATCGTT TCGTATTTATTGGTTGGTCTGGTTTGCTGCTCTTCCCCTGT GCCTTCATGGCCCTGGGGGGGATGGCTAACCGGCACCACC TTCGTTACTTCCTGGTACACCCACGGTCTAGCCAGTTCCT ATCTAGAAGGAGCTAACTTTTTGACCGTGGCGGTCTCTTC CCCCGCCGATGCCTTCGGCCATTCCCTCCTGTTCCTCTGG GGACCCGAAGCCCAAGGTAACCTGACCCGCTGGTTCCAA ATCGGTGGTTTGTGGCCCTTCGTTGCCCTCCACGGTGCCT TCGGTCTGATTGGCTTTATGCTGCGTCAGTTCGAAATTTC CCGTCTGGTTGGCATTCGTCCCTACAACGCCATCGCCTTC TCTGGTCCCATTGCGGTGTTTGTCAGTGTCTTTTTGATGTA CCCCTTGGGACAATCCAGTTGGTTCTTTGCCCCCAGCTTT GGGGTAGCGGGAATCTTCCGGTTCATTTTGTTCCTGCAAG GGTTCCACAACTGGACTTTGAACCCCTTCCACATGATGGG AGTGGCAGGGATTTTGGGCGGCGCCCTCCTCTGTGCTATC CACGGTGCCACGGTGGAAAACACCCTGTTTGAAGATGGG GAAGATTCCAATACTTTCCGGGCATTTGAACCCACCCAA GCAGAAGAAACCTATTCCATGGTGACCGCTAACCGTTTCT GGTCTCAGATTTTCGGTATTGCTTTCTCCAACAAGCGGTG GTTGCACTTCTTCATGTTGTTCGTGCCGGTAACTGGTCTG TGGATGAGTTCCGTCGGTATCGTCGGTTTAGCCTTGAACC TACGGGCCTATGACTTTGTCTCCCAGGAGCTACGGGCGG CGGAAGACCCGGAATTTGAAACTTTCTATACGAAAAACA TTTTGTTGAACGAAGGGATGCGCGCCTGGATGGCTCCCC AAGATCAACCCCATGAAAACTTTATCTTCCCTGAGGAGG TTCTCCCCCGTGGTAACGCTCTCTAA	Red is the sequence for gRNA recognition

psbD2 gene in *Synechocystis* 6803	ATGACCATTGCAGTCGGACGCGCCCCAGTCGAAAGAGGA TGGTTTGATGTCCTCGACGATTGGCTAAAGCGTGATCGTT TCGTATTTATCGGTTGGTCTGGTTTGCTACTCTTCCCCTGC GCCTTCATGGCCCTGGGGGGGATGGTTAACCGGCACCACC TTCGTTACTTCCTGGTACACCCACGGTCTAGCCAGTTCCT ACCTGGAAGGGGCTAACTTTTTGACCGTGGCGGTCTCTTC CCCCGCCGATGCCTTCGGCCATTCCCTCCTGTTCCTGTGG GGACCGGAAGCTCAAGGTAACCTGACCCGCTGGTTCCAA ATTGGTGGTTTGTGGCCCTTCGTTGCCCTCCACGGTGCCT TTGGATTGATTGGCTTCATGCTGCGTCAGTTCGAAATTTC CCGTCTGGTAGGCATTCGTCCCTACAACGCCATCGCTTTC TCTGGTCCCATTGCGGTATTTGTCAGCGTCTTTCTGATGT ACCCCTTGGGTCAATCGAGTTGGTTCTTTGCTCCCAGCTT TGGGGTAGCGGGAATCTTCCGGTTTATTTTGTTCCTACAA GGTTTCCACAACTGGACCCTGAACCCCTTCCACATGATGG GAGTAGCCGGTATTCTCGGTGGTGCCCTACTGTGTGCCAT CCACGGTGCCACGGTGGAAAACACCCTGTTTGAAGACGG TGAAGATTCCAACACCTTCCGGGCGTTTGAACCTACCCAA GCGGAAGAAACCTACTCCATGGTGACTGCCAACCGTTTC TGGTCTCAGATTTTCGGTATTGCTTTCTCCAACAAACGGT GGCTGCACTTCTTCATGTTGTTCGTTCCCGTAACTGGTTTG TGGATGAGTTCTGTGGGTATCGTCGGTTTGGCGTTGAACC TACGGGCTTATGACTTCGTTTCCCAGGAACTGCGGGCTGC TGAAGATCCGGAATTTGAAACGTTTTATACGAAAAACAT TTTGTTGAACGAAGGGATGCGCGCCTGGATGGCTCCCCA AGATCAACCCCATGAAAACTTTATCTTCCCTGAGGAAGT ACTGCCCCGGGGTAATGCTCTCTAA	Red is the sequence for gRNA recognition

Table S3.2 Strains and plasmids used in this Chapter 3.

Strains and plasmids	Description	Source
Strain		
E.coli strain XL1-Blue	Used for DNA cloning	Our lab
Synechocystis 6803	Wild type (WT) strain	Our lab
CK3068	Control strain containing the eyfp gene on pRSF1010 but without any promoters to drive it	(35)
CK01	Control strain containing the CRISPRi system but targeting to *eyfp* by the gRNA	This study
CK02	Control strain containing the CRISPR i_{RSW} system but targeting to *eyfp* by the gRNA	This study
P_{rhaBAD}-EYFP	Strain containing the eyfp gene on pRSF1010 with the P_{rhaBAD} promoter to drive it	This study
$P_{rhaBAD\text{-}RSW}$-EYFP	Strain containing the eyfp gene on pRSF1010 with the $P_{rhaBAD–RSW}$ promoter to drive it	This study
CRISPR i-D2	Strain containing the CRISPRi system with gRNA targeting to *psbD* gene of *Synechocystis* 6803	This study
CRISPR i_{RSW}-D2	Strain containing the CRISPR i_{RSW} system with gRNA targeting to *psbD* gene of *Synechocystis* 6803	This study
Plasmid		
pRL443	Plasmid used for conjugation	(45)
PRL623	Plasmid used for conjugation	(46)
pRSF1010	Broad-host-range shuttle vector	(43)
pCK3068	Plasmid containing the eyfp gene on pRSF1010 but without any promoters to drive it	(35)
pCRISPR i-eyfp	Plasmid containing CRISPRi system on pRSF1010 with gRNA targeting to *eyfp* gene	This study
pCRISPR i_{RSW}-eyfp	Plasmid containing CRISPR i_{RSW} system on pRSF1010 with gRNA targeting to *eyfp* gene	This study
pRhaBAD-eyfp	Plasmid containing the *eyfp* gene on pRSF1010 with P_{rhaBAD} to drive it	This study
pRhaBAD-RSW-eyfp	Plasmid containing the *eyfp* gene on pRSF1010 with $P_{rhaBAD\text{-}RSW}$ to drive it	This study
pCRISPR i-D2	Plasmid containing the CRISPRi system on pRSF1010 with gRNA targeting to *psbD* gene of *Synechocystis* 6803	This study
pCRISPR i_{RSW}-D2	Plasmid containing the CRISPR i_{RSW} system on pRSF1010 with gRNA targeting to *psbD* gene of *Synechocystis* 6803	This study

Table S3.3 List of primers used in this Chapter 3.

Primer name	Sequence 5' -> 3'	Purpose of primers
RHA_TrbcS_F1	cgctttcctggctttgcttcccactaattgacaattgacaattccccac	For plasmid pRhaBAD-eyfp
RHA_TrbcS_R1	acgggatggctttctgcaataattacagttttggcaattactaaaaaac	
RHA_rhaS_F2	gccaaaactgtaattattgcagaaagccatcccg	
RHA_rhas_R2	caggaaacagctatgaccgtattacatagtgtgg	
RHA_PlacOI_F3	gtaatacggtcatagctgtttcctgtgtgaaattg	
RHA_PlacOI_R3	aagtctcaattagctcactcattaggcacccc	
RHA_TpsbC_F4	gagtgagctaattgagacttttctgattttgc	
RHA_TpsbC_R4	tgaattgtggaacaccagcggggaaaggtttttg	
RHA_Prha_F5	cgctggtgttccacaattcagcaaattgtgaac	
RHA-Prha_R5	attataaacttacccgattcattacgaccagtctaaaaagc	
RHA_Prha_R6	ttctacctcctttgtatattataaacttacccgattcattac	
RHA_Prha_R7	cagctcctcgcccttgctcaccatttctacctcctttgtatattataaac	
EYFP_F	atggtgagcaagggcgaggag	
TrrnB_R	cattacgctgacttgacgggacacggttttaaagaaaaagggcagg	
PrhaBAD-RSW_KspAI_F1	ctgtcgcacctgctgcaatac	For plasmid pRhaBAD-RSW-eyfp
PrhaBAD-RSW_R1	agggcatcaagacgatgctggtatcaccggtattcattacgaccagtctaaaaagcgc	
PrhaBAD_RSW_R2	tgttgttacctccttagcagggtgctgccaagggcatcaagacgatgctgg	
PrhaBAD-RSW_F3	tggcagcaccctgctaaggaggtaacaacaagatggtgagcaagggcgaggag	
PrhaBAD-RSW_pstI_R4	aaagggcagggtggtgacac	
Rha_lguI_F1	ctggctttgcttccagatgtatgctcttcttaattgacaattgacaattccccac	
PrhaBAD_F	ccgtttttgcctaaatcagcttctacctcctttgtatattataaac	For plasmid pCRISPR i-eyfp
PrhaBAD_R	gagtcttgccacgccgagcacctggccacaattcagcaaattgtgaac	
Template2_R	gctgatttaggcaaaaacgg	
Template1_F	cgtggctttgcgcattaaagc	
Template_F3	tacagctgaaagcgaaaaaaaatgaccttcataaatcgc	
cpf1_BcuI_F	agagcgacaaaaagttttttgc	
cpf1_BcuI_R	aaggtcatttttttgtctagc	
Km_F2	gctagacaaaaaaatgacctttcgactctagagaggatctgtaac	

Km_R2	gaaggtcatttttttcgctttcagctgtaatccgg	
leader-rha_R	ggaggtagaagctgatttaggcaaaaacgg	
Rha_RSW-dcpf1_R1	tttattaacaaattcttgataaattgacatcttgttgttacctccttagcagg	For plasmid pCRISPR i_{RSW}-eyfp
dcpf1_start_F2	atgtcaatttatcaagaatttgttaataaatatag	
dCpf1_lguI_R2	tgtagtcaatatcaaaggttagctc	
EcoO109I_R	gatgagccgggctgaatgatc	For plasmid pCRISPR i-D2
OliI_F	agacctcagcgctattctgac	
Rhacasette_F	atgtctagctttaatgcggtagttagatcttaattgacaattgacaattccccac	
RHA_PlacOI_F3	gtaatacggtcatagctgtttcctgtgtgaaattg	
Rhacasette_R	tgataaattgacatttctacctcctttgtatattataaacttac	
qPCR_6803RnpB_F0	agtatcgagaggtactggctc	For q-PCR
qPCR_6803RnpB_R0	acccttggggagttatctatc	
qPCR_6803D1_F1	ctctaccaacaaccggatttatg	
qPCR_6803D1_R1	gcgatgaaggcaatgatgaag	
qPCR_6803D2_F2	ttacttcctggtacacccacg	
qPCR_6803D2_R2	gaaccagcgggtcaggttac	
qPCR_6803CP43_F3	ccgtggtaacgctctctaatac	
qPCR_6803CP43_R3	gattaatcagccgggcatttc	
qPCR_6803CP47_F4	ccttggtatcgcgttcatacag	
qPCR_6803CP47_R4	gccaactcatagagagccatag	
qPCR_6803psaA_F5	gataccgctcaccaccatttg	
qPCR_6803psaA_R5	cgaggatctctttcatgctatgg	

3.7 References

1. Williams JGK (1988) Construction of specific mutations in photosystem II photosynthetic reaction center by genetic engineering methods in *Synechocystis* 6803. *Methods in Enzymology*, (Academic Press), Vol Volume 167, pp 766-778.

2. Sun T*, et al.* (2018) Toolboxes for cyanobacteria: Recent advances and future direction. *Biotechnol. Adv.* 36(4):1293-1307.

3. Umena Y, Kawakami K, Shen JR, & Kamiya N (2011) Crystal structure of oxygen-evolving photosystem II at a resolution of 1.9 A. *Nature* 473(7345):55-60.

4. Barber J (2012) Photosystem II: the water-splitting enzyme of photosynthesis. *Cold Spring Harb Symp Quant Biol* 77:295-307.

5. Gao J, Wang H, Yuan Q, & Feng Y (2018) Structure and function of the photosystem supercomplexes. *Front Plant Sci* 9:357.

6. Eaton-Rye JJ & Sobotka R (2017) Editorial: Assembly of the Photosystem II Membrane-Protein Complex of Oxygenic Photosynthesis. *Front. Plant Sci.* 8.

7. Nickelsen J & Rengstl B (2013) Photosystem II assembly: from cyanobacteria to plants. *Annu Rev Plant Biol* 64:609-635.

8. Nixon PJ, Michoux F, Yu J, Boehm M, & Komenda J (2010) Recent advances in understanding the assembly and repair of photosystem II. *Ann Bot* 106(1):1-16.

9. Roose JL & Pakrasi HB (2004) Evidence that D1 Processing Is Required for Manganese Binding and Extrinsic Protein Assembly into Photosystem II. *J. Biol. Chem.* 279(44):45417-45422.

10. Roose JL & Pakrasi HB (2008) The Psb27 protein facilitates manganese cluster assembly in photosystem II. *J Biol Chem* 283(7):4044-4050.

11. Weisz DA*, et al.* (2019) A novel chlorophyll protein complex in the repair cycle of photosystem II. *Proc Natl Acad Sci U S A* 116(43):21907-21913.

12. Yao DC, Brune DC, & Vermaas WF (2012) Lifetimes of photosystem I and II proteins in the cyanobacterium Synechocystis sp. PCC 6803. *FEBS Lett* 586(2):169-173.

13. Bonisteel EM*, et al.* (2018) Strain specific differences in rates of Photosystem II repair in picocyanobacteria correlate to differences in FtsH protein levels and isoform expression patterns. *PLoS One* 13(12):e0209115.

14. Pospíšil P (2016) Production of Reactive Oxygen Species by Photosystem II as a Response to Light and Temperature Stress. *Front. Plant Sci.* 7.

15. Boehm M*, et al.* (2011) Investigating the early stages of photosystem II assembly in *Synechocystis* sp. PCC 6803: isolation of CP47 and CP43 complexes. *J. Biol. Chem.* 286(17):14812-14819.

16. Boehm M*, et al.* (2012) Subunit composition of CP43-less photosystem II complexes of Synechocystis sp. PCC 6803: implications for the assembly and repair of photosystem II. *Philos Trans R Soc Lond B Biol Sci* 367(1608):3444-3454.

17. Dobáková M, Sobotka R, Tichý M, & Komenda J (2009) Psb28 Protein Is Involved in the Biogenesis of the Photosystem II Inner Antenna CP47 (PsbB) in the Cyanobacterium Synechocystis sp. PCC 6803. *Plant Physiology* 149(2):1076-1086.

18. Komenda J*, et al.* (2004) Accumulation of the D2 protein is a key regulatory step for assembly of the photosystem II reaction center complex in Synechocystis PCC 6803. *J Biol Chem* 279(47):48620-48629.

19. Behler J, Vijay D, Hess WR, & Akhtar MK (2018) CRISPR-Based Technologies for Metabolic Engineering in Cyanobacteria. *Trends Biotechnol* 36(10):996-1010.

20. Li H*, et al.* (2016) CRISPR-Cas9 for the genome engineering of cyanobacteria and succinate production. *Metab. Eng.* 38:293-302.

21. Ungerer J & Pakrasi HB (2016) Cpf1 is a versatile tool for crispr genome editing across diverse species of cyanobacteria. *Scientific reports* 6:39681.

22. Wendt KE, Ungerer J, Cobb RE, Zhao H, & Pakrasi HB (2016) CRISPR/Cas9 mediated targeted mutagenesis of the fast growing cyanobacterium *Synechococcus elongatus* UTEX 2973. *Microbial cell factories* 15(1):115.

23. Qi LS*, et al.* (2013) Repurposing CRISPR as an RNA-guided platform for sequence-specific control of gene expression. *Cell* 152(5):1173-1183.

24. Yao L, Cengic I, Anfelt J, & Hudson EP (2016) Multiple Gene Repression in Cyanobacteria Using CRISPRi. *ACS Synth Biol* 5(3):207-212.

25. Huang CH*, et al.* (2016) CRISPR interference (CRISPRi) for gene regulation and succinate production in cyanobacterium *S. elongatus* PCC 7942. *Microbial cell factories* 15(1):196.

26. Gordon GC*, et al.* (2016) CRISPR interference as a titratable, trans-acting regulatory tool for metabolic engineering in the cyanobacterium *Synechococcus* sp. strain PCC 7002. *Metab. Eng.* 38:170-179.

27. Higo A, Isu A, Fukaya Y, Ehira S, & Hisabori T (2018) Application of CRISPR interference for metabolic engineering of the heterocyst-forming multicellular cyanobacterium *Anabaena* sp. PCC 7120. *Plant Cell Physiol.* 59(1):119-127.

28. Knoot CJ, Biswas S, & Pakrasi HB (2020) Tunable Repression of Key Photosynthetic Processes Using Cas12a CRISPR Interference in the Fast-Growing Cyanobacterium Synechococcus sp. UTEX 2973. *ACS Synth Biol* 9(1):132-143.

29. Kirtania P*, et al.* (2019) A single plasmid based CRISPR interference in Synechocystis 6803 - A proof of concept. *PLoS One* 14(11):e0225375.

30. Gordon GC & Pfleger BF (2018) Regulatory tools for controlling gene expression in cyanobacteria. *Adv. Exp. Med. Biol.* 1080:281-315.

31. Jin H, Lindblad P, & Bhaya D (2019) Building an inducible T7 RNA polymerase/T7 promoter circuit in *Synechocystis* sp. PCC6803. *ACS Synth Biol* 8(4):655-660.

32. Behle A, Saake P, & Axmann IM (2019) Comparative analysis of inducible promoters in cyanobacteria. *bioRxiv*:757948.

33. Kaczmarzyk D, Cengic I, Yao L, & Hudson EP (2018) Diversion of the long-chain acyl-ACP pool in Synechocystis to fatty alcohols through CRISPRi repression of the essential phosphate acyltransferase PlsX. *Metab Eng* 45:59-66.

34. Kelly CL, Taylor GM, Hitchcock A, Torres-Mendez A, & Heap JT (2018) A Rhamnose-Inducible System for Precise and Temporal Control of Gene Expression in Cyanobacteria. *ACS Synth Biol* 7(4):1056-1066.

35. Knoot CJ, Khatri Y, Hohlman RM, Sherman DH, & Pakrasi HB (2019) Engineered production of hapalindole alkaloids in the cyanobacterium *Synechococcus* sp. UTEX 2973. *ACS Synth Biol* 8(8):1941-1951.

36. Bhende PM & Egan SM (2000) Genetic evidence that transcription activation by RhaS involves specific amino acid contacts with sigma 70. *J. Bacteriol.* 182(17):4959-4969.

37. Ma AT, Schmidt CM, & Golden JW (2014) Regulation of gene expression in diverse cyanobacterial species by using theophylline-responsive riboswitches. *Appl. Environ. Microbiol.* 80(21):6704-6713.

38. Chi X*, et al.* (2019) Adopting a theophylline-responsive riboswitch for flexible regulation and understanding of glycogen metabolism in *Synechococcus elongatus* PCC7942. *Frontiers in microbiology* 10:551.

39. Blankenship RE (2014) *Molecular Mechanisms of Photosynthesis* (Wiley Blackwell) 2nd Ed.

40. Weisz DA*, et al.* (2017) Mass spectrometry-based cross-linking study shows that the Psb28 protein binds to cytochrome b559 in Photosystem II. *Proc Natl Acad Sci U S A* 114(9):2224-2229.

41. Heinz S, Liauw P, Nickelsen J, & Nowaczyk M (2016) Analysis of photosystem II biogenesis in cyanobacteria. *Biochim Biophys Acta* 1857(3):274-287.

42. Gibson DG*, et al.* (2009) Enzymatic assembly of DNA molecules up to several hundred kilobases. *Nat. Methods* 6(5):343-345.

43. Taton A*, et al.* (2014) Broad-host-range vector system for synthetic biology and biotechnology in cyanobacteria. *Nucleic Acids Res.* 42(17):e136.

44. Golden SS, Brusslan J, & Haselkorn R (1987) Genetic engineering of the cyanobacterial chromosome. *Methods Enzymol.* 153:215-231.

45. Elhai J, Vepritskiy A, Muro-Pastor AM, Flores E, & Wolk CP (1997) Reduction of conjugal transfer efficiency by three restriction activities of *Anabaena* sp. strain PCC 7120. *J. Bacteriol.* 179(6):1998-2005.

46. Wang D*, et al.* (1995) Discontinuous movements of DNA and RNA in RNA polymerase accompany formation of a paused transcription complex. *Cell* 81(3):341-350.

47. Kashino Y*, et al.* (2002) Proteomic Analysis of a Highly Active Photosystem II Preparation from the Cyanobacterium Synechocystis sp. PCC 6803 Reveals the Presence of Novel Polypeptides. *Biochemistry* 41(25):8004-8012.

48. Dai GZ, Qiu BS, & Forchhammer K (2014) Ammonium tolerance in the cyanobacterium *Synechocystis* sp. strain PCC 6803 and the role of the *psbA* multigene family. *Plant Cell Environ* 37(4):840-851.

Chapter 4

Control of expression of the PSII assembly factor CtpA

Chapter Contributions: All data in this chapter were generated by VMJ.

4.1 Summary

The c-terminal protease CtpA cleaves the carboxy-terminus of the D1 protein in a critical regulatory step of PSII assembly. Without processing of the D1 c-terminus, the Mn_4CaO_5 cluster cannot assemble, as the c-terminus of the mature peptide supplies a ligand to the catalytic metal center. To study the events of the Photosystem II lifecycle immediately following this processing step in more detail, I wished to control the expression of *ctpA* in S6803. Originally, I thought to use a reversible CRISPR inhibition strategy to control *ctpA* expression in the same way as I used it in Chapter 3 to turn the expression of the *psbD* gene on and off. However, a CRISPR inhibition system with one guide RNA targeted near the start codon of *ctpA* was not sufficient to achieve repression. I constructed three different strategies to more tightly control either reversible inhibition of *ctpA* in the WT strain or reversible expression in the *ctpA* deletion strain. In the first, the Rha-RSW inducible promoter was used to drive expression of *ctpA* on an RSF1010 based plasmid in the ΔCtpA strain. In the second, a Nickel-inducible promoter was used to drive *ctpA* expression on a plasmid in the ΔCtpA strain. In the third, *ctpA* was expressed exogenously on a plasmid in the ΔCtpA strain, with CRISPR-inhibition targeted to just past the start codon of the gene. The efficacy of these strategies to reversibly express the CtpA protein is assayed and discussed.

4.2 Introduction

A defining step in PSII synthesis is the photoassembly of the catalytic Mn_4CaO_5 cluster from soluble Mn^{2+} ions, Ca^{2+} ions, and water. This step in the assembly process may only occur after the C-terminus of the immature pD1 polypeptide is processed by the protease CtpA (c-terminal

protease). In the interest of studying the steps of assembly and photoactivation that occur around this processing step, I wished to target the *ctpA* gene for inhibition in the same reversible manner as we targeted *psbD* in the CRISPRi-RSW D2 strain (Chapter 3, (1)). However, I found that this CRISPR inhibition system was not suitable to target *ctpA* without some modification. Previously, we found that our rhamnose-inducible CRISPRi-RSW system was able to reduce expression of the D2 subunit by 97-99% by targeting the gRNA just past the *psbD* (gene that codes for D2) start codon (1). We implemented that same system in S6803, identical to the CRISPRi-RSW D2 system, except the gRNA was switched for one targeted to just past the *ctpA* start codon. However, no functional repression of CtpA activity was observed (Figure 4.1). So, we implemented a number of alternate strategies to control CtpA expression in *Synechocycstis* sp. PCC 6803 in a completely reversible fashion.

The most obvious alternate strategy, given that we have the deletion strain of *ctpA* in the lab (6), was to do the opposite of CRISPR-inhibition. I inducibly expressed *ctpA* in its deletion strain. I chose the Rha-RSW inducible promoter from which to express *ctpA*, as we observed that it is well-controlled in S6803. Alternatively, I also chose to use a Nickel-inducible promoter from S6803 to drive *ctpA* expression in the ΔCtpA strain, given that it was shown to have very low basal expression (7).

The third approach that I implemented was to improve the CRISPR-inhibition strategy. Because we and other groups have had success in achieving close to 100% repression using CRISPRi, and because we weren't sure how low of a basal expression level could be achieved with any inducible promoter, I altered the CRISPR inhibition strain to try to achieve maximal repression of Ctpa. To to this, I expressed CtpA from a constitutive promoter with low expression level in the deletion strain. On the same plasmid, I introduced the inducible CRISPR-inhibition

targeted to just past the start codon of *ctpA*. The rationale was that this expression system would improve the CRISPR inhibition because the TSS is now close to where the guide RNA is targeted.

This chapter will show the implementation of each of these systems, as well as growth, PSII activity, and level of D1 processing. Unfortunately, the original CRISPRi system failed to fully inhibit *ctpA* expression and the inducible promoters are somewhat leaky, allowing *ctpA* expression in the absence of inducers. So far, a fully reversible expression strategy has been elusive.

4.3 Results

4.3.1 CRIPSRi-RSW CtpA

To inhibit expression of *ctpA*, a CRISPR-inhibition plasmid was designed to target that gene. A guide RNA targeted to just past the start codon of *ctpA* in S6803 was chosen (Fig. 4.1A,B, full

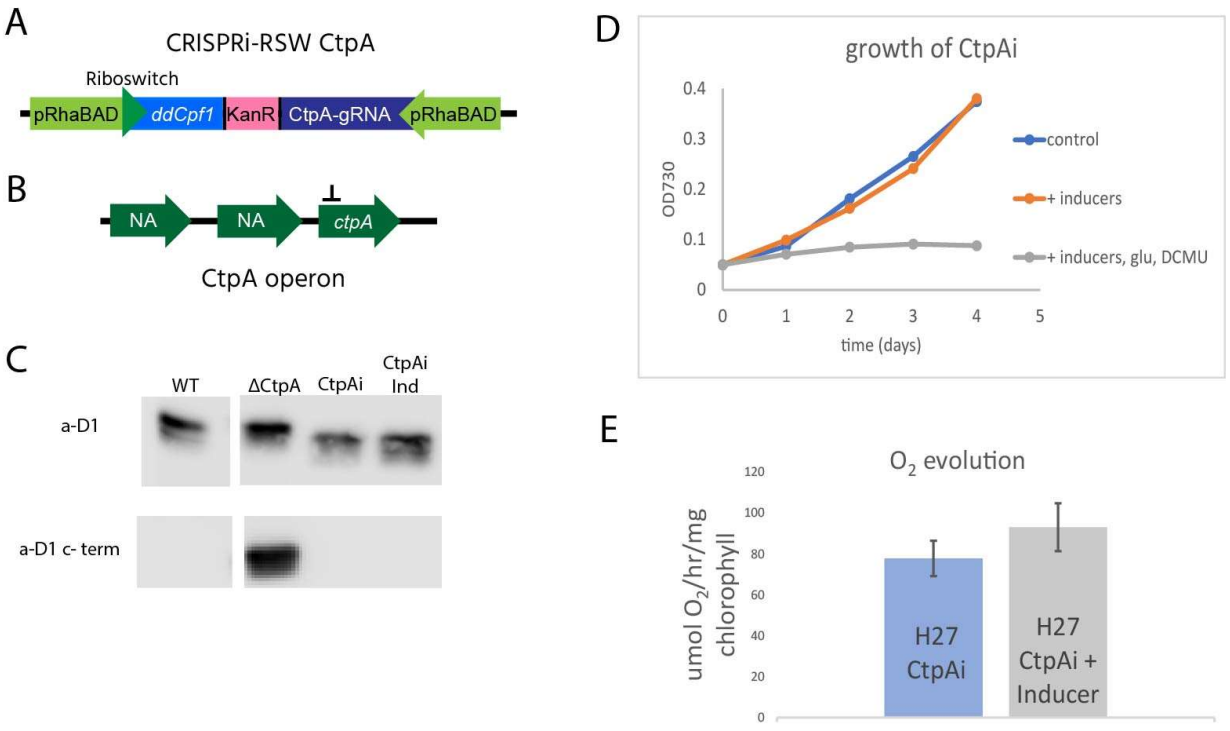

Figure 4.1 A) CRISPRi-RSW CtpA construct B) CtpA operon. Guide RNA target indicated by line. C) Western blot for D1 protein and D1 c-terminus D) growth of CtpAi strain with and without inducers added E) PSII activity (oxygen evolution rate) of CtpAi strain with and without inducer added.

plasmid map in Fig. S4.1) and cloned into the CRISPR-inhibition plasmid used in Chapter 3 (1), where the D2-targeting gRNA was swapped for one targeting *ctpA*. This plasmid-based system uses a rhamnose-inducible promoter coupled to a theophylline-controlled riboswitch to regulate expression of DNase-dead Cpf1 (Cas12a), and a rhamnose-inducible promoter to control expression of the guide RNA(s). This plasmid, called pCRISPRi-RSW CtpA, was introduced into

the H27 background of S6803. I called the strain H27 CtpAi. To test the activity of the CRISPRi system in the presence of inducers (5 g/L rhamnose and 2 mM theophylline), growth, PSII activity, and presence of the D1-c-terminus were measured. Figure 4.1C shows a western blot for both the D1 protein and the c-terminus of the D1 protein. As expected, the WT cells do not have any D1-c-terminus that cross-reacts with the antibody, while the deletion strain of CtpA does. Additionally, a shift in the molecular weight of D1 is observable by western blot, with a slightly higher molecular weight in the ΔCtpA strain, as expected due to the presence of the D1 c-terminus. The uninduced CtpAi strain did not contain the D1 c-terminus, as expected. However, it was expected that, in the induced strain of the CRISPRi targeting CtpA, the D1 c-terminus would be present and D1 have a higher molecular weight, but that was not observed. Accordingly, the induced CtpAi strain behaved similarly to the H27 strain and was not deficient in growth or photosynthesis (Figure 4.1 D,E). Several colonies were tested for growth and oxygen evolution, and none were inhibited.

In thinking about why this inhibition strategy was not able to repress CtpA to an extent to affect the level of D1 processing, there were a number of possibilities. First of all, it must be noted that we do not have a good antibody for CtpA, so its presence could not be directly measured. Secondly, we did not perform qPCR to test for *ctpA* transcript level, so we do not know what the degree of inhibition was, if any. So, I have several hypotheses for what may be occurring but I do not have evidence for which one is the case. We know that this CRISPRi system works in S6803, as evidenced in Chapter 3, so we can be confident that ddCpf1 is expressed in the presence of inducers. However, it is possible that inhibition does take place, and CtpA levels are decreased in the cell, but not to a degree to cause a noticeable difference in the amount of D1 able to be processed. As an enzyme, CtpA could be present at a very low level and still functional. So, it is possible that CtpA expression is inhibited but not to a degree that D1 is no longer processed or

growth is inhibited. Growth of these induced cultures at higher light may exacerbate a phenotype. The second, related possibility is that, as has been observed by other groups (2, 3), CRISPRi is less effective the further away the guide RNA is from the transcription start site of a gene. So, given the place of *ctpA* as the third gene in its operon, it is possible that there is a reduced level of repression from what we saw with the D2 protein. However, while *ctpA* is in an operon, it does seem to have an internal transcription start site (4, 5), and so whether this is the case is unclear. However, either way, it seems that this system was not working to inhibit CtpA to a degree to inhibit photosynthesis. Another possibility is that CtpA has an exceedingly long lifetime in the cell. So, following induction of ddCpf1, even if no new CtpA is expressed, the enzyme present in the cell is sufficient to maintain photosynthetic activity at normal levels. I measured protein content and PSII activity after 4 days, which would be an exceedingly long lifetime, so this seems unlikely.

One way to potentially improve inhibition would be to multiplex guide RNAs, with one targeted to the first, unannotated gene in the *ctpA* operon in addition to the gRNA targeting CtpA (Fig. 4.1 B). This strategy would improve repression if in fact the reason for continued CtpA expression is that the gRNA is too far from the TSS. However, the function of the first two genes in the operon is unknown, and this may have unintended consequences in the cell. So, we tried three alternate strategies to reversibly express CtpA.

4.3.2 Rhamnose-Theophylline inducible CtpA

To reversibly express *ctpA*, we reversed the CRISPR-inhibition approach. Rather than inhibit CtpA in a 'WT' strain, CtpA expression would be induced in its deletion strain. This deletion strain was constructed previously in the lab (6). To induce *ctpA*, it was expressed from the rhamnose-inducible RhaBAD promoter with a theophylline riboswitch on a replicating plasmid

(Fig. 4.2A, full plasmid Fig. S4.2), and introduced into the ΔCtpA strain (Fig. 4.2B). I called this plasmid pRhaRSWCtpAKanR (RRCK). When transformants containing the RRCK plasmid were assayed, however, it became clear that CtpA was active even in the uninduced strain. A western blot for the D1 c-terminus and the D1 subunit (Fig. 4.2C) shows the absence of the D1 c-terminus in the RRCK strain, and the presence of D1 at its mature, processed molecular weight. Similarly, the RRCK strain grew at the same rate as WT (Fig. 4.2 D). When oxygen evolution of the strains was measured, RRCK evolved oxygen at the same rate as WT. Therefore, we concluded that the promoter was leaky enough to allow expression of enough CtpA to maintain photosynthetic activity, even when uninduced.

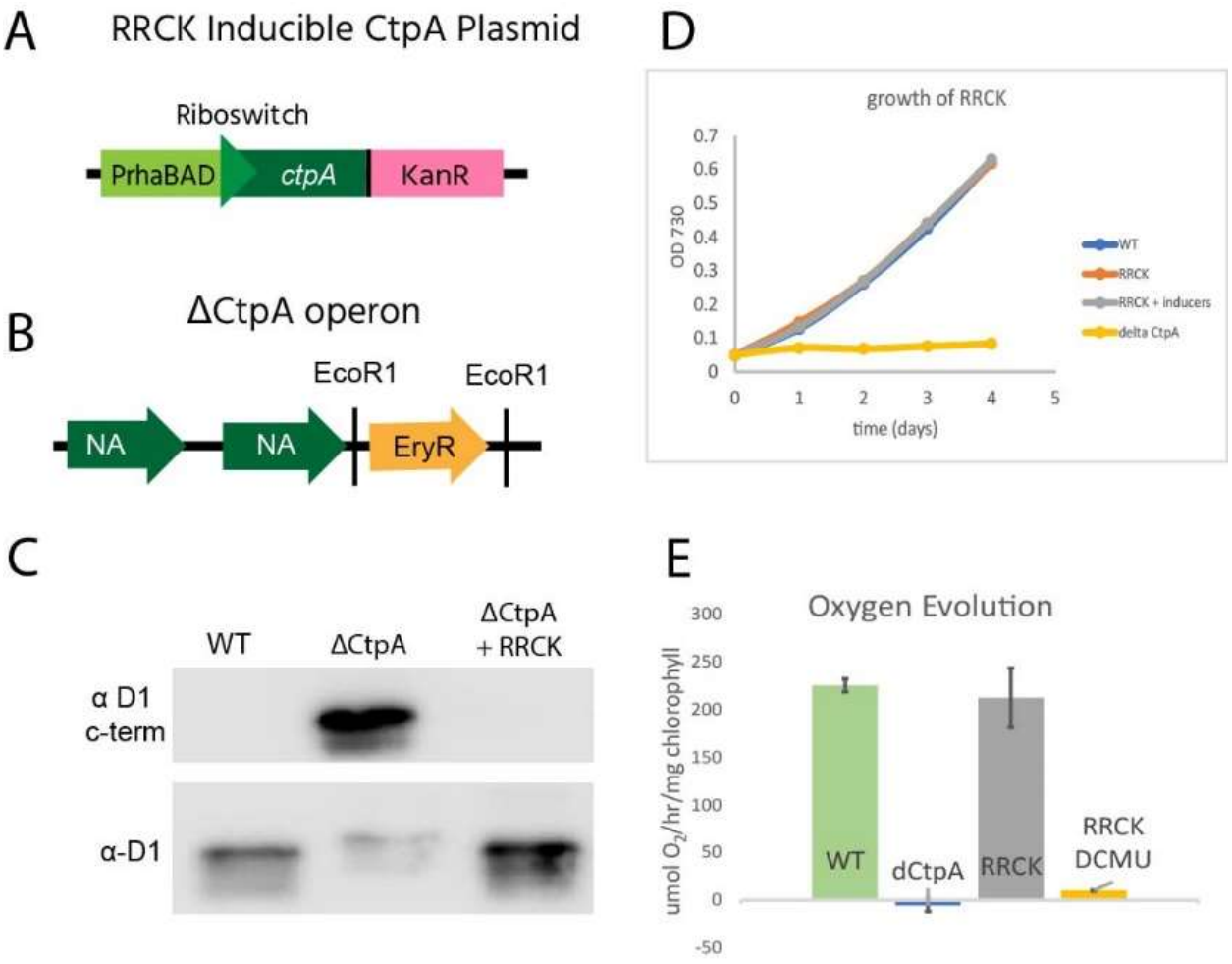

Figure 4.2 RRCK plasmid in Synechocystis sp. PCC 6803. A) RRCK construct. A rhamnose-theophylline promoter drives *ctpA* expression. B) The ΔCtpA construct. The CtpA gene was replaced by an erythryomycin resistance cassette using homologous recombination. See (6) for details. C) western blot for D1 subunit of PSII and the c-terminus of D1, which is removed by CtpA. D) growth of WT, ΔCtpA, and RRCK strain with and without inducers E) PSII activity of WT, ΔCtpA, and RRCK strains.

4.3.3 Nickel-inducible CtpA

Because the RRCK strain had leaky expression of CtpA, I wanted to find a different inducible promoter with lower basal expression to directly control expression of CtpA in its deletion strain. I chose the nickel-inducible promoter, PnrsB, from S6803. This promoter's activity was characterized in (7) as having a very low basal expression level in regular BG11 growth media, which does contain trace amounts of Co^{2+}. It is the promoter controlling expression of the *nrsBACD* operon in Synechocystis, which responds to toxic Ni^{2+} and Co^{2+} ions, and transports them out of the cells. This transport system also requires the native S6803 two-component system encoded by the *nrsRS* operon, where NrsS senses Ni^{2+} ions and phosphorylates NrsR which activates transcription of *nrsBACD* and *nrsRS* (8, 9). The PnrsB promoter was introduced in front of *ctpA* on an RSF1010 plasmid backbone, and I called the plasmid pNrsB CtpA. The plasmid pNrsB CtpA was introduced into the ΔCtpA strain (Fig. 4.4A). The full plasmid map is shown in Figure S4.4. I called the strain PnrsB CtpA.

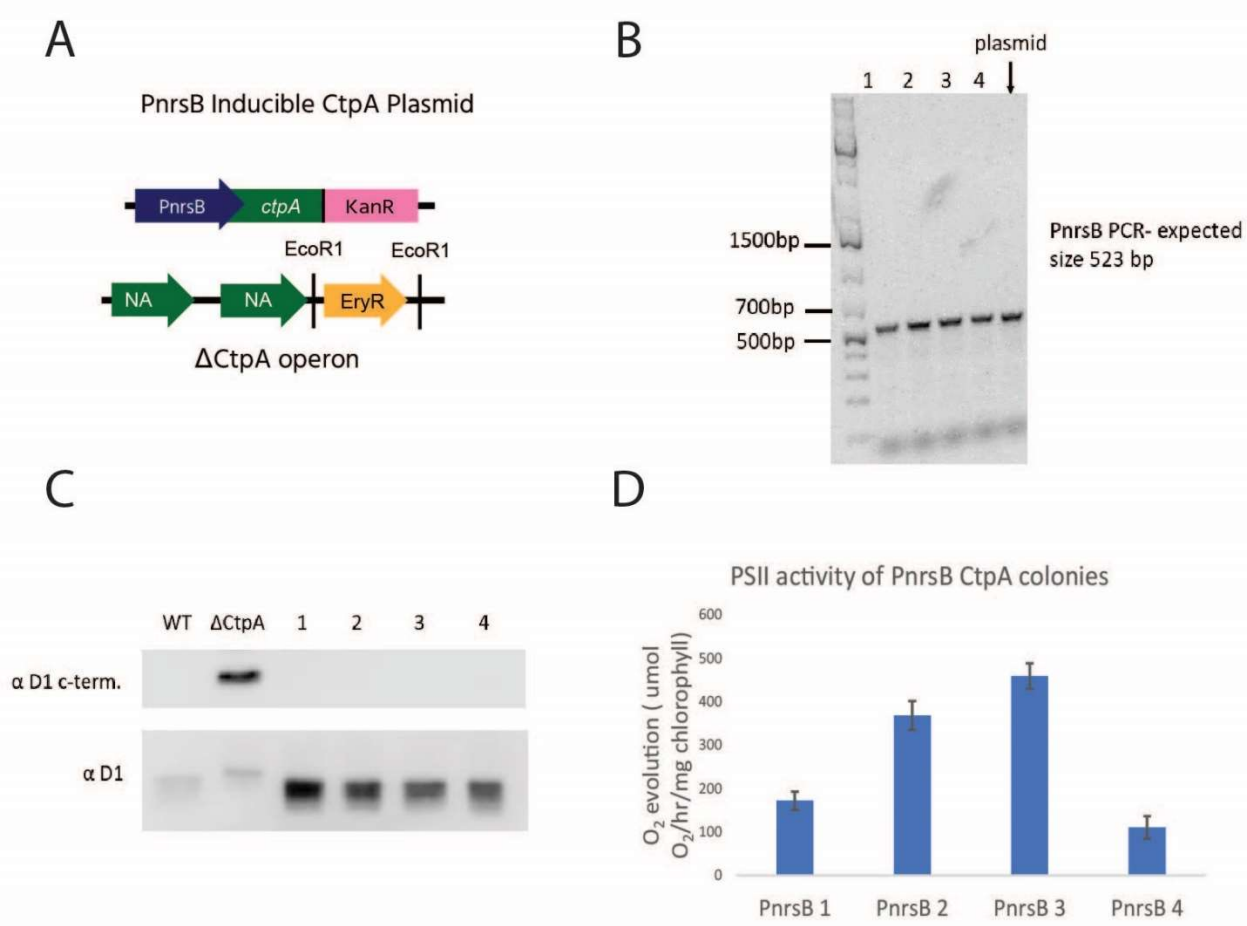

Figure 4.3 A) PnrsB CtpA construct**.** B) PCR check that PnrsB CtpA plasmid is intact in S6803 colonies assayed. Primers used were RRCK PCR 2Rev and PnsrB CtpASeq1 (See Fig. S4.4) C) Western blot for D1 protein and D1 c-terminus are shown for WT S6803, deltaCtpA, and 4 PnrsB CtpA colonies (1-4) D) PSII activity (oxygen evolution) of selected PnrsB CtpA colonies.

In Figure 4.3B, a PCR check of the plasmid fragment containing the PnrsB promoter from the S6803 strains is shown. In Figure 4.3C, a western blot shows that, in the PnrsB strains, the D1 protein is fully processed. The protein is at its mature molecular weight, and the c-terminus is absent. Figure 4.3D shows PSII activity of the PnrsB strains. While activity amongst the strains was variable, they all evolve oxygen even in the absence of inducer.

There are a ways to try to lower the basal expression from the PnrsB promoter, including growing the cells under lower light, which seemed to lower expression in (7), and growing the cells in BG11 -Co^{2+} in acid-washed flasks.

4.3.4 Pslr0701 CRISPRi-RSW CtpA

The final strategy to further tighten control of CtpA expression, to obtain a system in which, when CtpA is expressed, cells are fully photosynthetic, and when it is not, cells are unable to grow autotrophically, I developed the CRISPRi strategy further. In this strategy, *ctpA* was expressed from a weak constitutive promoter from S6803 (Pslr0701, described in (10)) on a plasmid in addition to the CRISPRi-RSW CtpA system. We then introduced this plasmid into the ΔCtpA strain of S6803. So, we had a system in which *ctpA* was expressed directly from a known weak promoter, not further down in an operon, in the deletion strain. From the same plasmid, *ddcpf1* is expressed from rhamnose-theophylline inducible promoter (Fig. 4.4), and the gRNA still targets just past the *ctpA* stop codon. I called this strain P0701 CtpA. I have transformed the P0701 CtpA plasmid in to ΔCtpa 6803, and am waiting for colonies to form to assay them for CtpA presence and activity.

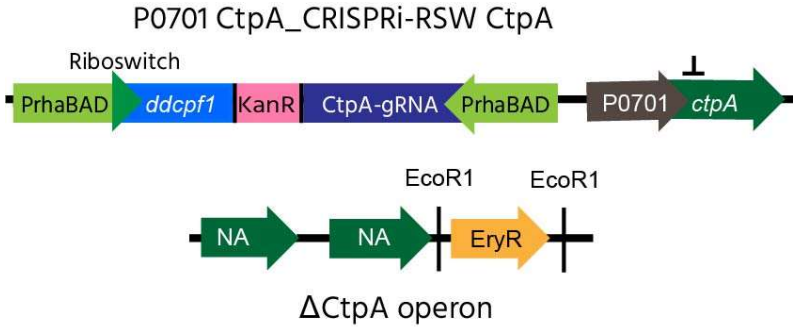

Figure 4.4. Pslr0701 CRISPRi-RSW CtpA construct and ΔCtpA construct

4.4 Discussion

A number of expression strategies were developed and tested for reversibly expressing *ctpA* but achieving a functional zero level of repression was elusive. It seems that, even when expressed at what was expected to be a very low level, as with the leaky inducible promoters, CtpA is able to process D1 at a high enough rate to maintain wild type or close-to wild type rates of photosynthesis. It is possible that growing these uninduced cells (either RRCK or the PnrsB CtpA strain) under stressful conditions such as high light or low temperature may exacerbate a phenotype. However, under the normal growth conditions that were assayed in this work, the strains behaved nearly identically to WT.

It is difficult to determine where the CRISPRi system was failing without qPCR data, especially in absence of CtpA antibody. An immediate future direction to determine the level of CtpA expression in all of the strains would be to do qPCR. Additionally, a His-tag or other known epitope could be engineered onto CtpA in the strains to allow for greater ease of western blotting.

0701 CtpA still needs to be assayed for CtpA presence and functionality. It is possible that CtpA may repressed to a sufficient level to inhibit photosynthesis in these cells. However, given that CtpA seems to be functional even at very low levels, whether or not this strategy will be successful is unclear.

4.5 Materials and Methods

4.5.1 Strains and growth conditions

All cloning work was performed in *E. coli* strain XL1-Blue grown in LB medium in culture tubes or on agar plates at 37 °C, supplemented with 50 μg/ml kanamycin, 20 μg/ml chloramphenicol, or 100 μg/ml ampicillin, as needed. *Synechocystis* 6803 cells were cultured in BG11 medium supplemented with 30 μg/ml kanamycin, 5 mM glucose, 10 μM DCMU, 3 μg/mL erythromycin as needed, under continuous white light at 30 μmol photons m^{-2} s^{-1} at 30 °C. Cultures were grown in 125-ml glass flasks or on agar plates. ΔCtpA strains were grown under the same conditions, but with a layer of kimwipes over the plate or around the flask to dim the light exposure To monitor growth, 150 μL of cells suspension was loaded onto a 96-well plate and OD at 730 nm was measured on a plate reader (BioTek, VT).

4.5.2 Strain Generation

S6803 H27 is described in (11). A Myc/6xHis tag was added to the c-terminus of the *slr1645* gene, followed by a gentamicin resistance cassette. The ΔCtpA strain is described in (6). The *ctpA* gene was replaced by an erythromycin resistance cassette.

Plasmids and strains used in this study are listed in Table S4.1, and all primers used in this study are listed in Table S4.2. All plasmids were constructed by Gibson Assembly (12), using linear fragments purified from PCR products or digested plasmid preps. All plasmids used in this study are based on the broad host replicating plasmid pRSF1010 (13). All PCR amplifications were performed using Phusion High-fidelity DNA polymerase (Thermo Scientific). Plasmids and PCR products were purified using the GeneJET (Thermo Scientific) plasmid miniprep kit and gel extraction kit, respectively. Oligonucleotides were designed using the SnapGene software (GSL

Biotech LLC) and synthesized by IDT (Coralville, IA). The sequences of all the plasmids constructed in this study were verified using Sanger sequencing (Genewiz, NJ).

pCRISPRi-RSW-CtpA

The pCRISPRi-RSW CtpA plasmid was assembled from the pCRISPRi-RSW D2 plasmid described previously in chapter 3 (1). That plasmid was double digested with BcuI and EcoO1091 to create the backbone. Fragment 1 was amplified using the primers Cpf1_BcuI_F and BcuI_R. Fragment 2, containing the CRISPR repeats, was amplified in two segments. Primer Template_F3 and crRNA_CtpA_R were used and Template_2R and crRNA_CtpA_F were used to amplify fragments that were PCR stitched together to form Fragment 2. Fragment 3 was amplified using the primers EcoO1091_F and EcoO1091_R.

pRhaRSWCtpA KanR

The RRCK plasmid (pRhaRSWCtpAKanR) was derived from the pRhaBAD-RSW-eyfp plasmid described in (1), in which EYFP is under the rhamnose-riboswitch inducible promoter. The EYFP gene was swapped for *ctpA*. That plasmid was double digested with XhoI and EcoRI as the backbone. Fragment 1 was amplified from the plasmid using primers RRCK_Frag1FOR and RRCK_Frag1REV. Fragment 2 was amplified from WT 6803 using primers RRCK_Frag2FOR and RRCK_Frag2REV. Fragment 3 was amplified from the plasmid using primers RRCK_Frag3FOR and RRCK_Frag3REV. The fragments and backbone were assembled using Gibson assembly. Bi-parental conjugation was performed with the 623 plasmid in the WM3064 (DAP auxotrophic) strain of *E.coli* to introduce the plasmid to ΔCtpA 6803.

Pslr0701 CtpA CRISPRi

The pslr0701 CtpA CRISPRi plasmid was derived from the pCRISPRi-RSW CtpA plasmid and pSL2750 described in (10), which expresses EYFP from the promoter associated with the S6803 gene slr0701. The pCRISPRi-RSW CtpA plasmid was double digested with MluI and Eco01091 to create the backbone. Fragment 1 and Fragment 4 were amplified from that plasmid with 0701CtpA_1FOR and 0701CtpA_1REV, and 0701CtpA_4FOR and 0701CtpA_4REV, respectively. Fragment 2 was amplified from pSL2750 using primers 0701CtpA_2FOR and 0701CtpA_2REV. Fragment 3 was amplified from S6803 using primers 0701CtpA_3FOR and 0701CtpA_3REV. The plasmid was introduced to S6803 H27 delta CtpA using tri-parental mating with the 443 helper plasmid, plated on a filter on BG11+5%LB+ 5mM glucose and transferred to BG11 Kan30 for selection.

PnrsB CtpA

The PnrsB plasmid is derived from the RRCK plasmid. That plasmid was double digested using ScaI and HindII to create the backbone. Fragment 1 was amplified from the plasmid using PnrsB_1FOR and PnrsB_1REV, while Fragment 3 was amplified using PnrsB_3FOR and PnrsB_3REV. Fragment 2 was amplified from S6803 genomic DNA using PnrsB_2FOR and PnrsB_2REV. The fragments and backbone were assembled using Gibson assembly and transformed to ΔCtpa H27 6803 using biparental mating with the WM3064 strain of *E.coli* with the 623 helper plasmid.

A tri-parental conjugation method was used, except where indicated, to transfer all pRSF1010 derivative plasmids to *Synechocystis* 6803 cells (14), using a helper strain of *E. coli* containing the pRL443 and pRL623 plasmids (15, 16). Transformants were isolated on BG11 agar

plates containing 20 μg/mL kanamycin, 5mM glucose, 10 uM DCMU, 3 mM erythromycin, as needed. Isolated *Synechocystis* 6803 transformants were checked by PCR to confirm presence of the desired constructs.

4.5.3 Western blot analysis

Cyanobacterial cells were harvested and broken by bead beating as described previously (17) with minor modifications. Cells were re-suspended in RB buffer (25% glycerol (wt/vol), 10mM $MgCl_2$, 5mM $CaCl_2$, 50 mM MES buffer pH 6.0) and broken by vortexing with 0.17 mm glass beads. Membrane fraction was isolated by centrifugation, re-suspended in RB, and solubilized by addition of β-D-dodecyl maltoside (DDM) to a final concentration of 0.8%. After incubation on ice in dark for 30 min, the solubilized membranes were separated from the insoluble material by centrifugation at gradually increasing speed from 120×g to 27,000×g at 4 °C for 20 min. The solubilized membranes were then stored at −80 °C for future use. The protein content was determined using bicinchoninic acid (BCA) protein assay reagent (Thermo Scientific).

SDS-PAGE was performed by loading the same amount of isolated membrane proteins on a 12.5% acrylamide resolving gel. After electrophoresis, proteins were transferred to a polyvinylidene difluoride (PVDF) membrane (Millipore), blocked using 5% bovine serum albumin (BSA) for 3 h at room temperature, and then separately incubated with the primary rabbit antibodies raised against D1 and D1 c-terminus polypeptides overnight at 4°C. The horseradish peroxidase (HRP)-conjugated secondary antibody goat anti-rabbit IgG (H+L)-HRP conjugate (Bio-Rad) was diluted at 1:5,000 in 1.5% BSA. Bands were visualized using chemiluminescence reagents (EMD Millipore, Billerica, MA, USA) with an ImageQuant LAS-4000 imager (GE Healthcare).

4.5.4 Measurement of Photosystem II activity

PSII activity was analyzed *in vivo* using a custom-built clark-type electrode. Samples were incubated at 30°C in the light prior to measurement in the presence of 1 mM potassium ferricyanide and 0.5 mM 2,6-dichloro-*p*-benzoquinone as electron acceptors to measure PSII-specific oxygen evolution rates.

4.6 Supporting Information

Figure S4.1 Plasmid Map of CRISPRi-RSW CtpA

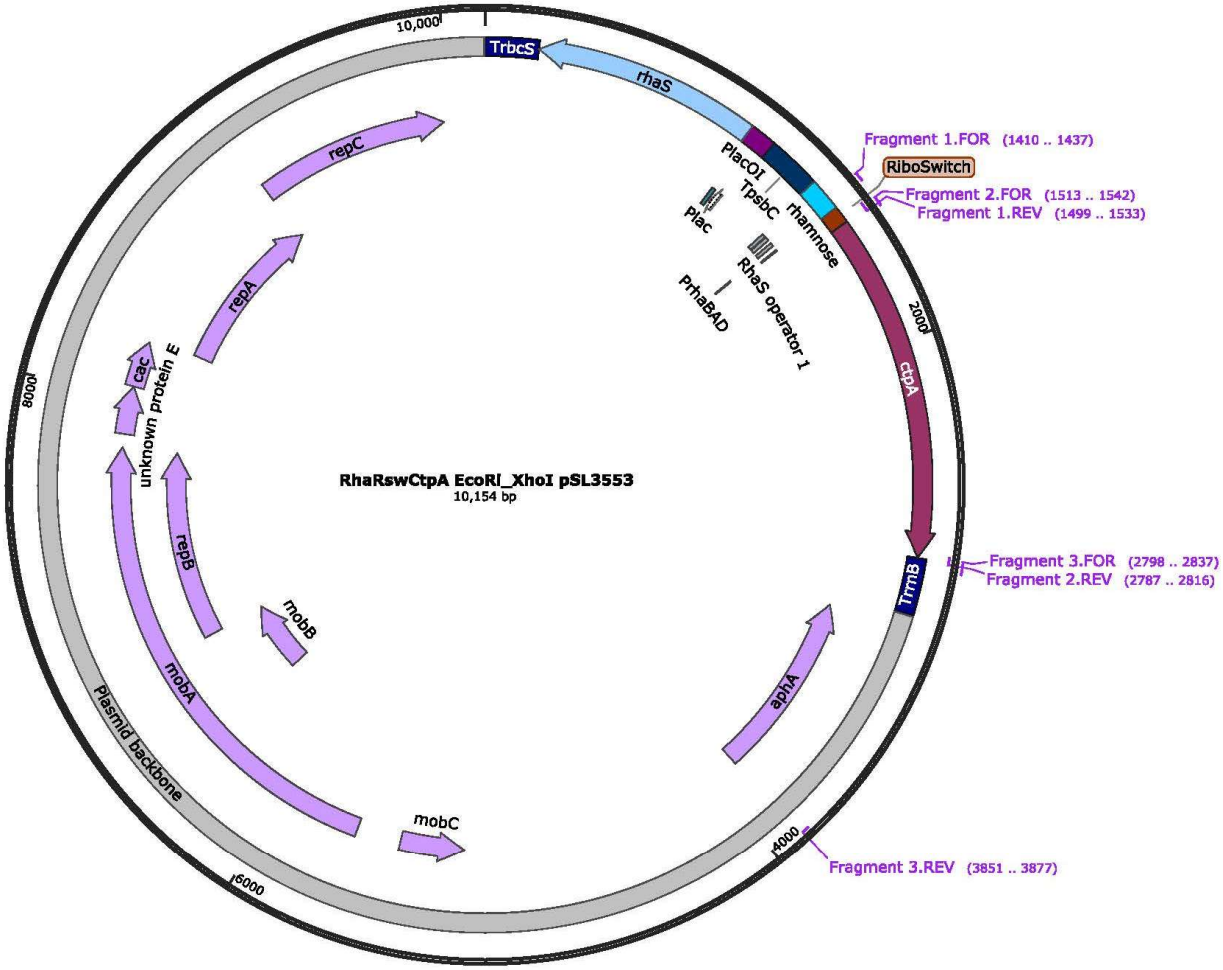

Figure S4.2 Plasmid Map of RRCK

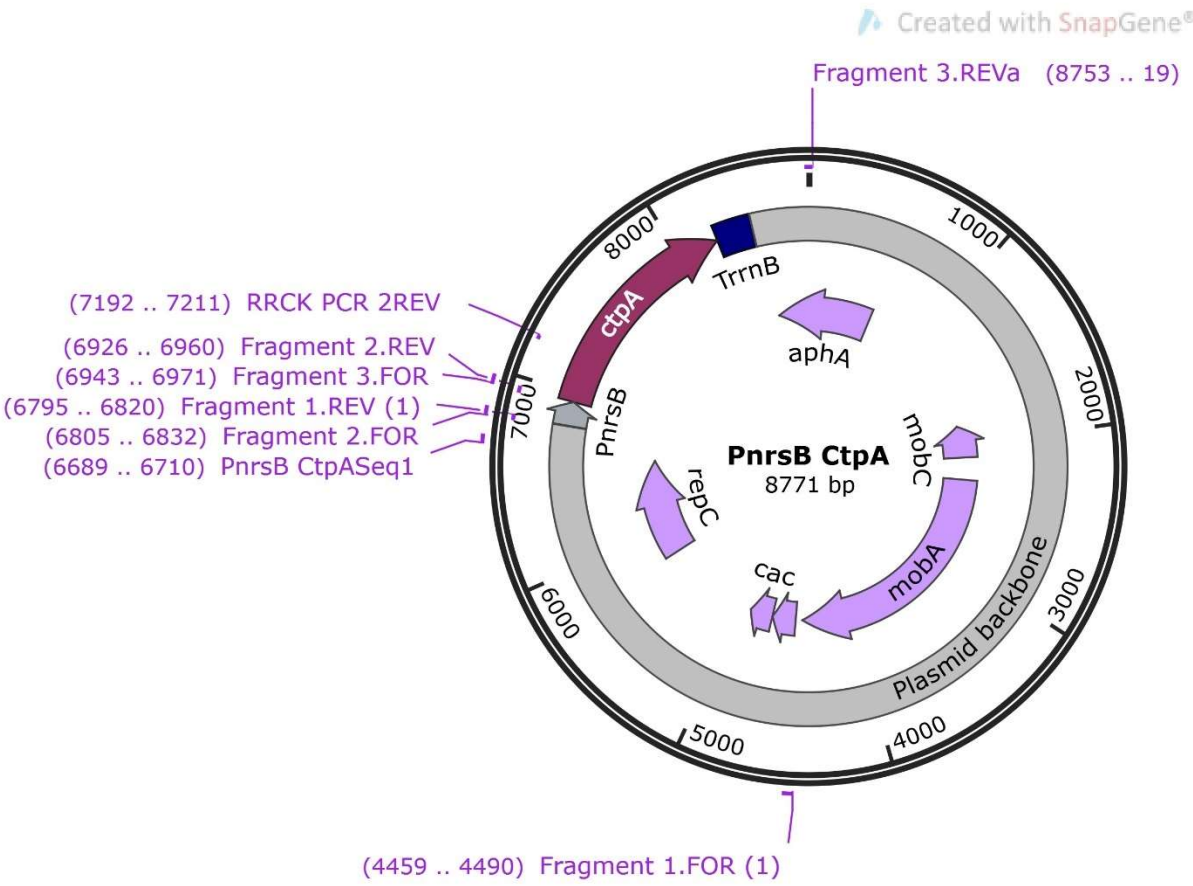

Figure S4.3 Plasmid Map of PnrsB-CtpA

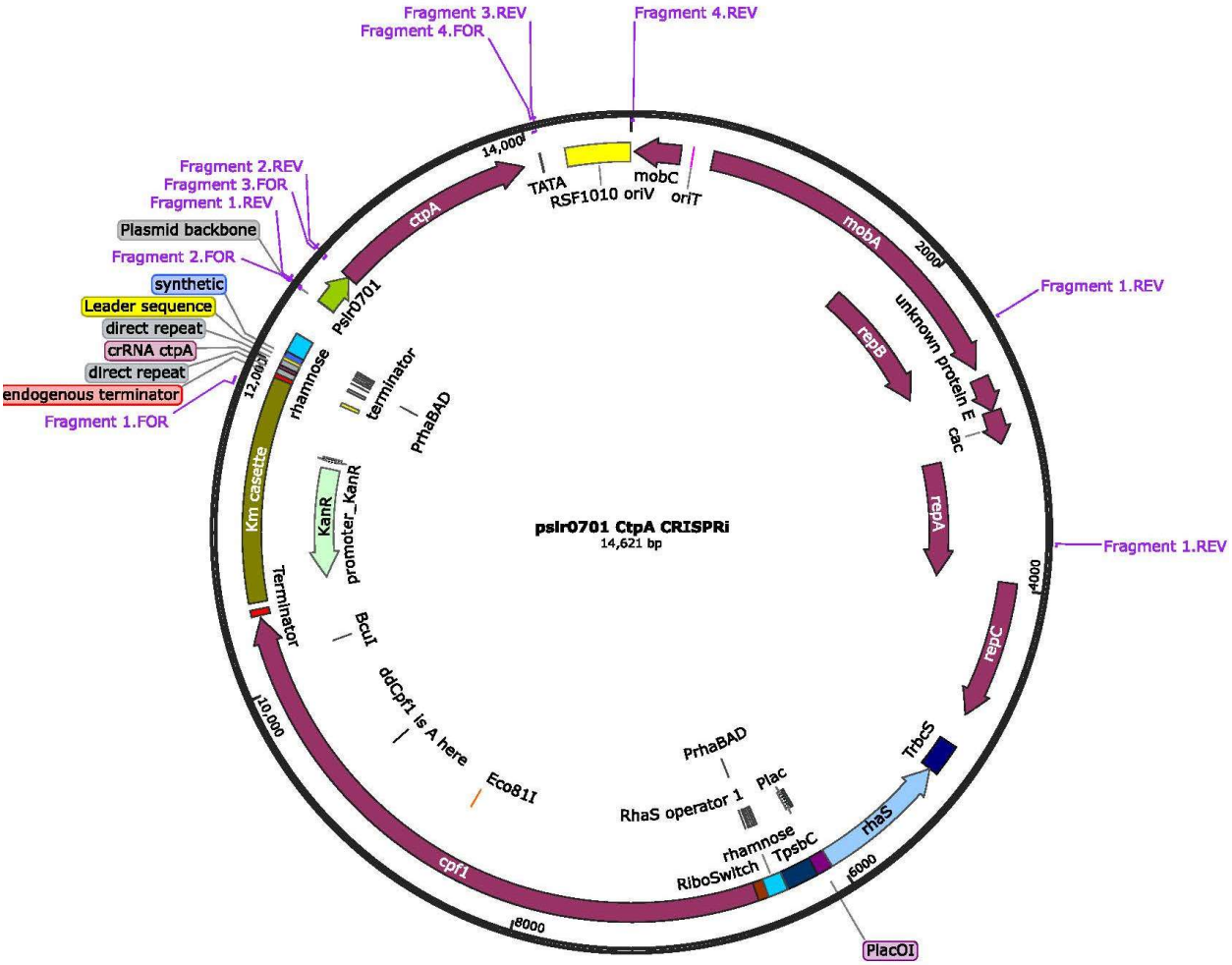

Figure S4.4 Plasmid Map of pslr0701 CRISPRi CtpA

Table S4.1 Strains and Plasmids used in Chapter 4

Plasmid or Strain name	**Description**	**Source**
H27 6803	S6803 strain with c-terminal His/Myc tag on Psb27. GmR	(11)
pCRISPRi-RSW CtpA	CRISPR-inhibition plasmid with guide RNA targeting CtpA	This study
H27 CtpAi	H27 S6803 strain with pCRIPSRi-RSW CtpA plasmid. GmR, KanR	This study
H27 ΔCtpA	H27 6803 strain with deletion of CtpA gene, GmR, EryR	(6, 18)
pRhaRSWCtpAKanR (RRCK)	Plasmid with CtpA under the rhamnose-riboswitch inducible promoter, KanR	This study
H27 ΔCtpA RRCK	H27 ΔCtpA strain with RRCK plasmid. GmR, EryR, KanR	This study
pslr0701 CtpA CRISPRi	pCRISPRi-RSW CtpA with CtpA expressed under Pslr0701 promoter	This study
0701 CtpA CRISPRi	H27 ΔCtpA strain with p0701 CtpA CRISPRi plasmid. GmR, EryR, KanR	This study
pnrsB CtpA	RSF1010 based plasmid with CtpA under PnrsB promoter	This study
PnrsB CtpA	H27 ΔCtpA strain with pNrsB CtpA plasmid. GmR, EryR, KanR	This study

Table S4.2 Primers used in Chapter 4

Primer Name	**Primer Sequence**
EcoO1091_F	ccgtttttgcctaaatcagcttctacct
EcoO1091_R	gatgagccgggctgaatgatc
Cpf1_BcuI_F	agagcgacaaaaagttttttgc
BcuI_R	tagcgatttatgaaggtcatttttttc
Template2_R	gctgatttaggcaaaaacgg
Template_F3	tacagctgaaagcgaaaaaaaatgaccttcataaatcgc
crRNA_ctpA_F	gtctaagaactttaaataatttctactgttgtagatGGCTTTAGCTTTTTCTTTG
crRNA_ctpA_R	atctacaacagtagaaattatttaaagttcttagacGCAAAGAAAAAGCTAAAGC
RRCK_Frag1FOR	taacgagaaggtcgcgaattcaggcgct
RRCK_Frag1REV	cgtttacccatCTTGTTGTTACCTCCTTAGCAGGG
RRCK_Frag2FOR	TAACAACAAGatgggtaaacggacaaggcg
RRCK_Frag2REV	ggctctagtattagttgggcttgtgagccg
RRCK_Frag3FOR	cccaactaatactagagccaggcatcaaataaaacgaaag
RRCK_Frag3REV	CGGGAAACGTCTTGCTCGAGGCCGCGA
0701CtpA_1FOR	gactgtgctggtcattaaacgcgtattcaggctgacc
0701CtpA_1REV	agttctcgggacggccagccgg
0701CtpA_2FOR	gccgtcccgagaactaagacaaaaattactggg
0701CtpA_2REV	tttacccatcctcccatttcttctctgtct
0701CtpA_3FOR	aatgggaggatgggtaaacggacaaggcg
0701CtpA_3REV	ggcggccaatcttatcacgcagggg
0701CtpA_4FOR	gataagattggccgccacatgaggc
0701CtpA_4REV	tgatcgaccgagacagctgcggg

PnrsB_1FOR	ACGCCTGTTATACTATGAGTACTCACGCACAG
PnrsB_1REV	tggtggaagtgGGAAGCAAAGCCAGG
PnrsB_2FOR	CTTCCcacttccaccagcaaaattcgca
PnrsB_2REV	tttacccataccacctcaaattgggaatttgtcca
PnrsB_3FOR	tgaggtggtatgggtaaacggacaaggcg
PnrsB_3REV	GTCTGGAAAGAAATGCATATCGATTTGCCATTCTCACC

4.7 References

1. Liu D, Johnson VM, & Pakrasi HB (2020) A Reversibly Induced CRISPRi System Targeting Photosystem II in the Cyanobacterium Synechocystis sp. PCC 6803. *ACS Synthetic Biology* 9(6):1441-1449.

2. Santos M, Pacheco CC, Yao L, Hudson EP, & Tamagnini P (2021) CRISPRi as a Tool to Repress Multiple Copies of Extracellular Polymeric Substances (EPS)-Related Genes in the Cyanobacterium Synechocystis sp. PCC 6803. *Life (Basel)* 11(11).

3. Yao L, Cengic I, Anfelt J, & Hudson EP (2016) Multiple Gene Repression in Cyanobacteria Using CRISPRi. *ACS Synth Biol* 5(3):207-212.

4. Mitschke J*, et al.* (2011) An experimentally anchored map of transcriptional start sites in the model cyanobacterium Synechocystis sp. PCC6803. *Proc Natl Acad Sci U S A* 108(5):2124-2129.

5. Kopf M*, et al.* (2014) Comparative analysis of the primary transcriptome of Synechocystis sp. PCC 6803. *DNA Res* 21(5):527-539.

6. Roose JL & Pakrasi HB (2004) Evidence that D1 processing is required for manganese binding and extrinsic protein assembly into photosystem II. *J Biol Chem* 279(44):45417-45422.

7. Englund E, Liang F, & Lindberg P (2016) Evaluation of promoters and ribosome binding sites for biotechnological applications in the unicellular cyanobacterium Synechocystis sp. PCC 6803. *Sci Rep* 6:36640.

8. Garcia-Dominguez M, Lopez-Maury L, Florencio FJ, & Reyes JC (2000) A gene cluster involved in metal homeostasis in the cyanobacterium Synechocystis sp. strain PCC 6803. *J Bacteriol* 182(6):1507-1514.

9. Lopez-Maury L, Garcia-Dominguez M, Florencio FJ, & Reyes JC (2002) A two-component signal transduction system involved in nickel sensing in the cyanobacterium Synechocystis sp. PCC 6803. *Mol Microbiol* 43(1):247-256.

10. Liu D & Pakrasi HB (2018) Exploring native genetic elements as plug-in tools for synthetic biology in the cyanobacterium Synechocystis sp. PCC 6803. *Microb Cell Fact* 17(1):48.

11. Roose JL & Pakrasi HB (2008) The Psb27 protein facilitates manganese cluster assembly in photosystem II. *J Biol Chem* 283(7):4044-4050.

12. Gibson DG*, et al.* (2009) Enzymatic assembly of DNA molecules up to several hundred kilobases. *Nat. Methods* 6(5):343-345.

13. Taton A*, et al.* (2014) Broad-host-range vector system for synthetic biology and biotechnology in cyanobacteria. *Nucleic Acids Res.* 42(17):e136.

14. Golden SS, Brusslan J, & Haselkorn R (1987) Genetic engineering of the cyanobacterial chromosome. *Methods Enzymol.* 153:215-231.

15. Elhai J, Vepritskiy A, Muro-Pastor AM, Flores E, & Wolk CP (1997) Reduction of conjugal transfer efficiency by three restriction activities of *Anabaena* sp. strain PCC 7120. *J. Bacteriol.* 179(6):1998-2005.

16. Wang D*, et al.* (1995) Discontinuous movements of DNA and RNA in RNA polymerase accompany formation of a paused transcription complex. *Cell* 81(3):341-350.

17. Kashino Y*, et al.* (2002) Proteomic Analysis of a Highly Active Photosystem II Preparation from the Cyanobacterium Synechocystis sp. PCC 6803 Reveals the Presence of Novel Polypeptides. *Biochemistry* 41(25):8004-8012.

18. Liu H, Roose JL, Cameron JC, & Pakrasi HB (2011) A genetically tagged Psb27 protein allows purification of two consecutive photosystem II (PSII) assembly intermediates in Synechocystis 6803, a cyanobacterium. *J Biol Chem* 286(28):24865-24871.

Chapter 5

Psb27 contributes to non-photochemical quenching during its participation in the PSII life cycle

This Chapter was adapted, with permission, from:

Johnson, V.M., Biswas, S., Roose, J.L., Liu, H, and Pakrasi, H.B. (2022). Psb27, a photosystem II assembly protein, enables quenching of excess light energy during its participation in the PSII lifecycle. *Photosynth. Res*. DOI: 10.1007/s11120-021-00895-3.

Chapter contributions:

Data presented in Figures 5.4, S5.1B, S5.1C were generated by VMJ.

5.1 Summary

Photosystem II (PSII), the enzyme responsible for oxidizing water into molecular oxygen, undergoes a complex lifecycle during which multiple assembly proteins transiently bind to and depart from PSII assembly intermediate complexes. Psb27 is one such protein. It associates with the CP43 chlorophyll-binding subunit of PSII to form a Psb27-PSII sub-complex that constitutes 7-10% of the total PSII pool under normal growth conditions. Psb27 remains bound to PSII assembly intermediates and dissociates prior to the formation of fully functional PSII. In this study, we compared a series of Psb27 mutant strains in the cyanobacterium *Synechocystis* sp. PCC 6803 with varied expression levels of Psb27: wild type (WT); *psb27* genetic deletion (Del27), genetically complemented *psb27* (Com27); and over-expressed Psb27 (OE27). The Del27 strain demonstrated decreased non-photochemical fluorescence quenching, while the OE27 strain showed increased non-photochemical quenching and tolerance to fluctuating light conditions. Multiple flashes and fluorescence decay analysis indicated that OE27 has the least affected maximum PSII quantum yield of the mutants. OE27 also displayed a minimal impact on the half-life of the fast component of Q_A^- reoxidation over multiple flashes, indicating robust PSII function. We propose that the close association between Psb27 and CP43, and the absence of a fully functional manganese cluster in the Psb27-PSII complex, create a PSII sub-population that dissipates excitation energy prior to its recruitment into the functional PSII pool. Efficient energy dissipation prevents damage to this pre-PSII pool and allows for efficient PSII repair and maturation. Participation of Psb27 in the PSII life cycle ensures high quality PSII assembly.

5.2 Introduction

Photosystem II (PSII) is a unique enzyme, in that it routinely experiences damage caused by one of its substrates, light, and its derivative reactive oxygen species. Additionally, PSII is assembled modularly from chlorophyll-containing subunits, which themselves are sensitive to damage by absorption of light prior to complete PSII assembly. On the organismal level, this photo-damage is detrimental to fitness unless a protective mechanism is adopted to dissipate excess light energy, both during assembly and under photoactive conditions. Cyanobacteria have several known mechanisms of excitation energy quenching and redistribution, collectively called non-photochemical quenching (NPQ). These include quenching via the orange carotenoid protein (OCP), which, in its light-induced active state, uncouples the excitation energy transfer from phycobilisome antennas to PSII, reducing its functional cross section (1, 2). Another mechanism is via IsiA, a chlorophyll-containing homolog of CP43, which forms oligomeric ring structures under stress conditions (3) (4). These rings are thought to absorb and dissipate excess light energy as a means of photoprotection. Additionally, during assembly, the reaction center proteins of PSII are associated with carotenoid-containing quenching proteins known as HLIPS for protection prior to their assembly into active PSII (5, 6). This mechanism relies on carotenoids' ability to quench both triplet chlorophyll and singlet oxygen. Cyanobacteria have two other mechanisms of fluorescence quenching and redistribution. These are state transitions, which regulate the distribution of excitation energy between PSII and PSI, and photoinhibition, which results from the high-light-induced inactivation of PSII caused by damage and degradation of the D1 protein.

Elucidation of photoprotective strategies that occur at the molecular level promises to inspire rational redesign of photosynthesis to sustainably meet current and future global food and energy demand (7). Recently, increasing the responsiveness of photoprotective quenching routes

to fluctuating light conditions has been observed to have a significant (15%) positive impact on crop yield under simulated field conditions (8). Overall, the increased availability of protective quenchers and accelerated recovery from NPQ in lower light conditions allowed for increased environmental adaptability and thus increased photosynthetic productivity.

Psb27, a small extrinsic membrane protein, is only bound to inactive PSII. It binds either to monomeric PSII during *de novo* assembly and repair, or to dimeric PSII during repair (9-12). It is thought to enable the efficient light-driven assembly (photoactivation) of the Mn-cluster (13, 14). In strains lacking Psb27, PSII can assemble fully, but photoactivation is slower and recovery from photodamage is slower as well (14-16). In the absence of both Psb27 and CP47, unassembled CP43 is degraded at a higher rate (17), which indicates that Psb27 stabilizes CP43 and allows a relatively larger amount of the pre-complex (Psb27-CP43) to form. Psb27 is not found in the structure of active PSII, but recently, structures of PSII assembly complexes bound to Psb27 have been elucidated using cryo-electron microscopy (18), (19). These structures reveal that Psb27 binds to the surface of Loop E of CP43 distal to the Mn binding site, or D1/D2 axis, which is consistent with two previous observations from mass spectrometry crosslinking and protein foot-printing (20, 21). These findings have suggested an allosteric role of Psb27 in maintaining PSII in a nonfunctional state, ready for the final steps of PSII assembly. However, the details of such structural arrangements remain unclear.

Psb27 is conserved across all oxygenic photosynthetic organisms. In *Arabidopsis thaliana*, Psb27 is not essential for PSII formation and photoautotrophic growth. Absence of Psb27, however, leads to decreased recovery of the photodamaged PSII complex (22), especially in fluctuating light (23). We suggest that a similar growth benefit may be conferred by Psb27 in

cyanobacteria, and we propose a mechanistic explanation for how Psb27-PSII contributes to optimal PSII function and eco-physiological fitness in cyanobacteria.

5.3 Results

This study analyzed four strains of *Synechocystis* sp. PCC 6803 for growth and photosynthetic parameters: WT, a deletion mutant of Psb27 (Del27), a strain complementing the deletion (Com27), and a weak over-expression line of Psb27 (OE27). Figure 5.1A shows the growth rates of these strains under standard lab conditions: constant, low level (30 µM photons m^{-2} s^{-2}) light. Figure 5.1B shows the growth rate under fluctuating light conditions: a 30-minute-high light/30-minute dark cycle. While the growth rates are quite similar, the OE27 strain under continuous light shows slower initial growth before catching up to the WT at about 4-5 days of growth. Under fluctuating light conditions, the growth rate of the strains is similar as well, but the OE27 strain overtakes the WT after several days of growth. Interestingly, under fluctuating light, the Del27 strain and Com27 strains also appear to overtake the WT.

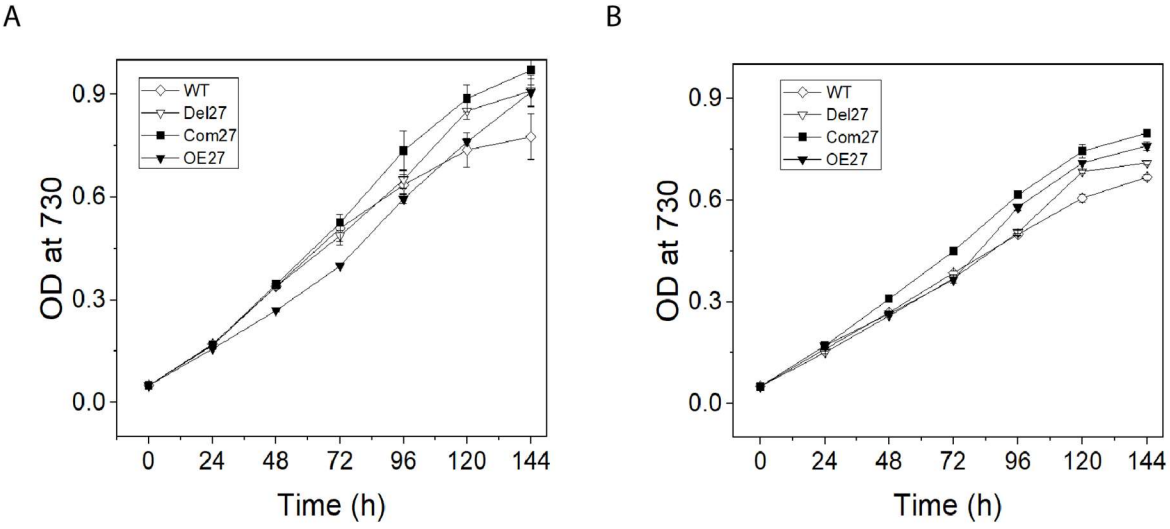

Figure 5.1 OE27 growth outpaces WT *Synechocystis* 6803 in fluctuating light. A) Growth under continuous light. This figure shows the growth curve of WT, Del27, Com27, OE27 under normal growth continuous light (30 µmol photons $m^{-2} \cdot s^{-1}$). B) Growth under 1200 µmol photons $m^{-2} \cdot s^{-1}$, 30 minute on-off cycles. Growth was shown as an average of three replicates.

To further test the photosynthetic parameters of these strains, cells were grown on BG-11 plates without antibiotics and the Fluorocam 800MF was used to assay for non-photochemical quenching. Figure 5.2A shows the NPQ trace collected for each of the four strains. Application of

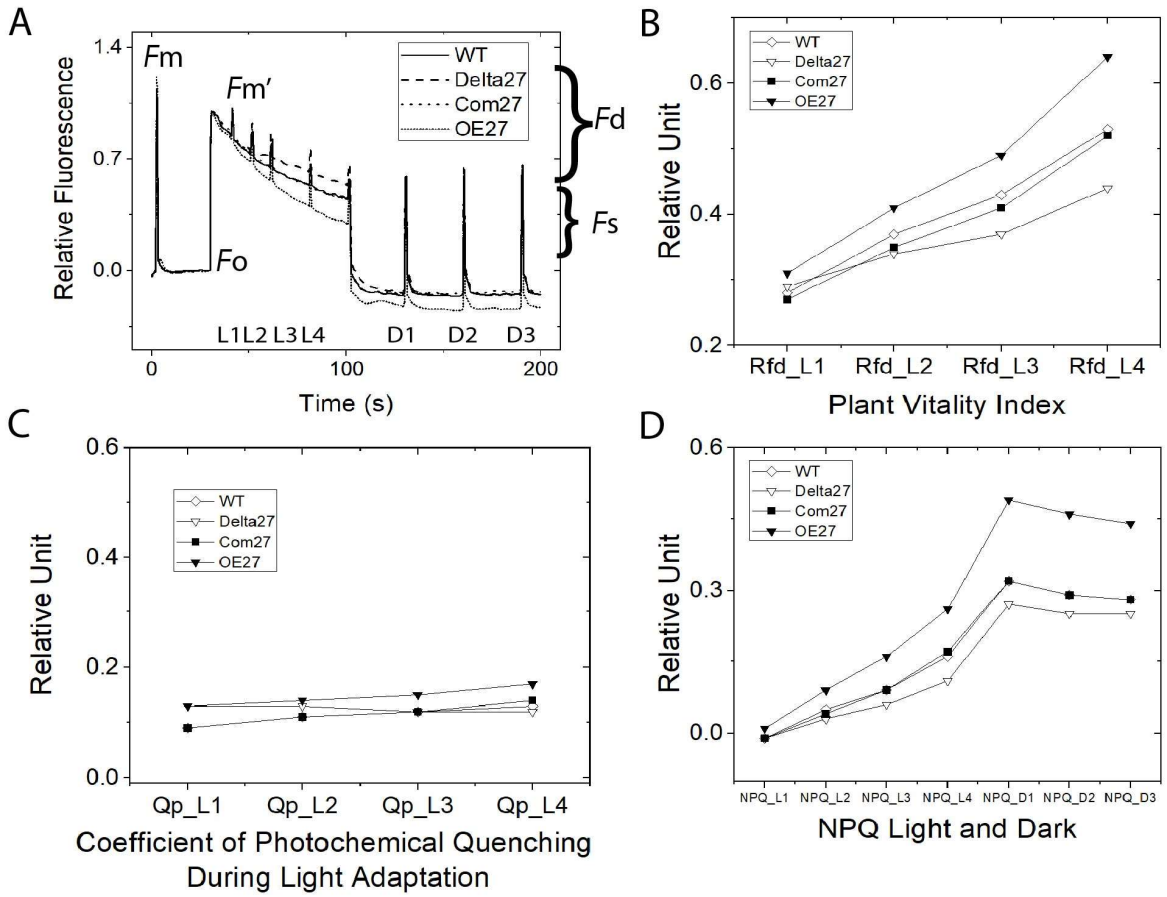

Figure 5.2: NPQ is increased in the Psb27 overexpression strain (A) NPQ traces from Fluorocam 800MF of four cell lines. Light and dark scheme are indicated with saturating pulses applied. *F*m, *F*d, and *F*s are marked for WT trace. Deconvolution of the traces followed manufacturer's protocol (Photo System Instruments, Brno, Czech Republic). (B) Plant vitality index Rfd (*F*d/*F*s) at intervals during light exposure. (C) Coefficient of quenching (*F*m'-*F*)/(*F*m'-*F*o'). (D) NPQ ((*F*m-*F*m')/*F*m'). Data are representative of 3 replicates.

a saturating pulse to the dark-adapted plate induced a maximum value of fluorescence, *F*m, by closing reaction centers. At that time there was no NPQ because the colonies had been fully dark-adapted. Following a dark relaxation, a sufficiently strong actinic light was applied and an initial rise in fluorescence was observed. This fluorescence was then partially quenched as a result of increasing competition with photochemical and non-photochemical events. Five saturating pulses

were applied under actinic illumination that transiently closed all the reaction centers and provided a value of maximal fluorescence in the light-adapted state, termed *F*m′. The difference between *F*m and *F*m*′,* is due to the contribution of NPQ. Figure 5.2B plots the plant vitality index, Rfd, derived from peak fluorescence, *F*m, attained during the first seconds of the transient, and the steady-state fluorescence, *F*s, in the light-adapted phase. In healthy photosynthetic cells, there is a larger value, as shown for WT and Com27, while Del27 has a slower rise than WT. Conversely, OE27 demonstrates an accelerated rise which means that this strain's overall physiological fitness is increased. Figure 5.2C shows the coefficient of photochemical quenching during actinic light conditions, which reflects the process of photosynthesis itself. Upon light illumination, enzymes in the Calvin-Benson Cycle activate fully, the metabolite pool size increases, and the carbon concentrating mechanism for feeding CO_2 to Rubisco is initiated. These factors lead to an increased electron sink from the photosynthetic electron transport chain and contribute to quenching. To our surprise, Del27 showed effectively no increase in the time range recorded, and WT and Com27 showed a gradual increase, in parallel with that of OE27. The values for WT and Com27, however, are less than that of the OE27. Figure 5.2D shows the NPQ recorded during the actinic and dark phases, derived from the difference of *F*m and *F*m′. OE27 has the highest NPQ levels, in contrast to the lowest level in Del27, with WT and Com27 in between.

Figure 5.3 shows Q_A^- reoxidation over 1000 flashes. Before the measurement, we performed dark-adapted fluorescence induction analysis, known as Kautsky induction (Fig. 5.3A). The dark-adapted *F*v/*F*m values of the four strains are comparable. This is the basis for NPQ and the following fluorescence kinetics analysis. The 'multiple flashes' experiment is modified from the S-state program equipped in the FL-200 fluorometer. It is a sequence of 1000 saturating flashes

over the course of 500s (see Materials and Methods). We used multiple flashes to compare the charge recombinations of the dark-adapted strains after a single flash and its associated S-state,

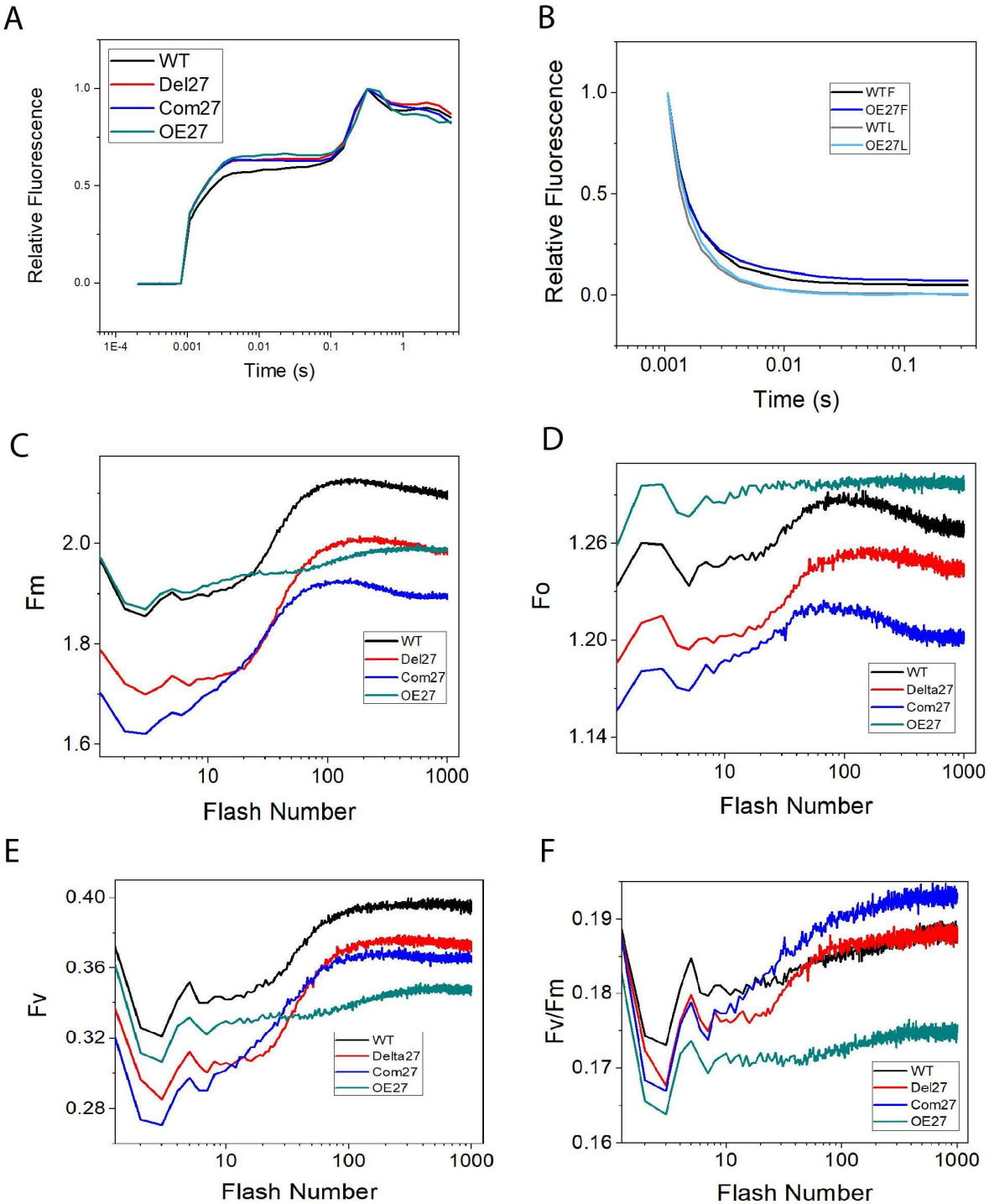

Figure 5.3: OE27 is resilient to light adaptation over 1000 flashes (A) Fluorescence induction (Kautsky effect); (B) Fluorescence decay over 500ms for WT and OE27 strains after first (F) and last (L, 1000) flashes. (C) *F*m fluctuation over 1000 flashes. (D) *F*o fluctuation over 1000 flashes. (E) *F*v derived from (C) and (D). *F*v value shows periodic

change which is the opposite of flash induced oxygen yield. Some studies use these values to derive S-state distribution analysis. (F) *F*v/*F*m maximum quantum yield of PSII chemistry.

and to compare the first charge recombination with recombination after multiple flashes. Each flash also contributes to the redox state of PSII and thus the thylakoids overall, so the observed values reflect the redox state changes after actinic light illumination over a longer time scale (>5 sec). Figure 5.3B compares the fluorescence decay after the first and last (1000) of the flashes for WT and OE27 (data of Del27 and Com27 are not shown for clarity), which is driven by charge transfer from the plastoquinone Q_A to Q_B in the PSII electron transport chain. To model the charge transfer kinetics between Q_A^- and the plastoquinone bound at the Q_B-binding site, we employed a double exponential decay. The fast exponential component describes the charge transfer between Q_A^- and plastoquinone bound at the Q_B site. The second exponential, intermediate, component describes plastoquinone exchange at the Q_B-binding site (24). Because the fluorescence decay was recorded for approximately 330 ms after the actinic flash (instrument intrinsic function), we did not consider a slow hyperbolic component ($T_{1/2}$ ranging in seconds) that would describe the $S_2Q_A^-$ charge recombination (25). Table 5.1 and Table 5.2 show the decay kinetics for all strains for the first and last flashes (data is in Table S5.2). Residuals for the fits are shown in Fig S5.2.

Table 5.1: Fluorescence decay kinetics after a single actinic flash

Strains and treatment	Fast component		Intermediate component	
	Amplitude (%)	$T_{1/2}$ (µs)	Amplitude (%)	$T_{1/2}$ (ms)
WTF	59.1	252.7	40.9	2.1
Del27F	60.5	273.2	39.5	2.2
Com27F	65.6	229.7	34.4	2.2
OE27F	68.0	237.9	32.0	2.6

Table 5.2: Fluorescence decay kinetics after 1000 actinic flashes

Strains and treatment	Fast component		Intermediate component	
	Amplitude (%)	$T_{1/2}$ (µs)	Amplitude (%)	$T_{1/2}$ (ms)
WTL	39.2	178.8	60.8	1.3
Del27L	42.4	195.1	57.6	1.3
Com27L	43.3	179.8	56.7	1.2
OE27L	50.2	243.9	49.8	1.6

The fluorescence decay kinetics for the fast and intermediate components after a single saturating flash are nearly the same for all the strains. However, after 1000 saturating flashes, the $T_{1/2}$ and amplitude for the fast component are considerably different for the OE27 strain compared to other strains (Table 5.2). The $T_{1/2}$ for the intermediate components for all the strains remain similar. The changes in the amplitudes for the intermediate component between the first flash and thousandth

flash would suggest increased photochemistry owing to cells transitioning from dark-adapted to steady-state conditions. After multiple saturating flashes, an overall increase in the electron transfer is also evident from a decline in the half-times of both the fast and intermediate components.

Because Psb27 is not found in active cyanobacterial PSII (26) (9, 20), deletion of Psb27 has a minimal impact on the PSII-associated electron transfer processes as compared to WT (Table 1 and 2), as expected. The minimal impact on the $T_{1/2}$ for the fast component in the OE27 strain could indicate the robustness of PSII. However, because Psb27 is not a component of active PSII, we hypothesize that more of the Psb27-bound PSII assembly intermediate is available in the OE27 strain. Increased Psb27 assures high quality, efficient PSII assembly based on previous functional analysis (15, 27). Under steady-state conditions, an increase in damage to PSII would make PSII maturation in the OE27 strain more efficient than in the other strains and thus a minimal impact on the electron-transfer kinetics is observed, as it is more reflective of new complex formation than adapting PSII centers to light.

Although the fit of the model employed to fit fluorescence decay was satisfactory (R^2=0.99), the sinusoidal pattern observed for the residuals (Figure S5.2) would suggest that a model employing a double exponential does not fully describe the relaxation processes taking place. We also did not consider the slow hyperbolic component for curve fitting, which could be contributing to the structure of the residuals.

Figure 5.3C shows *F*m changes over 1000 saturating flashes. OE27 shows less increase in *F*m than other strains, indicative of either a robust non-photochemical quenching, or NPQ, consistent with the results from Figure 5.2C. Figure 5.3D shows *F*o changes over 1000 flashes.

Figure 5.3E shows *F*v over the 1000 flashes, and Figure 5.3F shows *F*v/*F*m. Overall, OE27 shows less of a change over the 1000 flashes than the other strains.

5.4 Discussion

In our previous study (10), we demonstrated that within the PSII population, there is always a sub-population (7-10%) of monomeric Psb27-PSII. This population is characterized by loosely bound PsbO and the absence of a functional Mn cluster, and has severely defective Q_A^- reoxidation by forward electron transfer to Q_B. Fluorescence decay profiles in both Psb27-PSII (His27PSII) and Psb27-Δ*ctpA*PSII (His27Δ*ctpA*PSII) samples without DCMU treatment are similar to those treated with DCMU, an electron transport inhibitor that binds to the Q_B site. Compared with functional PSII (HT3-PSII), forward electron transfer from Q_A^- to Q_B in both Psb27-PSII and Psb27-Δ*ctpA*PSII is blocked, which has been observed previously (28). The results presented in this work demonstrate that Psb27-PSII is not only involved in PSII assembly, but also correlated with a photoprotective energy-dissipation mechanism. It is thought that the removal of the Mn cluster results in a rise of the redox potential of Q_A–, rendering electron transfer to Q_B less efficient and promoting direct relaxation of Q_A- without forming the triplet-state of chlorophyll, a precursor of harmful singlet oxygen (29-31).

In the absence of Psb27-PSII in Del27 cells of *Synechocystis* sp. PCC 6803, the NPQ analysis demonstrated the absence of a fluorescence quenching component. This phenotype is fully complemented in Com27 (Fig. 5.2A), which indicates that the Psb27-PSII protein complexes present in WT comprise a PSII quenching pool. In the overexpression strain of Psb27, non-photochemical quenching parameters are even higher than in WT *Synechocystis* sp. PCC 6803 (Fig. 5.2A and 5.2D). This finding supports the hypothesis that the Psb27-PSII subpopulation is involved in energy quenching and that the pool size can be modified by genetically controlling levels of Psb27. We propose that the altered conformation of Loop E of CP43 that is conferred by Psb27 binding contributes to the rearrangement of cofactors (carotenoids, chlorophylls,

plastoquinone) that enables the quenching capability of Psb27-PSII (18, 19, 21, 28). Psb27-bound PSII lacks a functional Mn cluster and has an altered low temperature chlorophyll fluorescence profile at 77K (9, 10), but the relation of these phenomena to enhanced non-photochemical quenching in Psb27-PSII requires further research.

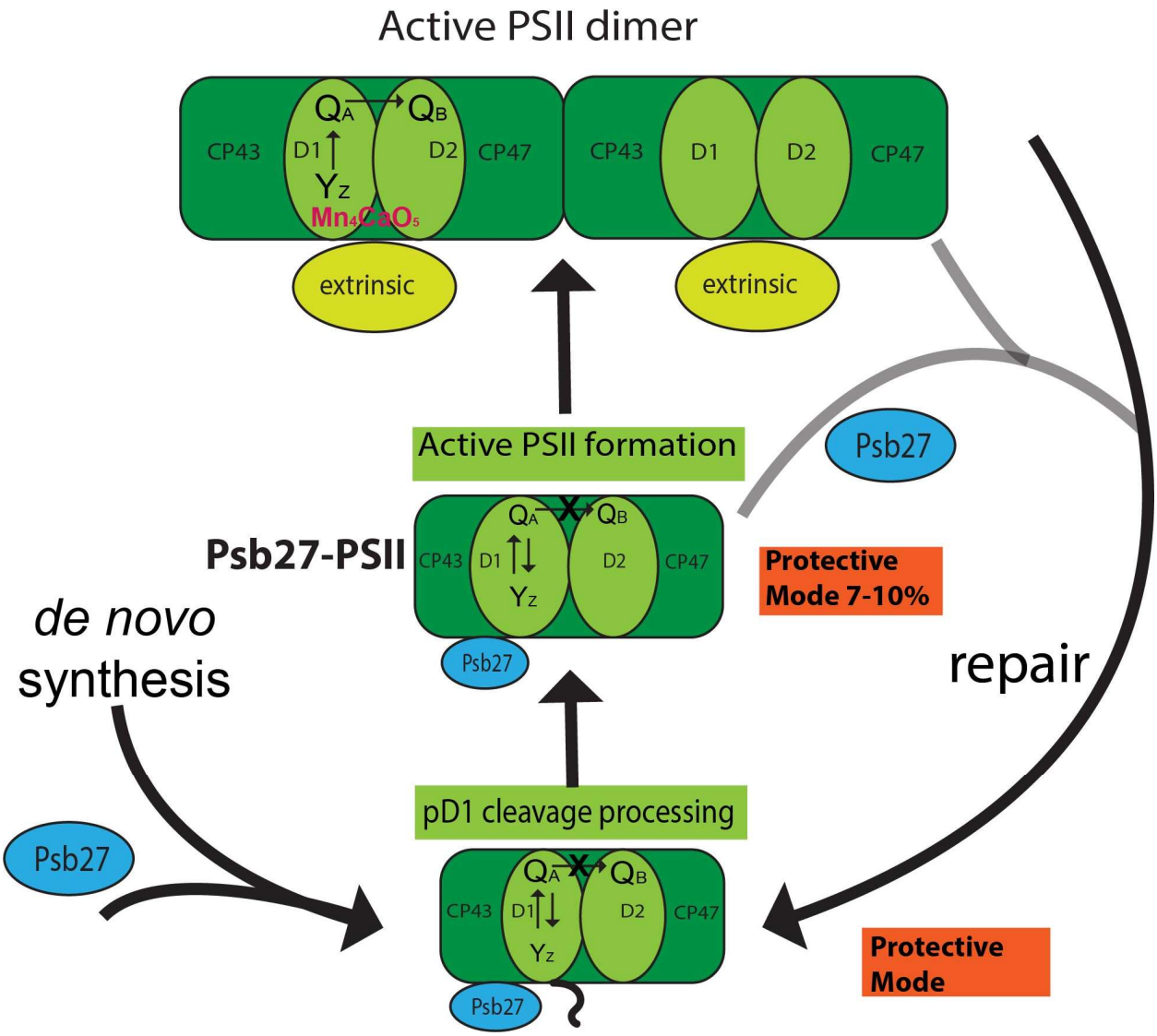

Figure 5.4 Schematic of the role of Psb27 in NPQ. Psb27 is the determining factor in the pool size of Psb27-PSII from both the synthesis and repair pathways. A larger pool of the quenching species Psb27-PSII forms when more Psb27 is present in the cell, which enables higher NPQ.

In Figure 5.3, we observed the behavior of PSII fluorescence induction and relaxation over the course of 1000 saturating flashes. We showed that OE27 is shows less of a change over time

as compared with the WT strain, indicating a higher resilience to light-induced change, and larger pool of PSII assembly complexes in this strain.

We propose a model for Psb27 as an agent of non-photochemical quenching of excitation in PSII assembly and repair intermediates in cyanobacteria (Fig. 5.4). Increased Psb27 levels lead to an increased pool of Psb27-PSII, ready to mature into active PSII as damage takes place or more PSII is needed, such as in a denser growth condition. This larger pool of non-photosynthetically active PSII can absorb light energy, dissipates it so as not to damage the protein subunits before PSII can function. Interestingly, (32) found that the ΔPsb27 strain had a higher rate of oxygen evolution following high light stress, indicating that quenching species are not present, raising the apparent rate compared to chlorophyll content. Our data are consistent with a model of Psb27 expression as the determining factor controlling the amount of Psb27-PSII intermediate complexes, which can quench excitation. It has been shown in previous work that PSII decouples from phycobilisome excitation energy transfer prior to manganese cluster assembly (33). It was also shown that, in the absence of PsbU, an extrinsic PSII subunit which binds following manganese (34). Our findings contribute another analogous strategy of the phenomenon decoupling excitation energy prior to full activation of PSII in order to prevent damage.

Cyanobacteria, in particular *Synechocystis* sp. PCC 6803, are widely used to study photosynthesis. However, unlike plants, cyanobacteria used for photosynthesis research are usually grown under continuous-light conditions in a constant-temperature growth chamber. In nature, these conditions are nonexistent. Not only are there night/day cycles of light and dark, but during the day light fluctuates due to variable shading caused by wind blowing tree branches, and current movement in a water column. An adaptive photoprotective mechanism under such conditions would have a more significant impact on eco-physiological fitness. We suggest that this

is why the quenching function of Psb27 in cyanobacteria has been overlooked until now. A more pronounced phenotype may be evident in a stronger overexpression strain, or with different varying light schemes other than the 30 min on/off cycle tested in this work. It is also likely that there are conditions under which over-expressing Psb27 is not advantageous, and the current level is a balance between a beneficial quenching state, and an over-protective mechanism.

5.5 Materials and Methods

5.5.1 Culture and Growth of *Synechocystis* sp. PCC 6803 strains

Wild type (WT), Psb27 deletion (Del27) (14), Psb27 complemented (Com27), and Psb27 Over-expression (OE27) of *Synechocystis* 6803 were grown in BG11 medium (35) at 30 °C under 30 μmol photons $m^{-2} \cdot s^{-1}$. The genetically modified strains were grown in BG11 supplemented with antibiotics as follows: 5 μg/mL chloramphenicol (Del27), 5 μg/mL chloramphenicol, 2 μg/mL gentamicin (Com27), 2 μg/mL gentamicin (OE27). For growth assays in liquid medium, cells were grown to mid log phase, harvested by centrifugation, washed in fresh BG11, and again centrifuged to pellet. The cell pellets were resuspended and diluted to $OD_{730} = 0.05$ in BG11 without antibiotics and grown with shaking (200 rpm). The OD_{730} was measured every 24 h on a μQuant Microplate spectrophotometer (Biotek Instruments).

5.5.2 Mutant Construction and Psb27 quantification

A complemented strain of the *Δpsb27* (Com27) was generated by inserting a copy of the psb27 locus (*slr1645*) containing 200 bp of upstream and downstream DNA and the coding region of the *slr1645* gene into the *psbA1* locus, a gene that is not expressed under lab growth conditions (Fig. S5.1A) (36) in the Del27 mutant background (14, 27). Briefly, psbA1 upstream and downstream DNA fragments were amplified using primers listed respectively in Table S5.1. The *psb27* DNA fragment was amplified using primer pair Psb27Comp5 and Psb27Comp3. Segregation of the modified psbA1 locus was verified by PCR analysis using A1segF and A1segR primers (Fig. S5.1B). The OE27 was generated by using the same construct as in Com27, with

psb27 under the native promoter, but introduced into the WT background. All primer sequences are listed in Table S5.1.

Cyanobacterial cells were harvested and broken by bead beating as described previously (37) with minor modifications. Cells were re-suspended in RB buffer (25% glycerol (wt/vol), 10mM $MgCl_2$, 5mM $CaCl_2$, 50 mM MES buffer pH 6.0) and broken by vortexing with 0.17 mm glass beads. Membrane fraction was isolated by centrifugation, re-suspended in RB, and solubilized by addition of β-D-dodecyl maltoside (DDM) to a final concentration of 0.8%. After incubation on ice in dark for 30 min, the solubilized membranes were separated from the insoluble material by centrifugation at gradually increasing speed from 120×g to 27,000×g at 4 °C for 20 min.

SDS-PAGE was performed by loading isolated membrane proteins on a same-chlorophyll basis on a 12.5% acrylamide resolving gel. After electrophoresis, proteins were transferred to a polyvinylidene difluoride (PVDF) membrane (Millipore-Sigma), blocked using 5% bovine serum albumin (Thermo-Fisher) for 2 h at room temperature, and then separately incubated with the primary rabbit antibody raised against Psb27 (Eaton-Rye lab) overnight at 4°C. The horseradish peroxidase (HRP)-conjugated secondary antibody goat anti-rabbit IgG (H+L)-HRP conjugate (Bio-Rad) was diluted at 1:5,000 in 1.5% BSA. Bands were visualized and quantified using chemiluminescence reagents (Millipore-Sigma) with a LI-COR Odyssey Fc (LI-COR Biotechnology) imager. Psb27 protein levels, on a per chlorophyll basis, in WT and OE27 are shown in Fig. S5.1C. OE27 has close to two times the Psb27 content of WT.

5.5.3 Fluorescence Analysis

For non-photochemical quenching (NPQ) analysis using the Fluorocam 800MF (Photon System Instruments, Brno, Czech Republic), cells were grown to mid log phase, harvested by

centrifugation, washed in fresh BG11, and again centrifuged to pellet. The cell pellets were resuspended and diluted to OD_{730} = 0.05 in BG11 without antibiotics and spotted (2 µL) to BG11 plates without antibiotics. WT and mutant cells were allowed to grow under the same temperature and light conditions as liquid culture for 3 weeks before NPQ analysis.

Fluorescence emission over many flashes was recorded on a double-modulation fluorometer (Photon System Instruments, Brno, Czech Republic) with a built-in analyzing program, FluorWin using a modified S-state program. 1000 flashes were delivered at 500 ms intervals over a period of 500 seconds. The sample concentration was adjusted to 5 µg/ml of Chl*a* in BG11. All samples were dark adapted for 5 min at room temperature before the measurements. Instead of using 10 actinic flashes that advance S-state by each flash, 1000 flashes (200 second duration) were used to test the Q_A^- reoxidation in three mutants versus WT. The charge recombination after first flash and last flash were numerically deconvoluted. The fluctuation of Fo, Fm, Fv was plotted against flash number.

To determine the charge transfer kinetics between Q_A^- and the plastoquinone bound at the Q_B-binding site, we employed a double exponential decay to fit the data in Table S2, where A_1 and A_2 are amplitudes, and T_1 and T_2 are time constants for the fast and intermediate components, respectively. To calculate respective decay $T_{1/2}$, the time constants were multiplied by Ln(2). F(t) is the fluorescence level, and Fo is the base fluorescence.

$$F(t) - Fo = A1 \exp\left(-\frac{t}{T1}\right) + A2 \exp\left(-\frac{t}{T2}\right) \qquad \text{(eq. 5.1)}$$

The first exponential (fast component) describes the charge transfer between the Q_A and plastoquinone bound at the Q_B site. The second exponential (intermediate component) describes plastoquinone exchange at the Q_B-binding site (24). Because the fluorescence decay was recorded for approximately 330 ms after the actinic flash, we did not consider a slow hyperbolic

component ($T_{1/2}$ ranging in seconds) that would describe the $S_2Q_A^-$ charge recombination (25). Residuals for the fits are shown in Fig S5.2.

5.6 Supporting Information

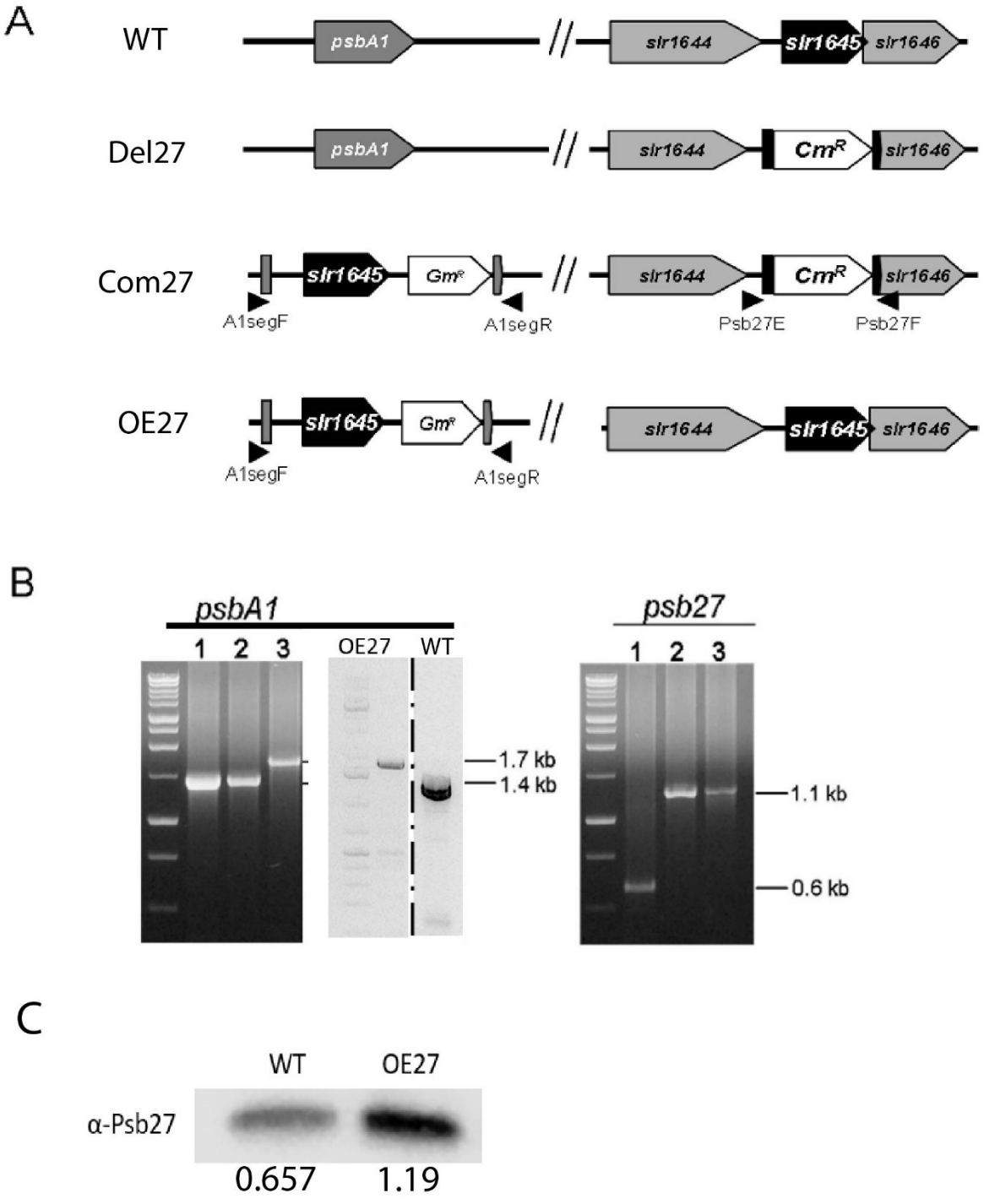

Fig. S5.1 *psbA1* and *psb27* loci of WT, Del27, OE27, and Com27 strains. (A) Diagrams of the *psbA1* and *psb27* loci in WT, Del27, OE27, and Com27 cells. The relative locations of the primers used for segregation analysis are labeled. (B) PCR analysis of the *psbA1* (left) and *psb27* (right) loci in WT (lane 1, WT), Del27 (lane 2) Com27 (lane 3), and OE27 cells. Dotted line indicates same agarose gel, but lane removed. The sizes of the various PCR products are shown to the right of each gel. (C) Western blot for the Psb27 protein. Samples were harvested at OD 0.5 and

solubilized membranes were loaded on an equal chlorophyll basis: 1ug chl./lane. Below the lanes are the relative pixel density for each band.

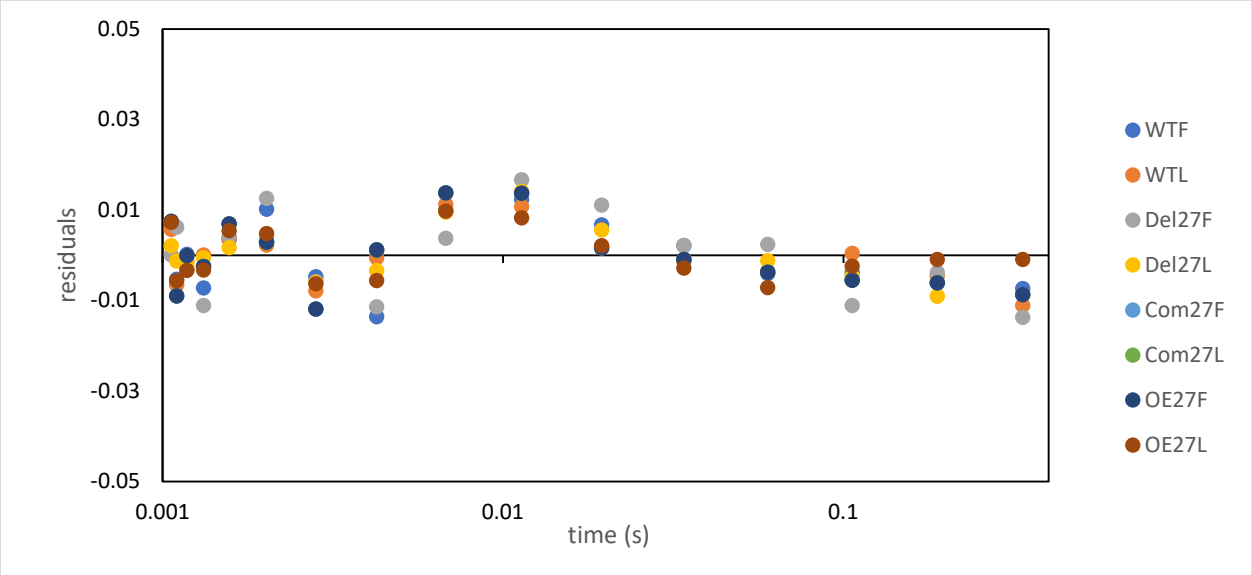

Fig. S5.2 Q_A reoxidation fit residuals

Table S5.1 primers used in Chapter 5

Primer	**Sequence (5' to 3')**
AlusFor	CCCAAGCTTAACAGGACCAAGCCTTG
AlusRev	ACATGCATGCTGGCATTGATTAACTTCCC
AldsFor	CGAGCTCGTGCCATTGCCATAACTG
AldsRev	CCGGAATTCCCTGGTCTCGATAATTGC
Psb27Comp5	AACTGCAGAACATTGCCCTCCAGGTGACCA
Psb27Comp3	CTAGTCTAGATCACACGCCCCGTTCAATGGAT
A1segF	ATGGCTTGATCTGGCATTTACG
A1segR	CCATTGCGAGAGTGCCCTTGAT

Table S5.2 Q_A reoxidation data for first, last flashes used in analysis (excel file attached)

5.7 References

1. Wilson A*, et al.* (2008) A photoactive carotenoid protein acting as light intensity sensor. *Proc Natl Acad Sci U S A* 105(33):12075-12080.
2. Wilson A*, et al.* (2006) A soluble carotenoid protein involved in phycobilisome-related energy dissipation in cyanobacteria. *Plant Cell* 18(4):992-1007.
3. Chen HYS, Bandyopadhyay A, & Pakrasi HB (2018) Function, regulation and distribution of IsiA, a membrane-bound chlorophyll a-antenna protein in cyanobacteria. *Photosynthetica* 56(1):322-333.
4. Ihalainen JA*, et al.* (2005) Aggregates of the chlorophyll-binding protein IsiA (CP43') dissipate energy in cyanobacteria. *Biochemistry* 44(32):10846-10853.
5. Knoppova J*, et al.* (2014) Discovery of a chlorophyll binding protein complex involved in the early steps of photosystem II assembly in Synechocystis. *Plant Cell* 26(3):1200-1212.
6. Niedzwiedzki DM*, et al.* (2016) Carotenoid-induced non-photochemical quenching in the cyanobacterial chlorophyll synthase-HliC/D complex. *Biochim Biophys Acta* 1857(9):1430-1439.
7. Ort DR*, et al.* (2015) Redesigning photosynthesis to sustainably meet global food and bioenergy demand. *Proc Natl Acad Sci U S A* 112(28):8529-8536.
8. Kromdijk J*, et al.* (2016) Improving photosynthesis and crop productivity by accelerating recovery from photoprotection. *Science* 354(6314):857-861.
9. Nowaczyk MM*, et al.* (2006) Psb27, a cyanobacterial lipoprotein, is involved in the repair cycle of photosystem II. *Plant Cell* 18(11):3121-3131.
10. Liu H, Roose JL, Cameron JC, & Pakrasi HB (2011) A genetically tagged Psb27 protein allows purification of two consecutive photosystem II (PSII) assembly intermediates in Synechocystis 6803, a cyanobacterium. *J Biol Chem* 286(28):24865-24871.
11. Grasse N*, et al.* (2011) Role of novel dimeric Photosystem II (PSII)-Psb27 protein complex in PSII repair. *J Biol Chem* 286(34):29548-29555.
12. Singh H (2017) The role of the low-molecular-weight proteins of the CP43 pre-assembly complex of Photosystem II. Doctor of Philosophy (University of Otago, Dunedin, New Zealand).
13. Avramov AP, Hwang HJ, & Burnap RL (2020) The role of Ca(2+) and protein scaffolding in the formation of nature's water oxidizing complex. *Proc Natl Acad Sci U S A* 117(45):28036-28045.
14. Roose JL & Pakrasi HB (2008) The Psb27 protein facilitates manganese cluster assembly in photosystem II. *J Biol Chem* 283(7):4044-4050.
15. Jackson SA, Hervey JR, Dale AJ, & Eaton-Rye JJ (2014) Removal of both Ycf48 and Psb27 in Synechocystis sp. PCC 6803 disrupts Photosystem II assembly and alters Q(A)(-) oxidation in the mature complex. *FEBS Lett* 588(20):3751-3760.
16. Davinagracia J (2021) The Role of Lipoprotein Psb27 in Photosystem II Biogenesis. Master of Science (University of Otago, Dunedin, New Zealand).
17. Komenda J*, et al.* (2012) The Psb27 assembly factor binds to the CP43 complex of photosystem II in the cyanobacterium Synechocystis sp. PCC 6803. *Plant Physiol* 158(1):476-486.

18. Zabret J*, et al.* (2021) Structural insights into photosystem II assembly. *Nat Plants* 7(4):524-538.

19. Huang G*, et al.* (2021) Structural insights into a dimeric Psb27-photosystem II complex from a cyanobacterium *Thermosynechococcus vulcanus*. *Proc Natl Acad Sci U S A* In Press.

20. Liu H, Huang RY, Chen J, Gross ML, & Pakrasi HB (2011) Psb27, a transiently associated protein, binds to the chlorophyll binding protein CP43 in photosystem II assembly intermediates. *Proc Natl Acad Sci U S A* 108(45):18536-18541.

21. Liu H*, et al.* (2013) Mass spectrometry-based footprinting reveals structural dynamics of loop E of the chlorophyll-binding protein CP43 during photosystem II assembly in the cyanobacterium Synechocystis 6803. *J Biol Chem* 288(20):14212-14220.

22. Chen H*, et al.* (2006) A Psb27 homologue in Arabidopsis thaliana is required for efficient repair of photodamaged photosystem II. *Plant Mol Biol* 61(4-5):567-575.

23. Hou X, Fu A, Garcia VJ, Buchanan BB, & Luan S (2015) PSB27: A thylakoid protein enabling Arabidopsis to adapt to changing light intensity. *Proc Natl Acad Sci U S A* 112(5):1613-1618.

24. Vass I, Kirilovsky D, & Etienne AL (1999) UV-B radiation-induced donor- and acceptor-side modifications of photosystem II in the cyanobacterium Synechocystis sp. PCC 6803. *Biochemistry* 38(39):12786-12794.

25. Biswas S & Eaton-Rye JJ (2018) PsbY is required for prevention of photodamage to photosystem II in a PsbM-lacking mutant of Synechocystis sp. PCC 6803. *Photosynthetica* 56:200-209.

26. Suga M*, et al.* (2015) Native structure of photosystem II at 1.95 A resolution viewed by femtosecond X-ray pulses. *Nature* 517(7532):99-103.

27. Roose JL (2008) Assembly and function of cyanobacterial photosystem II, Ph.D thesis. Washington University, St. Louis, MO.

28. Mamedov F, Nowaczyk MM, Thapper A, Rogner M, & Styring S (2007) Functional characterization of monomeric photosystem II core preparations from Thermosynechococcus elongatus with or without the Psb27 protein. *Biochemistry* 46(18):5542-5551.

29. Kato Y, Nagao R, & Noguchi T (2016) Redox potential of the terminal quinone electron acceptor QB in photosystem II reveals the mechanism of electron transfer regulation. *Proc Natl Acad Sci U S A* 113(3):620-625.

30. Rutherford AW, Osyczka A, & Rappaport F (2012) Back-reactions, short-circuits, leaks and other energy wasteful reactions in biological electron transfer: redox tuning to survive life in O(2). *FEBS Lett* 586(5):603-616.

31. Krieger-Liszkay A, Fufezan C, & Trebst A (2008) Singlet oxygen production in photosystem II and related protection mechanism. *Photosynth Res* 98(1-3):551-564.

32. Bentley FK, Luo H, Dilbeck P, Burnap RL, & Eaton-Rye JJ (2008) Effects of inactivating psbM and psbT on photodamage and assembly of photosystem II in Synechocystis sp. PCC 6803. *Biochemistry* 47(44):11637-11646.

33. Hwang HJ, Nagarajan A, McLain A, & Burnap RL (2008) Assembly and disassembly of the photosystem II manganese cluster reversibly alters the coupling of the reaction center with the light-harvesting phycobilisome. *Biochemistry* 47(37):9747-9755.

34. Veerman J*, et al.* (2005) The PsbU subunit of photosystem II stabilizes energy transfer and primary photochemistry in the phycobilisome-photosystem II assembly of Synechocystis sp. PCC 6803. *Biochemistry* 44(51):16939-16948.

35. Allen MM (1968) Simple Conditions for Growth of Unicellular Blue-Green Algae on Plates(1, 2). *J Phycol* 4(1):1-4.

36. Mohamed A & Jansson C (1989) Influence of light on accumulation of photosynthesis-specific transcripts in the cyanobacterium Synechocystis 6803. *Plant Mol Biol* 13(6):693-700.

37. Kashino Y*, et al.* (2002) Proteomic analysis of a highly active photosystem II preparation from the cyanobacterium Synechocystis sp. PCC 6803 reveals the presence of novel polypeptides. *Biochemistry* 41(25):8004-8012.

Chapter 6

Conclusions, Future Directions, and Additional Data

Chapter Contributions:

All data in this chapter were collected by VMJ.

6.1 Conclusions

In this thesis, I have demonstrated a range of approaches to studying Photosystem II (PSII) assembly and repair in the cyanobacterium *Synechocystis* sp. PCC 6803. In particular, a large part of my thesis work became developing and using synthetic biology tools to better understand aspects of this process. These synthetic biology tools are developed by and of interest to those lab members and members of the cyanobacterial research community who wish to do metabolic engineering of cyanobacteria, which are an attractive group of organisms for sustainably producing high-value small molecules or protein products (1-3). They are also powerful tools for studying basic biological processes such as photosynthesis. In particular, CRISPR-inhibition became of interest as a way to *reversibly* inhibit genes essential for Photosystem II assembly, so that processes in the complex PSII lifecycle could be studied in greater detail. Additionally, a number of different strategies were implemented and evaluated to control expression of the regulatory subunit CtpA, which was not effectively inhibited by the CRISPR-inhibition strategy.

This chapter will summarize conclusions from each previous chapter of the thesis, as well as additional data that did not turn into complete chapters and outline any future directions to be taken. Implications for future research will also be discussed.

6.2 Conclusions and Future Directions from Chapter 2

In Chapter 2, I described the identification and characterization of a PSII complex, which we called NRC for *no reaction center* (4). This finding was unexpected, as the complex we identified contained subunits of both the CP43 and CP47 PSII modules, but no reaction center subunits. In the structures of active PSII and assembly complexes that have been characterized, these modules

do not share any points of contact. In order to better understand when this complex forms during the PSII lifecycle, I set up a simple experiment where I grew large cultures of H47-S6803 and then divided them into four conditions: low (normal) light, high light, and low light plus lincomycin and high light plus lincomycin. The purpose was to halt protein synthesis with lincomycin and to cause damage (and degradation) of PSII with high light. I then isolated PSII from the cells grown under each of these four conditions and ran them on clear native PAGE. What I found was that NRC increased in the cells grown in high light and lincomycin, indicating that it forms as a damage product of PSII and not on the assembly pathway from newly synthesized subunits. We proposed that this complex forms as a part of the PSII repair pathway, where the undamaged antenna subunits remain waiting for insertion of new reaction center subunits and are protected from proteolytic degradation. It is also possible, however, that the complex we identified as NRC represents a mixture of degradation products that are not recycled back into active PSII. Additionally, the structure of this complex and its precise role in the PSII lifecycle remains uncharacterized.

A paper was published recently (5) in direct response to our publication (4), which claims that a stable complex composed of the CP43 and CP47 modules does not form, as we proposed. The authors of this study isolated the CP43 and CP47 modules separately and showed that they behave identically on a clear-native PAGE gel and glycerol gradient, the techniques used in our study. As a result, the complexes are indistinguishable by this method when both are present. They also claim that the detergent and lipid shell surrounding the module complexes caused us to misinterpret our predicted molecular weight based on analytical ultracentrifugation. While their hypothesis of two separate modules that behave identically would also be consistent with our data, our conclusions are reasonable. We do not have the ability to independently isolate these subunits

based on the mutants we have available. Also, our NRC complex was isolated with a his-tagged CP47 subunit, and so how the CP43 module would be pulled down in this experiment independently of CP47 is unclear. The authors suggest that the CP43 we see in the NRC band has dissociated from intact PSII during sample preparation or loading the gel. Figure 6.1 shows

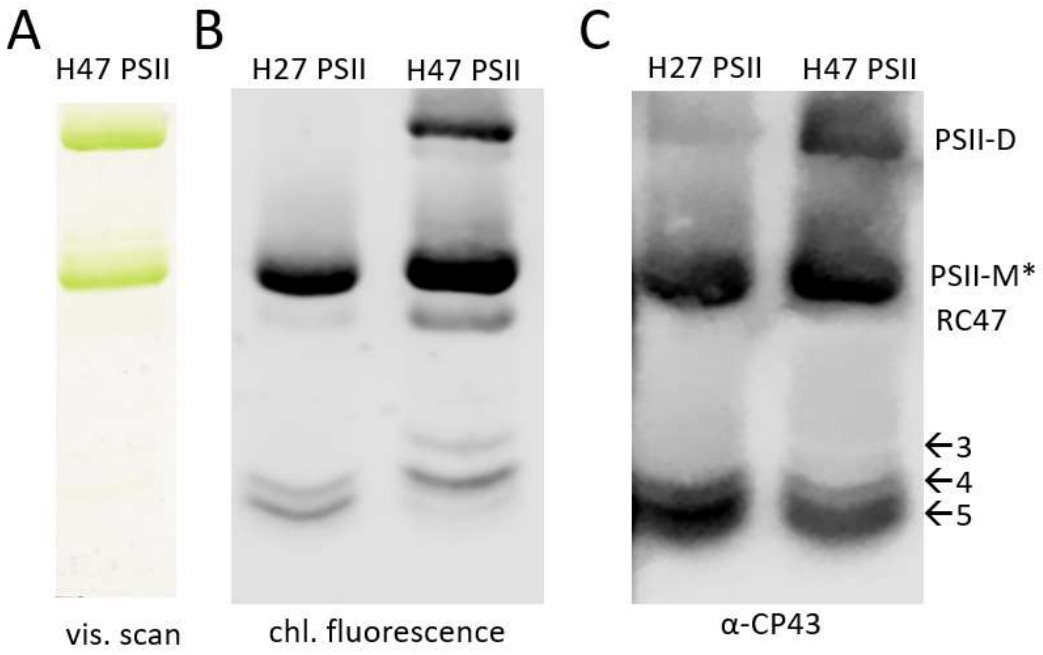

Figure 6.1, 4-16% CN PAGE of purified PSII. A) visible scan of H47 PSII B) chlorophyll fluorescence image of H27 and H47 PSII C) western blot for CP43 subunit in H27 and H47 on native gel. Bands 3, 4, 5 are chlorophyll containing bands, named for consistency with bands seen in other gels. Major bands are labeled PSII-D for PSII dimer, PSII-M for PSII monomer (the star indicates that the monomer observed is not necessarily active PSII, but inactive PSII or Psb27-PSII).

images of such a clear-native page gel in our hands. Fig. 6.1A is a visible light scan of the gel. The primary bands visible are those that contain chlorophyll, which in the case of purified H47 PSII are the PSII dimer, PSII monomer, RC47, and two lower molecular weight chlorophyll containing bands (those labeled 3 and 4). The visible bands are difficult to see, and so I also imaged the gel using the 700nm channel on our LICOR imager (Fig. 6.1B). This channel visualizes chlorophyll fluorescence. It should be noted that this fluorescence image is not quantitative, as not every

chlorophyll containing species fluoresces the same amount, but this mode of imaging is helpful to better visualize all the chlorophyll-containing bands. Figure 6.1B shows the chlorophyll fluorescence image of a CN-PAGE of His-Psb27 and H47 purified PSII. The H47 PSII has the same chlorophyll containing bands as are visible, with one additional faint band (5) able to be observed. Interestingly, the H27 PSII has a somewhat different subset of PSII-containing chlorophyll bands. Unlike H47 PSII, His-Psb27 does not pull down PSII dimers,

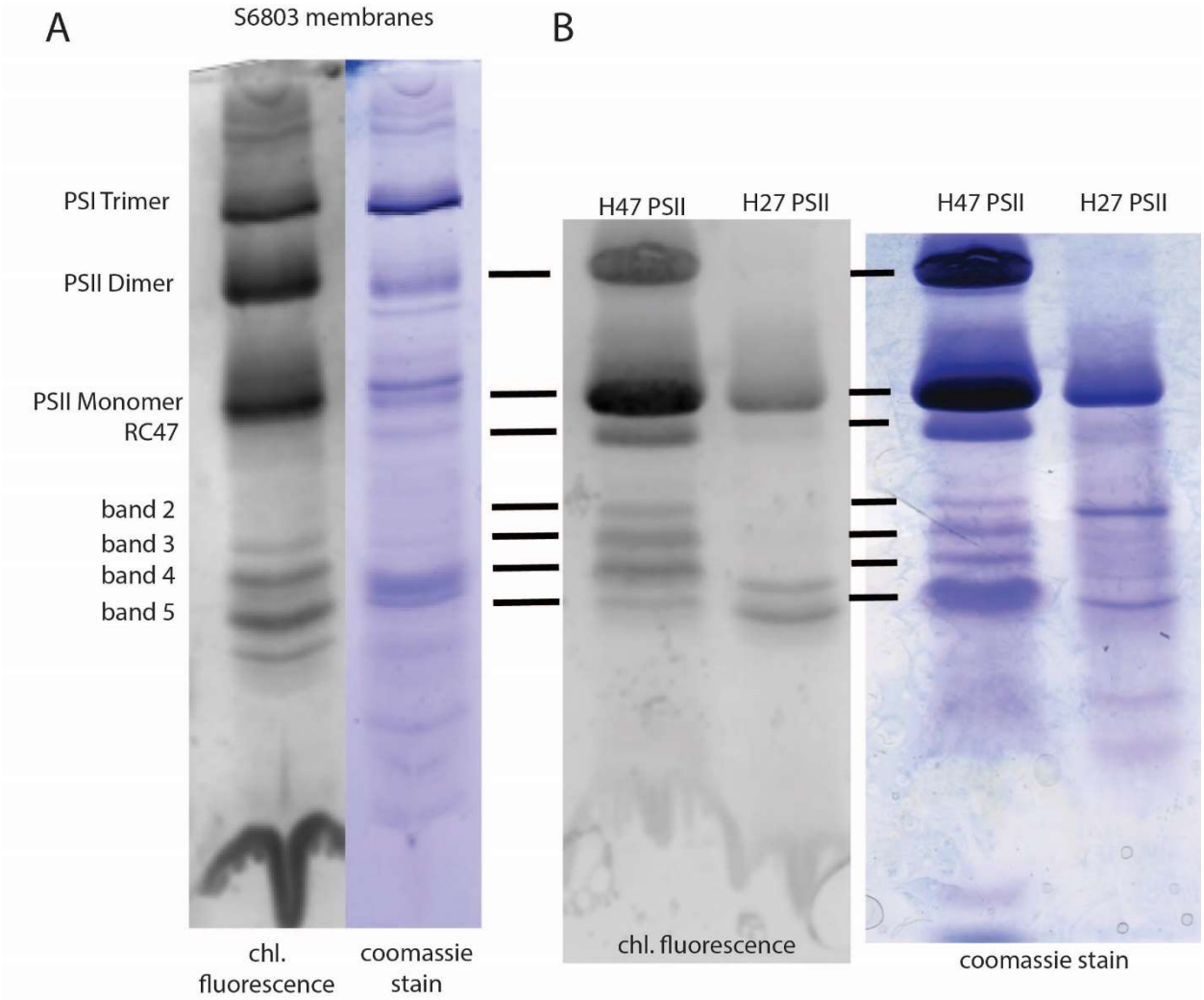

Fig. 6.2. A) CN-PAGE of S6803 membranes, imaged for chlorophyll fluorescence and Coomassie stained. B) CN-PAGE of purified PSII from the H47 and H27 strains. Major bands are labeled.

consistent with previous observations from our lab that Psb27 only associates with inactive PSII monomers during PSII assembly (6), although dimeric Psb27-PSII has been observed in the ΔPsbV mutant (7), and in cells under stressful conditions (8). His-Psb27 also does not pull down the PSII subcomplex RC47, as CP43/Psb27 are not found in that complex. So, the chlorophyll bands visible in H27 purified PSII are the monomer and two lower molecular weight chlorophyll bands (4 and 5). Presumably, these bands contain CP43, as Psb27 directly binds to CP43 and itself does not contain chlorophyll. In Figure 6.1C, a western blot for CP43 of the CN-PAGE of H27 and H47 purified PSII, confirms this. CP43 is present in the PSII dimer and monomer, as expected, and in the bands pulled down in His Psb27-PSII (4 and 5). In Figure 6.2, 4-16% CN-PAGE is shown for both thylakoid membranes from a WT cell (Fig.6.2A) and also of purified PSII, using either a His-CP47 tag or a His-Psb27 tag (Fig. 6.2B). 6.2A and 6.2B each show two different images of the same gel, In Figure 6.2A the gel was imaged for chlorophyll fluorescence, prior to being Coomassie stained and scanned for Figure 6.2B.

In 6.2A, the major protein bands present in WT membranes are the PSI trimer, PSII dimer, PSI monomer, PSII monomer, and a few lower molecular weight bands, which are not well characterized. These bands are of most interest to us, as given that they are made up of chlorophyll containing proteins that pull down using a tag on a PSII protein, indicating that they are involved in assembly of PSII. In 6.2B, you a subset of the chlorophyll proteins in the cell are pulled down with either H47 or H27 PSII. H47 pulls down the PSII dimer, PSII monomer, RC47, and a series of chlorophyll containing bands. H27 only pulls down the monomer and two of the lower molecular weight chlorophyll containing bands. These CN-PAGE gels can also be western-blotted (although the transfer is not always very even), as shown in Figure 6.1C and Figure 6.3B and 6.3D

One future direction that we propose in the paper to gain a more detailed understanding of how NRC, and all of the bands that we see in the clear-native PAGE gel, fit into the PSII lifecycle, is to set up an experiment where we use the stable isotope ^{15}N to label growing cultures for different periods of time, and then to isolate membranes or PSII complexes from these samples, run them on clear-native PAGE, cut out the bands, and use mass spectrometry to measure the relative incorporation of ^{15}N into peptides from various PSII subunits in each band. This approach would allow us to determine more definitively than the high-light and lincomycin experiment, the order of complex formation. This type of experiment, in concert with our CRISPR-i approach (see below), would allow us to determine more systematically the order of formation of PSII sub-complexes, beyond just the band that we had called NRC, and which the other paper calls a mixture of CP43m and CP47m. Further research in this area is warranted and may be complementary to future directions I propose for other chapters, below.

6.3 Conclusions and Future Directions from Chapter 3

In Chapter 3, I demonstrated the use of CRISPRi to reversibly target the photosystem II gene *psbD*, which codes for the D2 reaction center protein, for inhibition. I did this with the goal of studying PSII assembly *in vivo,* as opposed to other approaches to studying PSII which utilize deletion mutants of PSII subunit. This work represented a new framework for studying Photosystem II, in which, by inhibiting a subunit reversibly, the entire assembly process can take place *in vivo,* rather than being halted at a certain stage. While it is true that we are observing an ensemble process, as each cell will recover at a slightly different rate, observing membranes from cells at different stages of recovery will give a big-picture overview of which complexes

form in what order in the cells. Additionally, a future direction could be to try to discern cell-to-cell fluorescence variation. However, Synechocystis cells are so small that this could be difficult.

6.3.1 CRISPRi on Photosystem II proteins in *Synechococcus elongatus* UTEX 2973

In addition to the CRISPRi plasmid that was developed to target the D2 subunit of PSII in S6803, a plasmid was developed to target the same gene in the fast-growing cyanobacterium *Synechococcus elongatus* UTEX 2973. PSII was effectively inhibited in this strain when CRISPRi was induced, but, as this strain is an obligate photoautotroph, the inhibited cells do not grow and cannot be used to study PSII assembly. However, it is likely that engineering efforts in the lab by Deng Liu will soon lead to a strain of 2973 that is able to grow heterotrophically in the absence of PSII activity, and so this may lead to additional studies of PSII in that strain.

6.3.2 CN PAGE of D2-CRISPRi

The ultimate goal of using CRISPRi to inhibit PSII was to use that system to study PSII assembly during the recovery phase. We wished to identify any sub-complexes that formed during the process, and to identify any additional assembly factors that may be associated with those complexes. In order to analyze membrane samples from the timepoints during recovery, one way to look at them is by using clear native PAGE (CN-PAGE), as described above.

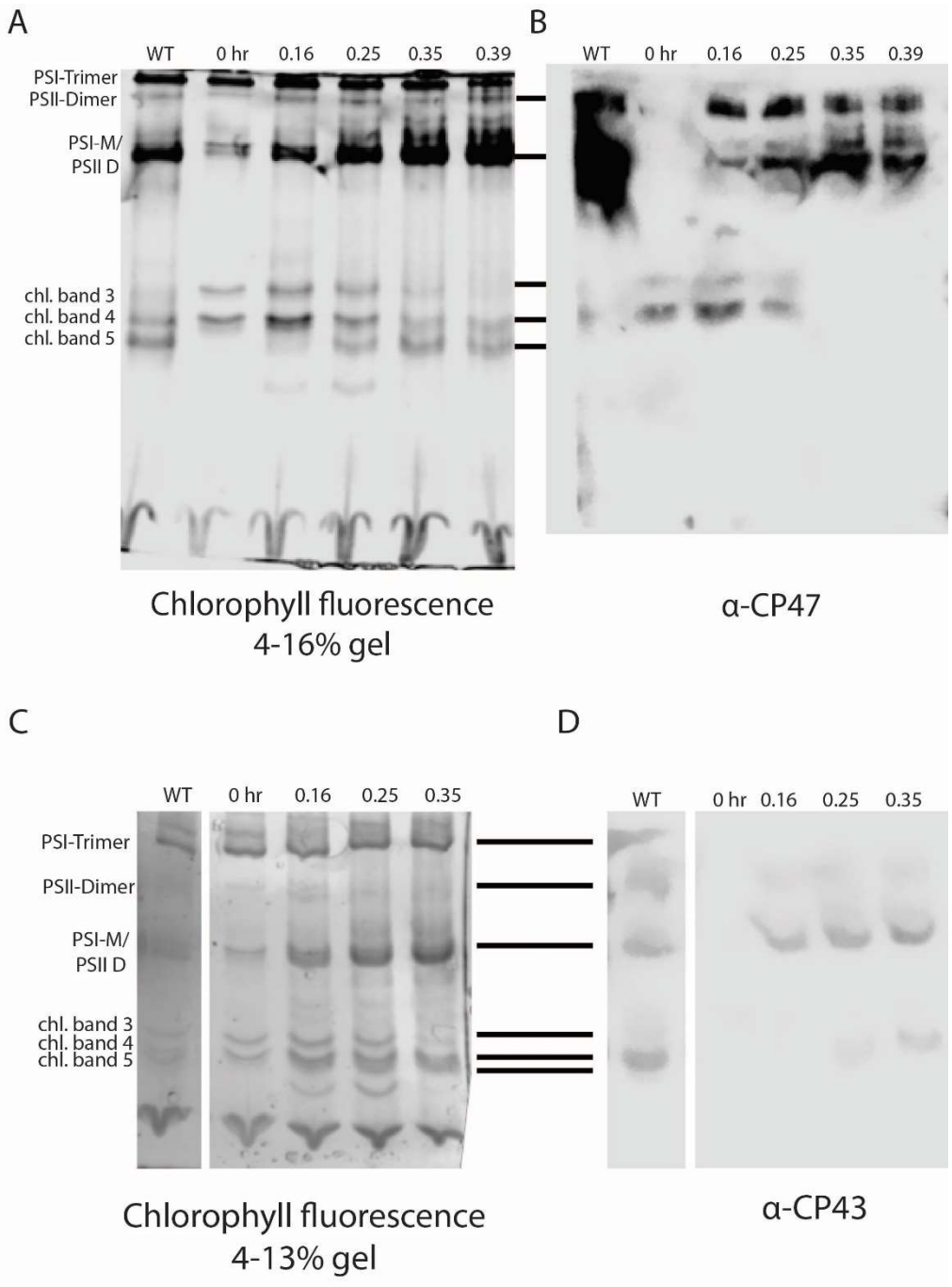

Figure 6.3. Clear-native PAGE of CRISPRi-D2 samples. The number indicated above indicates the Fv/Fm of sample at the timepoint it was taken during PSII recovery following removal of inducers. A) Chlorophyll fluorescence image of 4-16% CN PAGE of WT and CRISPRi samples during recovery. B) Same gel as in (A), transferred and western blotted with α-CP47 antibody. C) Chlorophyll fluorescence image of 4-13 % CN-PAGE of WT and CRISPRi samples during recovery. D) Same gel as in (B), transferred and blotted with α-CP43 antibody.

In Figure 6.3, CN-PAGE gels are shown with thylakoid membranes from both WT samples and from CRISPRi samples at timepoints during recovery. These gels are also blotted for either CP47 (Fig. 6.3B) or CP43 (Fig. 6.3D). As can be seen, αCP47 and αCP43 do seem to react with a different subset of the chlorophyll containing bands during recovery. Notably, the CP47 bands (band 3 and band 4) are quite prominent when PSII is at low levels due to depletion of CP43 and CP47, with band 3 present at lower levels and seemingly only when CP43 levels are very low. Band 4 is also present at higher abundance in the absence of CP43. Likewise, as expected, the CP43 containing bands (4 and 5) only appear after recovery has progressed a certain amount, as CP43 levels increase following release of inhibition. These findings may also support an interpretation where NRC is actually a mixture of CP43 and CP47 pre-complexes.

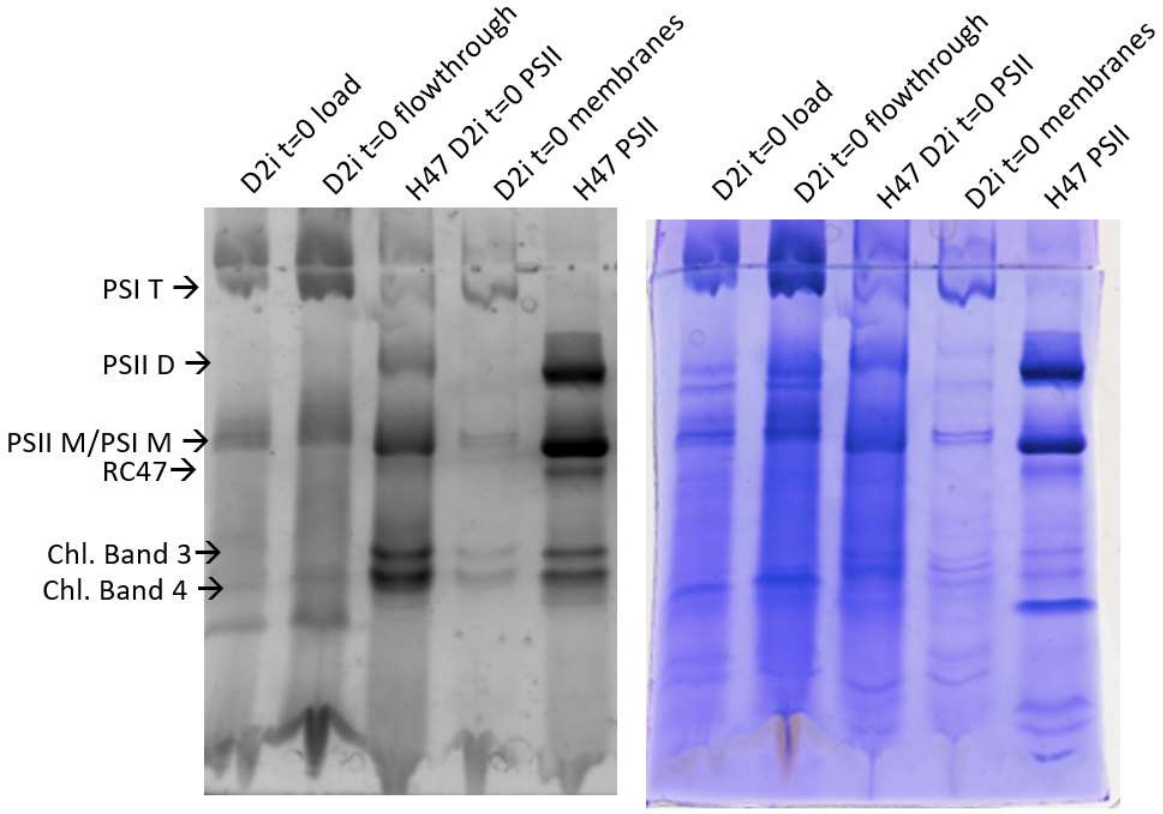

Figure 6.4 CN PAGE of H47 PSII preparation from t=0 membranes

Figure 6.4 shows CN PAGE images (chlorophyll fluorescence and Coomassie stained) of membranes and purified H47 PSII from the D2i cells at the highest level of inhibition. Intriguingly, PSII purified with the his-tagged CP47 from the cells at timepoint zero, when PSII activity is at a minimum, is devoid of RC47. The monomer present is presumably inactive, damaged PSII monomer. However, we would also expect to see some amount of RC47 as partially disassembled PSII that cannot join back with the CP43 module during repair. However, the D2 subunit is also a part of RC47, and so perhaps it is degraded to CP47m. The implication of this in interpreting the PSII lifecycle is unclear, but it suggests that RC47 plays a larger role in PSII assembly than in repair.

6.3.3 Membrane structure of S6803 during PSII degradation and recovery

We never planned such an experiment, but a potentially interesting avenue of investigation with our CRISPRi-RSW D2 strain would be to study the cellular architecture of cells in which we have inhibited PSII as PSII re-builds. PSII assembly has been linked to thylakoid membrane biogenesis, and PSII is also a major component of thylakoid membranes, which rely on the proteins which comprise the majority of their biomass to provide structure. Our CRISPRi-D2 strain would provide a unique platform to study how these processes are related.

6.4 Conclusions and Future Directions from Chapter 4

In Chapter 4, a number of expression strategies were outlined for reversibly expressing *ctpA*. Some of these strategies were constructed, but still need to be assayed for CtpA presence and functionality. In addition, it is difficult to determine where the CRISPRi system was failing without

qPCR data, especially in absence of CtpA antibody. Some future directions were discussed in the chapter, including to test the 0701 CtpA strain once colonies form, adding an epitope tag to CtpA in all of the constructs discussed so that its presence may be measured by western blot, and to perform qPCR to determine the transcript level of *ctpA* in all of the strains.

These expression strategies could also be tested for reversible expression of other genes.

On the whole, cyanobacterial transcription and translation are less-well described than in other model bacteria. Much work has been done from a synthetic biology standpoint, including evaluation of individual promoters and creation of promoter libraries, but understanding native gene expression and how it is regulated in the cell is also important.

Numerous factors influence the expression of genes. These include promoter strength, which is variable and dependent upon environment, including the presence of small-molecule transcriptional and translational inducers. Placement of a gene in an operon effects expression level, with genes early in the operon having higher expression levels. Rates of mRNA degradation, antisense RNAs, and ribosome binding strength also impact the amount of gene product produced, and the rate of protein degradation influences the cellular levels of a given protein. Many of these factors have been most highly studied in *E. coli*, but their exact mechanisms are less well studied in other organisms and in many cases not fully described even in *E. coli.* In particular, aspects of cyanobacterial transcription differ from that of *E. coli*, including RNAP structure, elongation rate, importance of divalent ion presence, proofreading, and terminators. Many promoters have different strengths and or induction ratios across bacterial and cyanobacterial species. As an example, the lac operon is not repressed in S6803 in the presence of LacI, but constitutively expressed. Furthermore, cyanobacterial transcription is not inhibited by Mn^{2+} ions and proceeds

more slowly than in *E.coli.* (9). Cyanobacteria also lack the Gre proofreading present in other bacterial species (10).

In order to have full control over expression of any given gene, these factors need to be understood. Empirically, libraries of promoter strengths of various synthetic and native promoter sequences in *Synechocystis* and other cyanobacteria have been tested and are available. However, the promoter strengths are not necessarily consistent between cyanobacterial species and whether or not they are expressed can also vary. Given the many variables, a more holistic understanding of cyanobacterial gene expression is necessary. On a deeper level, it is possible that our goal of achieving a true, functional 'off' state of an inducible promoter may not be possible, at least for a gene such as CtpA.

6.5 Conclusions and Future Directions from Chapter 5

In Chapter 5, I demonstrated that the overexpression strain of Psb27 (OE27) has higher overall levels of non-photochemical quenching (NPQ) than the WT strain. We hypothesized that the higher NPQ in this strain was a result of a higher level of the PSII assembly intermediate complex, Psb27-PSII. Many questions remain to be asked about the OE27 strain and NPQ. First of all, we have identified that Psb27 is expressed at a higher level, but is there truly more of the Psb27-PSII species present, as we hypothesize, and is this really the species that is contributing to increased cellular non-photochemical quenching? Recent structural work has shown that a PSII species containing Psb28 and Psb27 does have altered photochemistry and reduced singlet O_2 formation, which would be consistent with our findings (11, 12). Additionally, recent work by Avramov et al showed the effect of Psb27 overexpression on photoactivation (13). They found that Psb27 facilitated higher efficiency of photoactivation. Whether or how this finding may contribute to cellular NPQ is not clear.

An immediate future direction would be to isolate membranes from the overexpression strain and assess the membrane protein complexes that are present. We attributed the non-photochemical quenching properties of the strain to a higher abundance of the Psb27-PSII complex in the strain but did not directly show that more of this complex is present. Analyzing membranes from this strain by CN-PAGE and western-blot could be informative for telling what fraction of Psb27 is associated with PSII and if more is associated. In the study, we assayed the OE27 strain for NPQ but not PSII activity. PSII and whole-chain oxygen evolution can be measured on these strains. Finally, the study tested growth under constant light and a 30 min light/dark cycle, with the hypothesis that higher NPQ would be advantageous under changing light conditions. However,

no major difference was observed under this condition. In the future growth under different patterns of changing light, or stronger light intensities should be assayed.

6.6 Materials and Methods

6.6.1 Cell culture, PSII purification and protein analysis

Synechocystis 6803 cells were cultured in BG11 medium supplemented with 30 μg/ml kanamycin (CRISPRi-D2) or 5 μg/mL gentamicin (H47 and H27 strain), under continuous white light at 30 μmol photons m^{-2} s^{-1} at 30 °C. Cultures were grown in 125-ml glass flasks or on agar plates. The HT3 (His47) strain was a kind gift from Dr. Terry Bricker (Louisiana State University, Baton Rouge, LA) (14). Cyanobacterial cells were harvested and broken by bead beating as described previously (15) with minor modifications. Cells were re-suspended in RB buffer (25% glycerol (wt/vol), 10mM $MgCl_2$, 5mM $CaCl_2$, 50 mM MES buffer pH 6.0) and broken by vortexing with 0.17 mm glass beads. Membrane fraction was isolated by centrifugation, re-suspended in RB, and solubilized by addition of n-dodecyl β-D-maltoside (DDM) to a final concentration of 0.8%. After incubation on ice in dark for 30 min, the solubilized membranes were separated from the insoluble material by centrifugation at gradually increasing speed from 120×g to 27,000×g at 4 °C for 20 min. The solubilized membranes were then stored at −80 °C for future use. The protein content was determined using bicinchoninic acid (BCA) protein assay reagent (Thermo Scientific).

Histidine-tagged PSII complexes were purified by FPLC, as described previously (16), with minor modifications, and were stored in 25% glycerol (wt/vol), 10 mM $MgCl_2$, 5 mM $CaCl_2$, 0.04% n-dodecyl-β-D maltoside, and 50 mM MES buffer pH 6.0.

Protein electrophoresis was performed as described previously (17, 18). SDS-PAGE was performed by loading the same amount of isolated membrane proteins on a 12.5% acrylamide resolving gel. After electrophoresis, proteins were transferred to a polyvinylidene difluoride (PVDF) membrane (Millipore), blocked using 5% bovine serum albumin (BSA) for 2 h at room temperature, and then separately incubated with the primary rabbit antibodies raised against CP47 and CP43 proteins overnight at 4°C. The horseradish peroxidase (HRP)-conjugated secondary antibody goat anti-rabbit IgG (H+L)-HRP conjugate (Bio-Rad) was diluted at 1:5,000 in 1.5% BSA. Bands were visualized using chemiluminescence reagents (EMD Millipore, Billerica, MA, USA) with an ImageQuant LAS-4000 imager (GE Healthcare).

For immunoblotting, gels were transferred onto a PVDF membrane (MilliporeSigma, Burlington, MA, USA) followed by probing with specific antisera. Immunoblot imaging was performed with chemiluminescence reagents (MilliporeSigma, Burlington, MA, USA) on a LI-COR Odyssey Fc (LI-COR Biotechnology, Lincoln, NE, USA).

6.6.2 Clear native polyacrylamide gel electrophoresis

High resolution clear native PAGE was performed as described in (19). Clear native mini polyacrylamide gel, 4-13% or 4-16%, was prepared using a gradient maker. Protein samples containing 10ug total membrane proteins were loaded in each lane. Mini-gel was run at 4mA for 4 hours. Gels were imaged using a Li-COR Odyssey Fc (LI-COR Biotechnology, Lincoln, NE) using the 700 nm channel to visualize chlorophyll fluorescence.

6.7 References

1. Knoot CJ, Ungerer J, Wangikar PP, & Pakrasi HB (2018) Cyanobacteria: Promising biocatalysts for sustainable chemical production. *J Biol Chem* 293(14):5044-5052.

2. Lin PC & Pakrasi HB (2019) Engineering cyanobacteria for production of terpenoids. *Planta* 249(1):145-154.

3. Santos-Merino M, Singh AK, & Ducat DC (2019) New Applications of Synthetic Biology Tools for Cyanobacterial Metabolic Engineering. *Front Bioeng Biotechnol* 7:33.

4. Weisz DA*, et al.* (2019) A novel chlorophyll protein complex in the repair cycle of photosystem II. *Proc Natl Acad Sci U S A* 116(43):21907-21913.

5. Beckova M, Sobotka R, & Komenda J (2022) Photosystem II antenna modules CP43 and CP47 do not form a stable 'no reaction centre complex' in the cyanobacterium Synechocystis sp. PCC 6803. *Photosynth Res*.

6. Liu H, Roose JL, Cameron JC, & Pakrasi HB (2011) A genetically tagged Psb27 protein allows purification of two consecutive photosystem II (PSII) assembly intermediates in Synechocystis 6803, a cyanobacterium. *J Biol Chem* 286(28):24865-24871.

7. Huang G*, et al.* (2021) Structural insights into a dimeric Psb27-photosystem II complex from a cyanobacterium Thermosynechococcus vulcanus. *Proc Natl Acad Sci U S A* 118(5).

8. Grasse N*, et al.* (2011) Role of novel dimeric Photosystem II (PSII)-Psb27 protein complex in PSII repair. *J Biol Chem* 286(34):29548-29555.

9. Camsund D & Lindblad P (2014) Engineered transcriptional systems for cyanobacterial biotechnology. *Front Bioeng Biotechnol* 2:40.

10. Riaz-Bradley A (2019) Transcription in cyanobacteria: a distinctive machinery and putative mechanisms. *Biochem Soc Trans* 47(2):679-689.

11. Zabret J*, et al.* (2021) Structural insights into photosystem II assembly. *Nat Plants* 7(4):524-538.

12. Xiao Y*, et al.* (2021) Structural insights into cyanobacterial photosystem II intermediates associated with Psb28 and Tsl0063. *Nat Plants* 7(8):1132-1142.

13. Avramov AP, Hwang HJ, & Burnap RL (2020) The role of Ca(2+) and protein scaffolding in the formation of nature's water oxidizing complex. *Proc Natl Acad Sci U S A* 117(45):28036-28045.

14. Bricker TM, Morvant J, Masri N, Sutton HM, & Frankel LK (1998) Isolation of a highly active Photosystem II preparation from *Synechocystis* 6803 using a histidine-tagged mutant of CP 47. *Biochim Biophys Acta* 1409:50-57.

15. Kashino Y*, et al.* (2002) Proteomic Analysis of a Highly Active Photosystem II Preparation from the Cyanobacterium Synechocystis sp. PCC 6803 Reveals the Presence of Novel Polypeptides. *Biochemistry* 41(25):8004-8012.

16. Kashino Y*, et al.* (2002) Proteomic analysis of a highly active Photosystem II preparation from the cyanobacterium *Synechocystis* sp. PCC 6803 reveals the presence of novel polypeptides. *Biochemistry* 41:8004-8012.

17. Kashino Y, Koike H, & Satoh K (2001) An improved sodium dodecyl sulfate-polyacrylamide gel electrophoresis system for the analysis of membrane protein complexes. *Electrophoresis* 22:1004-1007.

18. Kashino Y*, et al.* (2002) Low-molecular-mass polypeptide components of a Photosystem II preparation from the thermophilic cyanobacterium *Thermosynechococcus vulcanus*. *Plant Cell Physiol* 43:1366-1373.

19. Wittig I, Karas M, & Schagger H (2007) High resolution clear native electrophoresis for in-gel functional assays and fluorescence studies of membrane protein complexes. *Mol Cell Proteomics* 6(7):1215-1225.

Appendix

Figures A.1 and Tables A1-11 were generated by VMJ.

A.1 Mass Spectrometry Data on Bands from purified H47 and H27 PSII

One experiment that I performed, and from which I have a lot of data, was to do bottom-up mass spectrometry on the lower-molecular weight bands that we observe when H47 or H27 PSII is run on a clear-native PAGE gel (Figure A.1). I did this experiment in collaboration with Haijun Liu in Washington University Biology Department, who ran the samples for me.

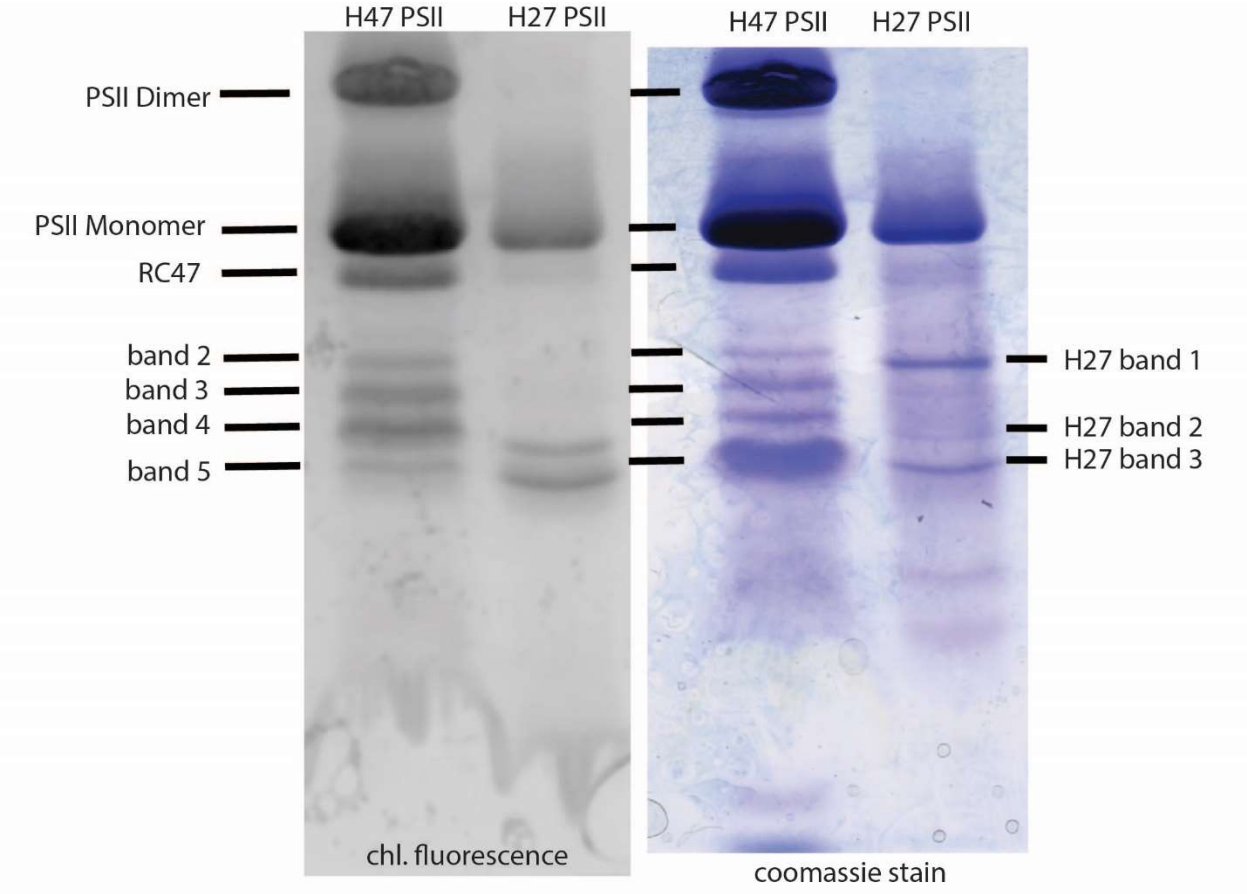

Figure A.1. CN-PAGE bands that were analyzed by bottom-up mass spectrometry.

Following is a series of tables with the PSII associated proteins identified in each sample from Figure A.1, and number of peptides from each protein from each band. The datasets were searched for known PSII associated proteins.

Table A.1 Peptides found in H47_D

Protein	**Peptide #**	**Coverage**
PsbB	920	0.665
PsbC	569	0.715
PsbD	435	0.446
PsbA	174	0.244
PsbY	122	1
PsbE	120	0.988
PsbF	70	0.977
PsbH	68	0.25
PsbK	50	0.867
PsbQ	49	0.57
PsbL	32	0.974
PsbU	26	0.557
PsbO	25	0.427

Table A.2 Peptides found in H47_M

Protein	Peptide Count	Coverage
PsbB	1103	0.69
PsbC	568	0.643
PsbD	490	0.403
PsbA	216	0.244
PsbY	145	1
PsbE	134	0.988
PsbQ	118	0.638
Psb27	115	0.563
PsbH	80	0.25
PsbF	74	1
PsbK	45	0.889
PsbL	33	1
PsbO	17	0.453
PsbU	14	0.557
Psb28	8	0.5

Table A.3 Peptides found in H47_RC47

Gene	Peptide #	Coverage
PsbB	271	0.44
PsbD	124	0.364
PsbO	71	0.631
PsbU	68	0.618
PsbE	56	0.58

PsbA	50	0.2
PsbQ	33	0.497
PsbH	16	0.219
PsbF	13	0.977
Psb28	12	0.5
PsbY	11	0.923

Table A.4 Peptides found in H47_2

Gene	**Peptide #**	**Coverage**
PsbB	230	0.521
PsbQ	89	0.557
PsbC	55	0.396
PsbO	45	0.427
PsbH	17	0.219
Psb27	11	0.289
PsbY	10	0.923
Psb28	6	0.5

Table A.5 Peptides found in H47_3

Gene	**Peptide #**	**Coverage**
PsbB	747	0.578
PsbC	396	0.617
PsbD	317	0.384
PsbA	156	0.244
PsbY	139	1
PsbE	102	0.988
PsbQ	98	0.597

Psb27	68	0.496
PsbO	67	0.609
PsbH	64	0.25
PsbU	54	0.618
PsbK	54	0.844
PsbF	48	0.977
PsbL	26	0.923
Psb28	10	0.357

Table A.6 Peptides found in H47_4

Gene	**Peptide #**	**Coverage**
PsbO	458	0.81
PsbB	387	0.558
PsbC	123	0.665
PsbQ	55	0.55
PsbY	27	0.923
cpcA	23	0.623
PsbH	21	0.219
Psb28	20	0.562
CpcB	16	0.593
PsbD	3	0.099
PsbK	3	0.822
PsbL	2	0.923
HliB	2	0.09

Table A.7 Peptides found in H47_5

Gene	Peptide #	Coverage
PsbO	2959	0.843
PsbC	188	0.665
PsbB	113	0.467
PsbQ	94	0.55
Psb28	52	0.562
Ycf48	34	0.596
PsbY	25	0.923
CpcA	17	0.531
Psb27	17	0.452
CpcB	7	0.331
PsbK	3	0.8
ApcB	2	0.099

Table A.8 Peptides found in H27_M

Gene	Peptide #	Coverage
PsbB	579	0.619
PsbC	281	0.737
PsbD	279	0.747
PsbF	123	1
PsbE	73	0.988
PsbY	37	1
PsbA	33	0.258
PsbH	21	0.25
PsaA	14	0.142
PsaF	13	0.642
PsaB	9	0.12
PsaL	6	0.401

PsbL	6	0.923
Psb27	6	0.422
PsaM	5	0.774
PsaE	3	0.541
PsaD	3	0.142
PsbK	2	0.822

Table A.9 Peptides found in H27_2

Protein	**Peptide #**	**Coverage**
PsbC	87	0.602
PsbO	52	0.609
CpcB	18	0.657
CpcA	17	0.531
PsbB	5	0.11
PsbY	5	0.923
OCP	2	0.06
PsbK	2	0.822

Table A.10 Peptides found in H27_3

Gene	**Peptide #**	**Coverage**
PsbC	460	0.654
PsbO	274	0.606
CpcA	162	0.512
PsbY	39	0.718
CpcB	172	0.25
PsbB	507	0.138
Psb28	112	0.393

ApcB	161	0.18
PsbK	45	0.8

In looking at this data, nothing surprising was observed. The results were mostly inconclusive. However, this data is a useful resource for future research. A separate data file with all the peptides found from the S6803 genome database is attached.

Table A.11 Supplementary Data file- list of all peptides identified from S6803 in samples listed

A.2 Materials and Methods

A.2.1 Clear-native PAGE analysis

High resolution clear native PAGE was performed. 1.5x160x160 mm clear native polyacrylamide gel, 4-16%, was prepared using a gradient maker. Protein samples containing 10 µg of Chl *a* were loaded in each lane. Gel was run at 4mA for 16 hours at 4° C. Gels were imaged using a Li-COR Odyssey Fc (LI-COR Biotechnology, Lincoln, NE) using the 700 nm channel to visualize chlorophyll fluorescence.

A.2.2 In-gel digestion and LC-MS/MS analysis

Protein samples were excised from the clear native polyacrylamide gel, destained and dehydrated with (1:1) 100mM ammonium bicarbonate:acetonitrile and digested in-gel with 13 ng/uL trypsin (Sigma, St. Louis, MO, USA) in 1mM TEABC. Following digestion, sample was extracted in 1% formic acid and subjected to LC-MS/MS.

Aliquots (5 µL, ~100 pmoles) of the peptide samples were separated online using a Dionex Ulimate 3000 RSLCnano pump and autosampler (Thermo Fisher Scientific, Waltham, MA, USA) and a column packed in-house utilizing ProntoSIL C18AQ, 3 µm particle size, 120 Å pore size (Bischoff, Stuttgart, Germany), in a 75 µm X 15 cm capillary. The mobile phase consisted of A: 0.1% formic acid in water and B: 0.1% formic acid in 80% acetonitrile/20% water (Thermo Fisher Scientific, Waltham, MA, USA). At a flow rate of 500 nL/min, the gradient was held for 5 min at 2% B and slowly ramped to 17% B over the next 30 min, increasing to 47% B over the next 30 min and then finally increasing to 90% B over 30 min and held at 90% for 10 min. The column was then allowed to re-equilibrate for 60 min with a flow of 2% B in preparation for the next injection.

The separated peptides were analyzed on-line by using a Q-Exactive Plus mass spectrometer (Thermo Fisher Scientific, Waltham, MA, USA) operated in standard data-dependent acquisition mode controlled by Xcalibur version 4.0.27.19. Precursor-ion activation was set with an isolation width of *m/z* 1.0 and with two collision energies toggled between 25 and 30%. The mass resolving power was 70,000 for precursor ions and 17,500 for product ions (MS2).

The raw data were analyzed using PEAKS Studio X (version 10.0, Bioinformatics Solution Inc., Waterloo, ON, Canada, www.bioinfor.com) and Protein Metrics Byonic and Byologic (Protein Metrics Inc., Cupertino, CA, www.proteinmetrics.com) (33). PEAKS was used in the *de novo* mode followed by DB, PTM, and SPIDER modes. Search parameters included a precursor-ion mass tolerance of 10.0 ppm and a fragment-ion mass tolerance of 0.02 Da. Variable modifications included all built-in PTMs. The maximum allowed modifications per peptide were 3; and the maximum missed cleavages were 2; false discovery rate, 0.1%. SPIDER (function) was used to

identify unknown spectra by considering homology searches, sequence errors, and residue substitutions to yield a more confident identification.